GROWTH AND MORPHOLOGY OF CLASSICAL AND SUPERSPACE CRYSTALS

GROWTH AND MORPHOLOGY OF CLASSICAL AND SUPERSPACE CRYSTALS

PROMOTOREN: PROF. DR. P. BENNEMA
PROF. DR. A. JANNER

GROWTH AND MORPHOLOGY OF CLASSICAL AND SUPERSPACE CRYSTALS

Proefschrift

ter verkrijging van de graad van doctor in de
wiskunde en natuurwetenschappen
aan de Katholieke Universiteit te Nijmegen,
op gezag van de Rector Magnificus,
Prof. Dr. J.H.G.I. Giesbers,
volgens besluit van het College van Dekanen
in het openbaar te verdedigen
op donderdag 17 april 1986
des namiddags te 2 uur precies

door

Bernard Dam

geboren te Arnhem

krips repro meppel

1986

Het is mij een genoegen ieder te danken die aan de totstandkoming van dit proefschrift heeft bijgedragen.

In het bijzonder mijn ouders, die mijn studie mogelijk maakten en mij altijd in mijn keuze hebben gestimuleerd.

De medewerkers en studenten van de Afdeling Vaste Stof Chemie/Vaste Stof Fysica III. Hier is mijn enthousiasme voor de wetenschap ontstaan; wetenschap niet alleen als handwerk, maar ook als object van studie.

De gastvrijheid op de afdeling theoretisch fysica, waar ik veel geleerd heb over superruimte en waar bovendien de ruimte was om over de moeilijkheden in het onderzoek te praten.

Tenslotte ieder die me buiten de faculteit nabij was. Met name Henny die het niet nalaat het niet met me eens te zijn, Gerard en zijn zorg waarvoor ik hem nooit heb mogen bedanken en Guus waarmee ik een historie deel. Hun scepsis, zorg en vriendschap vormen het complement van dit proefschrift.

O dit is vreemd bedrog. Subtiele logen
verwisseling des wezens en des schijns.

Frederik van Eeden
in 'Het Lied van Schijn en Wezen, III'.

Contents

Samenvatting 8

1. Introduction 10

2. Impurity action and the morphology of KDP-type crystals

2.1 On the occurrence of growth bands on spheres of single crystals of KH_2PO_4 and $NH_4H_2PO_4$ 19

2.2 In-situ observation of surface phenomena on {100} and {101} potassium dihydrogen phosphate crystals 25

2.3 In-situ observation of surface phenomena on {100} KDP related to growth kinetics and impurity action 36

2.4 The growth spiral morphology on {100} KDP related to impurity effects and step kinetics 42

2.5 The mechanism of tapering on KDP-type crystals 56

3. Layer growth on reconstructed silicon surfaces

3.1 A 'rough heart' model for 'edge' dislocations which act as persistent growth sources 69

4. The morphology of modulated K_2SO_4-type structures

4.1 Observation of bands of faces on incommensurate Rb_2Zr_4 single crystals 75

4.2 Morphological determination of modulated-cell parameters of Rb_2Zr_4 79

4.3 A superspace approach to the structure and morphology of $((CH_3)_4N)_2ZnCl_4$ 87

4.4 In-situ observation of a roughening transition of the $(10\bar{1}2)$ satellite crystal surface of modulated $((CH_3)_4N)_2ZnCl_4$ 96

4.5 Crystal form and surface morphology of modulated β-K_2SO_4-structures 101

5. Calaverite: An anomaly resolved

5.1 The incommensurate morphology of calaverite ($AuTe_2$) crystals 123

5.2 The incommensurate morphology of calaverite ($AuTe_2$) crystals, part II 127

Curriculum vitae 143

Samenvatting

In dit proefschrift is de relatie onderzocht tussen kristalstructuur en kristalmorfologie, met name in het geval van gemoduleerde verbindingen.

Kristalmorfologie is door de eeuwen heen gezien als een goede indicator voor de inwendige kristalstructuur. Dit, ondanks het feit dat, zoals we nu weten, oppervlakte reconstructie en verontreiniging aanleiding kunnen geven tot anomalieën. Deze beide laatste effecten worden hier geillustreerd met een artikel over tapering (hfst. 2.5), een anomale groeivorm op KH_2PO_4, en een beschouwing over een mogelijk groeimechanisme op gereconstrueerde silicium oppervlakken (hfst. 3). In de meeste gevallen is de morfologie echter inderdaad een getrouwe afspiegeling van de inwendige structuur en regelmaat van het kristal.

Zelfs als de normale regelmaat van het 3-dimensionale rooster verbroken is door een periodieke verstoring, is deze extra periodiciteit te herkennen in de kristalmorfologie (hfst 4. en 5.). Zo werden op enige gemoduleerde K_2SO_4-type kristallen extra, zogenaamde satellietvlakken gevonden. De orientatie en de verdeling van de satellieten kon gecorreleerd worden aan de lengte van de modulatie golf en de superruimtesymmetrie van de gemoduleerde structuur. Het bleek bovendien dat de ruimtegroep symmetrie van de verschillende gemoduleerde fasen van $((CH_3)_4N)_2ZnCl_4$ ondergroepen zijn van één enkele 4-dimensionale superruimtegroep, die het gemoduleerde patroon invariant laat.

Met optisch microscopie werden de nieuw ontdekte satellietvlakken in situ, d.w.z. tijdens de groei in een waterige oplossing, bestudeerd. Net als op normale kristalvlakken werden groeispiralen en etsputten aangetoond, zelfs op satellieten met een incommensurabele orientatie. Dit duidt erop dat ook satellietvlakken thermodynamisch stabiele orientaties zijn, met een randenergie groter dan nul. Zo gauw de lengte van de modulatiegolf verandert (als functie van de temperatuur bijvoorbeeld) veranderen ook de orientaties van de satellietvlakken. In-situ microscopie maakte het mogelijk dit proces aan het satellietoppervlak te volgen. Een nieuw soort verruwingsovergang werd hierbij waargenomen (hfst. 4.4).

Met genoemde in situ techniek werd overigens eerst ervaring opgedaan tijdens een studie naar de invloed van verontreinigingen op de kinetiek van groeilagen op KH_2PO_4. Minime concentraties aan Cr^{3+}-ionen bleken de groei aanmerkelijk te vertragen en bij lage oververzadiging zelfs een totale blokkering van de groei te veroorzaken (hfst. 2.2 en 2.3). Verder werd uit de vorm van de groeispiralen op KH_2PO_4 een mogelijk groeimechanisme afgeleid (hfst. 2.4).

Terwijl de morphologie van kristallen in het algemeen een onderwerp is met vele praktische toepassingen, lijkt de studie naar de stabiliteit van satellietvlakken in eerste instantie een onderwerp van slechts wetenschappelijk belang. Echter, ook 'normale' kristalstructuren kunnen met behulp van een commensurabele modulatie vereenvoudigd beschreven worden (hfst. 5.2). Aangezien satelliet vlakken zich als normale kristalvlakken lijken te gedragen, kan worden aangenomen dat de resultaten van dit onderzoek van belang zullen blijken woor de verdere ontwikkeling van de morfologische theorie. Dit met name gezien het feit dat vele kristalstructuren gezien kunnen worden als verstoorde kubische of hexagonale bolstapelingen.

In de nu volgende introductie zal in eenvoudige termen een overzicht gegeven worden van de historie van de studie der kristalvormen. In het kort zal daarbij in algemene termen worden nagegaan hoe bij gemoduleerde kristallen de morfologische concepten aangepast dienen te worden.

1. Introduction

I-1 General

The investigation of crystal morphology is an area of research where one is confronted with both the internal crystal structure and the structure of the crystal ambient mother phase. The same applies to study of crystal surface morphology. Though crystals are famous for their flat and shining surfaces, microscopically stepped structures can be observed on them. The geometry of these so-called growth figures is the 2-dimensional analogue of the crystal form.

Crystal form and surface structure are important problems in such diverging fields as katalysis, biology (the formation of bone, teeth and, unfortunately, kidney stones) and the manufacturing of semiconductors.

The discovery of modulated crystals gave a new dimension to both X-ray and morphological crystallography. The diffraction pattern of a substance with one periodic distortion wave is described in terms of (3+1) base vectors; accordingly for the crystal symmetry (3+1) dimensional superspace groups were introduced. Given the innate relation between crystal structure and its morphology, it is not surprising that also in the crystal morphology the effects of such modulations can be traced.

In this introduction we will give a historical review of the development of the relation between crystal structure and crystal morphology. It will be shown how the crystal lattice concept emerged from the study of crystal morphology. Later in the history of crystal morphology the more thermodynamic aspects became important.

The question how these concepts have to be modified in the modulated case is discussed in I-4, whereas this introduction is concluded with section I-5 which gives a scope and summary of the subjects treated in this thesis.

I-2 Morphology and the crystal lattice

The science of crystallography started with the study of the beautiful flat faces, which characterizes crystalline matter. It was found that on all crystals of the same substance, the angles between corresponding faces have a constant value (Steno, 1669). The crystals were also found to have a tendency to separate, when broken, along certain characteristic planes. This observation tempted Guglielmini to the idea that upon splitting the crystal again and again one would

obtain as ultimate unit a miniature crystal with plane faces. This concept was followed by Haüy (1784). According to him the smallest possible unit, the molécule intégrante, constitutes in a regular stacking the crystal structure. Important crystal faces will be parallel to the faces of this molécule intégrante. The most important contribution of Haüy is his view that other secondary faces, not parallel to the faces of a molécule intégrante, are in fact simple stepped arrays of these building units. Abstracting from this structural picture the Law of Rational Indices was formulated. In short it states the following. If we select the directions of three non-coplanar edges of a crystal as its reference axes, the intercepts p_1, p_2, p_3 and p'_1, p'_2, p'_3 made on them by any pair of faces relate as small integers

$$\frac{p'_1}{p_1} : \frac{p'_2}{p_2} : \frac{p'_3}{p_3} = h_1 : h_2 : h_3 \qquad (1)$$

Limited as we are by experimental errors such a hypothesis can never be derived from experiment. But it contains in its extrapolation from observed facts the concept of a 3-dimensional lattice of translations.

The lattice concept was made explicite by the Bravais derivation of the 14 space lattices. Accordingly, the law of Rational Indices was reformulated. The morphological importance (MI) of a certain crystal face is said to increase with an increase of the reticular density of the lattice plane parallel to that face. Equivalent is the inverse relation (Friedel), which states that the MI increases with an increasing distance between the equivalent lattice planes. The concept of morphological importance (MI) is a statistical one. It is a measure of the frequency of occurrence of a certain orientation. Sometimes also the size of a crystal face is taken into account.

With the advent of X-ray crystallography the electron density lattice became available. Moreover the diffraction pattern gradually gave more and more insight in the atomic coordinates within the unit-cell of the lattice. The morphological lattice and the lattice of electron density do not have to coincide. Still, a remarkable correspondence between the results of the two techniques was found. Due to the Donnay-Harker extension of the Bravais-Friedel law, in fortitious cases space group determination from morphological data appeared to be possible. In this extension the distance between equivalent lattice planes (and hence the MI) can be reduced through the pseudo-translational elements of the space group such as scew axes and glide planes. The extinction conditions of the diffraction pattern thus have their morphological counterpart, though the latter are only indirectly observed.

The distinction between the morphological lattice and the lattice obtained by X-ray diffraction is put forward again by Donnay and Donnay. They showed that the MI of certain orientations is reduced if within one lattice plane distance two equivalent bond structures are present. In this case the lattice is reduced to a kind of sublattice. Already in 1947 M. Buerger employed the reverse line of thought. He deduced that the crystal form of superstructures should follow the Bravais rule applied to its basic structure rather than to the superstructure lattice.

I-3 Thermodynamic aspects

Nowadays the study of crystal morphology is concerned more with the nature of the two-dimensional interface which a crystal surface provides. Only in first approximation the crystal surface structure is obtained from an infinite lattice by cleaving the crystal along a certain plane, and replacing one semi-infinite crystal by the mother phase. Due to the lack of inversion symmetry of the crystal at the surface, distortions such as lattice relaxation, surface reconstruction and surface enrichment are not unusual. Another important factor determining the eventual surface structure is adsorption and, in general, the interaction with the ambient phase.

The flatness of the crystal surface, in fact the existence of an interface, is determined by the strength of the lateral surface bonds. Taking in first approximation the cleavage structure as the crystal surface structure, the surface free energy will be smallest the more of the crystalline bonds lie within the lateral surface plane. The maximum of the natural repeat distance for the surface free energy is of course equal to the distance between equivalent lattice planes, d(hkl). Here, h,k and l are the indices of the crystal face normal vector with respect to the reciprocal lattice base vectors.

Another approach is based on the properties of steps on the crystal surface, i.e. the boundary of a mono-layer differing d(hkl) in height with the rest of the crystal surface. If the edge free energy of any step on a (hkl)-surface is zero, the crystal surface is not restricted to remain flat. Due to the fact that the creation of a step does not cost any free energy, a so-called roughening of the crystal surface is the result. It depends on the geometry of the crystal faces whether due to the roughening a crystal face is rounded off or disappears. On a roughened crystal surface under growth conditions layer growth is substituted by a normal growth mechanism characterized by a linear growth rate as a function of supersaturation. The temperature of this transition, the roughening temperature T_R, is related both to the

strength and geometry of the lateral surface bonds, and to the interaction of the crystal surface with the surrounding crystal motherphase. Hence T_R depends on the orientation of the crystal surface. The observation of coherent step structures is a strong indication that the surface under observation is thermodynamically stable, with a non-zero edge free energy. In this way the study of crystal morphology has become involved partly in surface science partly in crystal growth.

I-4 The morphological laws and modulated structures

The advent of the concept of incommensurately modulated crystals demanded for a reconsideration of the theories relating crystal form to crystal structure. A modulation can be seen as a periodic distortion of the (basic) crystal structure. The distortion can be a displacement wave, a spin density wave or an occupation wave. The essence of the new approach describing both incommensurate and commensurate modulations (superstructures) is that one considers the modulation as an extra periodicity to be treated independently from the three of the ordinary space lattice. In this way a concise description can be given of a modulated structure whether the periodicity of the modulation fits with the basic lattice or not (the commensurate and the incommensurate case, respectively). In reciprocal space this approach amounts to the use of four or more base vectors instead of three. Thus it is possible again to describe the diffraction pattern of an one-dimensionally modulated incommensurate structure with one set of integers (four), which is impossible when using only three base vectors. As crystal morphology is described in terms of face normals, the law of Rational Indices applies to a reciprical lattice also. It is quite natural then to apply in the description of the morphology of modulated crystals the same four base vectors as in the diffraction case. In chapter 4. and 5. it is shown that this extension is a very fruitful one. Nevertheless, the crystal has not a three-dimensional lattice anymore in real space. It appears thus that the existence of fundamental periodicities rather than 3-dimensional lattice symmetry is the key concept governing crystal morphology. The Bravais concept of lattice planes with a high reticular density is lost but the Friedel law remains applicable. The d(hklm) remains a reliable measure for the MI of a (hklm) face, though we propose that d(hklm) is no longer considered as the distance between equivalent lattice planes, but rather as the fronts of Fourier electron density waves.

What modification has to made to the classical thermodynamical approach to crystal morphology? A distinction has to be made between (hkl0) and (hklm) orientations, the so-called main and satellite faces. The bond structures within d(hkl0) will become modulated somewhat, but they are in principle the same as in the non-modulated phase. The d(hklm) slices along satellite orientation however have been formed together with the advent of the modulation; their orientation is directly coupled to the length and the orientation of the fourth base vector. One could say that whithin such thick slices it is not too difficult to construct new bond structures to explain the observed stability of the satellite faces. The question then is why mainly satellite orientations with low m indices are found. This suggests a stronger coupling with the modulation wave than only the effect of the increased slice thickness.

In chapter 4. a stabilized step model is introduced. This model takes into account that on main (hkl0) faces the edge free energy will become modulated. Thus certain stepped orientations on these main faces will become stabilized. This model more closely predicts the existence of only certain low m satellite faces. On the other hand the structural insight it gives is still poor. It must be admitted then that the description of the morphology of modulated crystals is still in a geometric stage. The enormous succes of the classical law of Rational Indices gives us some hope that in future also the bonding structure of satellite faces will become understood, with the help of the extended morphological laws presented in this thesis. Note, by the way, that also behind the Law of Rational Indices is the idea of simple stepped surface structures. The molécule intégrante can be compared with the main lattice and the stepped, secondary orientations with the satellite orientations.

I-5 Scope and summary

In this thesis the relation between crystal morphology and crystal structure is investigated for classical and modulated crystals.

Though the classical crystal form is generally thoroughly investigated, in chapter 2 we start with the observation of a strange phenomenon on $NH_4H_2PO_4$ crystals. This paper is the first to ascribe a morphological feature to the presence of a modulation in the crystal structure. However, the modulated nature of this substance could not be confirmed yet. The rest of this chapter is classical and deals with the effects of ionic impurities on the crystal form and surface morphology of crystals of the same type of crystal structure. With optical microscopy it was possible to observe the layer by layer

growth process on a crystal surface. The addition of minute quantities of ionic impurities had a dramatic effect on the advancement of the growth layers. Changes in shape and even a total blocking of the growth layers was observed.

The reconstructed silicon surfaces discussed shortly in chapter 3. are a kind of intermediate structures. Though the internal structure of these crystals is classical, at the surface the lattice has a periodicity different from the crystal lattice. Here one can speak of a surface modulation, which appears to be able to stabilize certain crystal faces also. In 3.1 a possible mechanism of repeated nucleation on such a surface is discussed.

In the K_2SO_4-type crystals treated in chapter 4 the 3-dimensional crystal structure is modulated. It is found that the orientation and distribution of the resulting satellite faces is strongly coupled to the length of the modulation wave and the superspace symmetry of the crystal structure. This superspace group describes the symmetry of several modulated phases, some commensurate some incommensurate. The classical space groups of the commensurate phases appeared to be subgroups of the superspace group. With optical microscopy the surface of the newly discovered satellite faces was studied in-situ, i.e. during growth in a saturated aquous solution. As on normal crystal surfaces growth spirals and etch pits were observed, even on crystals with an incommensurate orientation. This suggests that satellite faces are thermodynamically stable orientations, with an edge free energy larger than zero. As soon as the length of the modulation wave changes (as a function of temperature) also the orientation of the satellite faces changes. In-situ microscopy enabled us to follow the surface changes during this process. A new kind of roughening transition was observed, which appeared to be of a first order nature.

The thesis is concluded with a study on the morphology of the mineral calaverite. Based on data found in the litterature about 80 satellite faces were identified. Thus a more than one hundred years old problem in morphological litterature is solved.

The thesis is mainly a collection of journal articles. Some repition of ideas and views can not be excluded therefore. It is hoped on the other hand that following the development of certain lines of thought will add to the understanding of the problems presented here.

Litterature

- Crystal form and structure, C.J. Schneer editor (Dowden, Hutchinson & Ross, 1977).

- J.G. Burke: Origins of the science of crystals (University of California Press, 1966).

- B.K. Vainshtein: Modern Crystallography I, Springer Series in Solid State Sciences 15 (Springer Verlag, Berlin, 1984).

- J.P. van der Eerden, thesis (University of Nijmegen, 1979).

- P. Bennema and I. Sunagawa, in: Preparation and Properties of Solid State Materials, Vol. VII, Ed. W.R. Wilcox (Dekker, New York, 1982) p1.

- P.M. de Wolff, T. Janssen and A. Janner, Acta Cryst. A37 (1981) 625.

- A. Janner in: Symmetries and properties of non-rigid molecules: A comprehensive survey, Eds. J. Marnani and J. Serre (Elsevier, Amsterdam, 1983) Studies in Physical and Theoretical Chemistry, Vol.23, p461-486.

2. Impurity action and the morphology of KDP-type crystals

ON THE OCCURRENCE OF GROWTH BANDS ON SPHERES OF SINGLE CRYSTALS OF KH_2PO_4 AND $NH_4H_2PO_4$

B. Dam, P. Bennema and W.J.P. van Enckevort
RIM, Laboratory of Solid State Chemistry

and

A. Janner
Institute for theoretical physics,
Faculty of Science, Catholic University of Nijmegen,
Toernooiveld, NL-6525 ED Nijmegen, The Netherlands.

Introduction

This slightly rewritten abstract on the growth bands on crystalline spheres of ADP and KDP may seem a bit out of place. It is included, as it presents the first attempt to relate crystal morphology to a modulation wave. Its central hypothesis states that a modulation is capable to stabilize the morphology and to retard growth in PBC-zones perpendicular to the modulation wave vector. The fact that this hypothesis will be confirmed and refined in chapter 4 and 5 of this thesis is the principle reason for reproducing this abstract here.

Abstract 6^{th} International conference on Crystal Growth, Extended Abstracts IV p18, Moscow, 1980.

It was reported in 1965 that on spheres of ADP and KDP special growth bands occur [1]. These experiments have been repeated and the following interesting results were found for ADP and KDP. As indicated in fig.1, on spheres of ADP the F faces {101}, {100} and the 'stabilized S faces' $\{\bar{1}1\bar{2}\}$ and $\{11\bar{2}\}$ occur (for a PBC analysis of the KDP-type structure see Hartman [2]). Very interesting are the four 'A' bands, one of which runs from $(01\bar{1})$ to $(\bar{1}10)$, in zone with the PBC [111]. For the other set of bands, the so-called 'B' bands, the beginning and the origin is not quite clear. Assuming that it starts approximately in (130) and ends in $(11\bar{2})$ the band is in zone with $[3\bar{1}1]$. Both types of bands consist of about 100 well separated flat areas, each with its own orientation. Most intriguing is the fact that the point group symmetry of the bands is 222 and <u>not</u> $\bar{4}2m$, the point group of ADP.

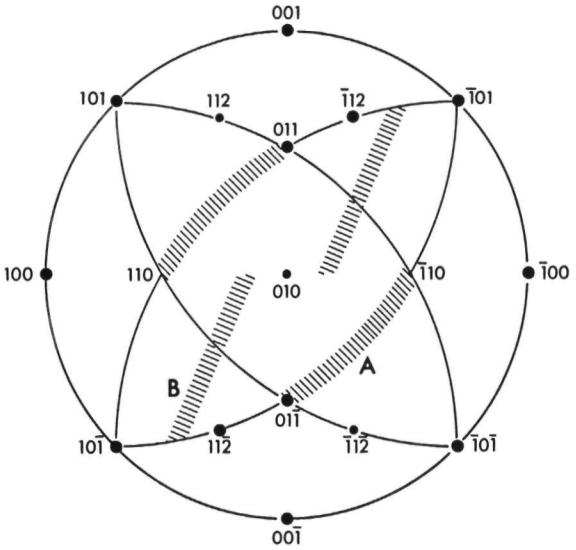

a

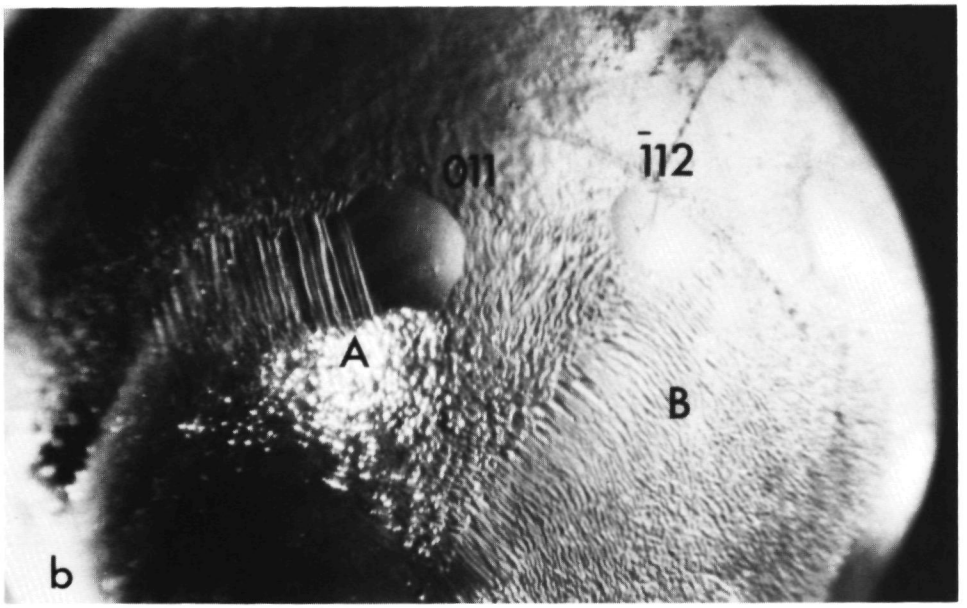

Fig.1.

a) Stereogram of a sphere of ADP

b) Corresponding picture of a grown ADP crystal sphere (20x).

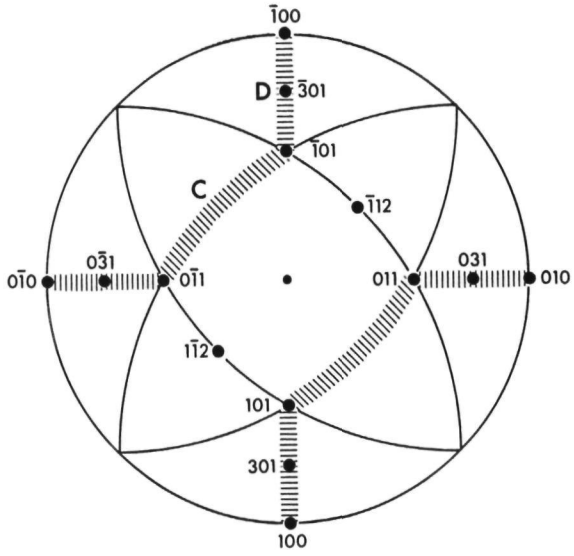

a

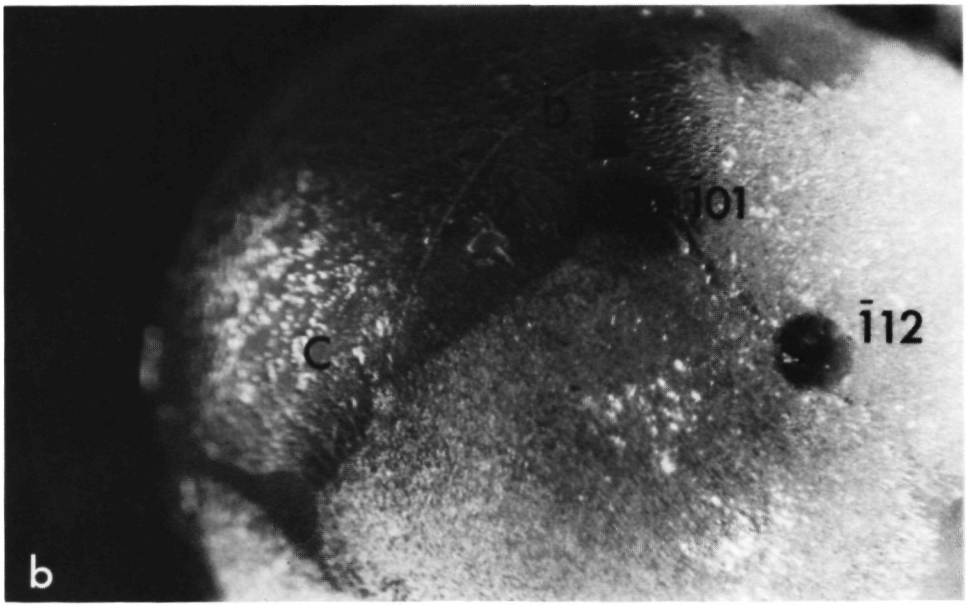

Fig. 2.

a) Stereogram of a sphere of KDP

b) Corresponding picture of a grown KDP crystal sphere (20x).

As can be seen from fig. 2a,b on KDP only the F-face {101} and one of the two sets of tetragonal bisphenoids {$\bar{1}$12} develop. No {100} F-faces develop, since probably due to metal impurities the [001] zone does not grow. Two types of well defined bands occur, which are indicated as 'C' and 'D' and lie in zone with the PBC's <111> and <001> respectively. Within the latter band the {301} S-faces were observed. The point group symmetry of the bands now is equivalent to the one of the KDP structure: $\bar{4}$2m.

We offer the following preliminary explanation for the occurrence of the growth bands. We assume that ADP and KDP are modulated crystals. This means that apart from the ideal structure there are periodic perturbations with wave lengths which in our case are say 100 elementary cell parameters (a≈b≈c). We introduce the following hypothesis: band shaped area's on a sphere are delayed in growth if:

1) They are more of less parallel to a modulation direction;

2) Lay in zone with a PBC, which is (more of less) perpendicular to the modulation (To modulation and PBC's the symmetry of a point group applies).

Our hypothesis is outlined in fig.3.

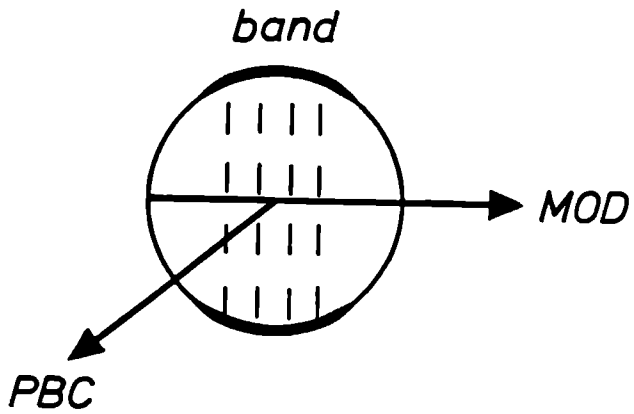

Fig.3. Sketch of the geometrical arrangement of a growth band, a PBC direction and the modulation wave vector.

Perpendicular to the modulation we have through the whole crystal equidistant phase planes. The more of these planes are cut by a certain area on the sphere the more 'elastic strain' is felt by this area, the slower the growth. This effect becomes especially visible if a certain orientation is in zone with a PBC. The further from the centre the more the band is blurred out. All bands except B start and end in F faces, contaning a PBC as in fig.3. Using our hypothesis, each of the bands can be described as a combination of a PBC and a modulation vector. In table I the inferred modulation directions are given, while the last column denotes the observed configurational symmetry of the growth bands.

Table I

compound	band	modulation	PBC	pointgroup
ADP	A	<10$\bar{1}$>	<111>	222
ADP	B	<10$\bar{1}$>	<3$\bar{1}$1>	222
KDP	C	<1$\bar{1}$0>	<111>	$\bar{4}$2m
KDP	D	<001>	<100>	$\bar{4}$2m

Assuming that the basic structure is unaffected, the point group reduction to 222 must be due to the nature of the modulation wave. Further, a problem arises with band B. Its presence can only be explained by the presence of a hitherto unidentified PBC, e.g. <3$\bar{1}$1> assuming a relaxation of the asumption of the perpendicularity of modulation and PBC.

As yet we have no independent X-ray information -like satellites- on the presence of modulation waves in ADP or KDP. The list of modulated structures is growing fastly however. Recently, about 30 structures have been identified as being modulated structures [4].

Addendum 1986

As to the postulated modulated character of KDP and ADP it must be remarked that no evidence for it ever appeared. On the other hand, even in view of the latest litterature, such a modulation in KDP (or ADP) is not excluded [5]. Presently, X-ray diffraction studies are performed on KDP, which explicitely examine the possible existence of any satellite diffraction spots [6].

Also the proposed <3$\bar{1}$1> PBC could not be confirmed [7].

Another point that calls for further study is the symmetry reduction in the configuration of the growth bands found in ADP: instead of a $\bar{4}$2m a 222 symmetry is found. Moreover, recent experiments revealed that of the two mirror images possible in a 222 point group, only one is found. Even when taking independently nucleated crystals, always only one form is found. Both phenomena remain an interesting problem in the field of morphological crystallography.

References

1) P. Bennema, Z. für Kristallogr. 121 (1965) 312.

2) P. Hartman, N. Jb. Min. Mh. 4, (1959) 73.

3) A. Janner and T. Janssen, Phys. Rev. B15, (1980) 643.

4) A. Janner and T. Janssen, Acta Cryst. A36, (1980) 399; A36, (1980) 408.

5) R. J. Nelmes, W. F. Kuhs, C. J. Howard, J. E. Tibbals T. W. Ryan, J. Phys. C.: Solid State Phys. 18 (1985) L711.

6) R.J. Nelmes, personal communication 1986.

7) M. Aguilo and C.F. Woensdregt, J. Crystal Growth (1984) 527.

Journal of Crystal Growth 69 (1984) 306–316
North Holland Amsterdam

IN SITU OBSERVATION OF SURFACE PHENOMENA ON {100} AND {101} POTASSIUM DIHYDROGEN PHOSPHATE CRYSTALS

B DAM and W J P VAN ENCKEVORT

RIM Laboratory of Solid State Chemistry Faculty of Science Catholic University Toernooiveld 6525 ED Nijmegen The Netherlands

Received 17 February 1984 manuscript received in final form 25 July 1984

Surface patterns on the {100} and {101} faces of KH_2PO_4 (KDP) crystals growing in a stagnant aqueous solution were studied by in situ interference contrast reflection microscopy The contrast of the image registered by a video camera was enhanced to such an extent that steps as low as 80 A could be observed The effect of supersaturation and Cr^{3+} impurity addition on the behaviour of steps and the shape of growth hillocks was studied and it appeared that crystal growth is a complicated non steady state process On {100} the effect of volume diffusion of the growth units could be positively identified Also it was found that at low supersaturation the surface morphology is similar to the pattern observed at higher supersaturation after Cr^{3+} addition Below 2% supersaturation even a blocking of step growth occurred This suggests that metal or other impurities play a significant role in the crystal growth process at low supersaturation

1. Introduction

The influence of supersaturation and impurity concentration on the kinetics and morphology of KDP-type crystals has been investigated by numerous authors (see ref [1] and references therein) However, few have considered the surface morphology of these crystals Ex situ (after removal of the crystal from the solution) growth spirals with macrosteps of about 350 Å were observed on {101} KDP by Van Enckevort et al [2] However, shut off effects, introducing artifacts on the surfaces, never can be excluded in these experiments The only in situ studies, carried out by Davey and Mullin [3,4] and Torgeson and Jackson [5] dealt with the behaviour of very high steps on growing {100} surfaces of $NH_4H_2PO_4$ (ADP)

Recently the technique to observe very low steps (10–50 Å) on crystals growing in aqueous solutions has been improved very much Whereas for CdI_2 Tsukamoto [6] applied transmission microscopy and Jetten et al [7] used reflection microscopy with oblique illumination for potassium hydrogen phthalate, we found that for KDP reflection differential interference contrast microscopy is the most sensitive method

This reflection method enabled us to observe the influence of supersaturation and impurity concentration on the behaviour of high and low steps on both the pyramidal {101} and the prismatic {100} faces of KDP On the basis of these observations some conclusions can be drawn regarding the mechanism of step growth and impurity adsorption

2 Experimental

The specimen crystals for the in situ observations were prepared by cutting plates parallel to {101} and {100} surfaces from larger, high quality KDP crystals The as-grown surfaces then can be studied since, contrary to misoriented surfaces, no inclusion formation takes place there This is important because inclusions lying just below the surface seriously deteriorate the image In some cases also small inclusion free KDP crystals were used

Solutions were prepared from Merck p a and suprapur chemicals in which the iron content has a weight percentage of 10^{-3} and 10^{-5}, respectively

To carry out in situ observations under well

controlled temperature conditions (±0.05°C), crystals were grown in a thermostated, stagnant, aqueous solution. The crystals were then observed by reflection microscopy using oblique illumination with closed aperture diaphragm. This method has been described in detail in a previous work on potassium hydrogen phthalate [7].

To increase the sensitivity of the in situ method the majority of the observations was carried out by application of reflection differential interference contrast microscopy (DICM). For that purpose an inverted type metallurgical Reichert MeFII microscope, fitted with a high intensity mercury light source (250 W) was used. The crystals were placed in a non-thermostated growth cell in such a manner that a layer of 1 mm solution was present between the crystal and the observation window. This optical window had a thickness of 1 mm.

For both systems the image was recorded on tape by means of a high sensitivity video camera, which was connected to an analogue contrast amplifier in order to increase the image contrast to a large extent. In this way details not detectable by visual observation could be revealed clearly on the video monitor.

Compared to the video image obtained by the oblique illumination technique the image obtained by DICM is considerably better showing very small height differences and less disturbing diffraction phenomena.

3. Growth patterns on {100} faces at high supersaturation

3.1 General features

In situ observations on KDP generally show that crystal growth is not a steady state process. On the {100} as well as on the {101} surfaces the configuration of steps and hillocks changes within several minutes. This shows that the currently used growth rate versus supersaturation curves obtained from bulk growth parameters, such as increase in weight or advancement rate of faces, give only a stochastic result. Even if external growth parameters such as temperature and supersaturation are kept constant, a continuous competition between different growth centres can be observed.

An example of a hillock overwhelmed by a sudden flow of macrosteps originating from another source is given in fig. 1. The competition between shallow hillocks (presumably consisting of monomolecular steps) and macrosteps is presented in fig. 2. When the macrosteps hit the small hillocks, wavelike instabilities are formed in the macrosteps, whose lifetimes depend on the orientation of the bunch with respect to the hillock. Both phenomena were observed at high supersaturation ($T_{eq} - T = 10°C$, $\sigma = \Delta c/c \simeq 15\%$) and the growth velocity normal to {100} was of the order of 10^{-7} m/s (≃ 10 mm/24 h).

At the {100} surface a very strong orientational dependence of the step velocity is found. For the ratio of the advancement rates of steps running towards the [001] direction versus those of the same height running towards [010] we found $v_{[001]}/v_{[010]} \simeq 1/10$ ($v_{[001]} = \simeq 10^{-5}$ m/s). Though surface diffusion might play a role in this orientational dependence of the step velocity [8,9], step integration [10] as the rate limiting factor cannot be excluded.

Apart from the orientational dependence, also a height dependence of the step velocity is found, though less pronounced. In this high supersaturation range we observed in the fastest growth direction [010] low steps of about 100 Å running twice as fast as higher ones of about 1000 Å. Going from [010] to [001] this height dependence decreases to zero for steps running towards [001]. Only at very high supersaturations a small height dependence is also seen in this slow direction.

From the fact that a height dependence of step velocities mainly exists for the faster directions, it can be concluded that in stagnant solutions insufficient volume diffusion retards the velocity of high steps (assuming now a direct step integration mechanism). Surface diffusion cannot account for this effect because some velocity difference between high and low steps would than have to exist in all directions.

The importance of volume diffusion is confirmed by two other observations. In the first place we found that steps moving along the edge with another {100} face are accelerated, whereas steps

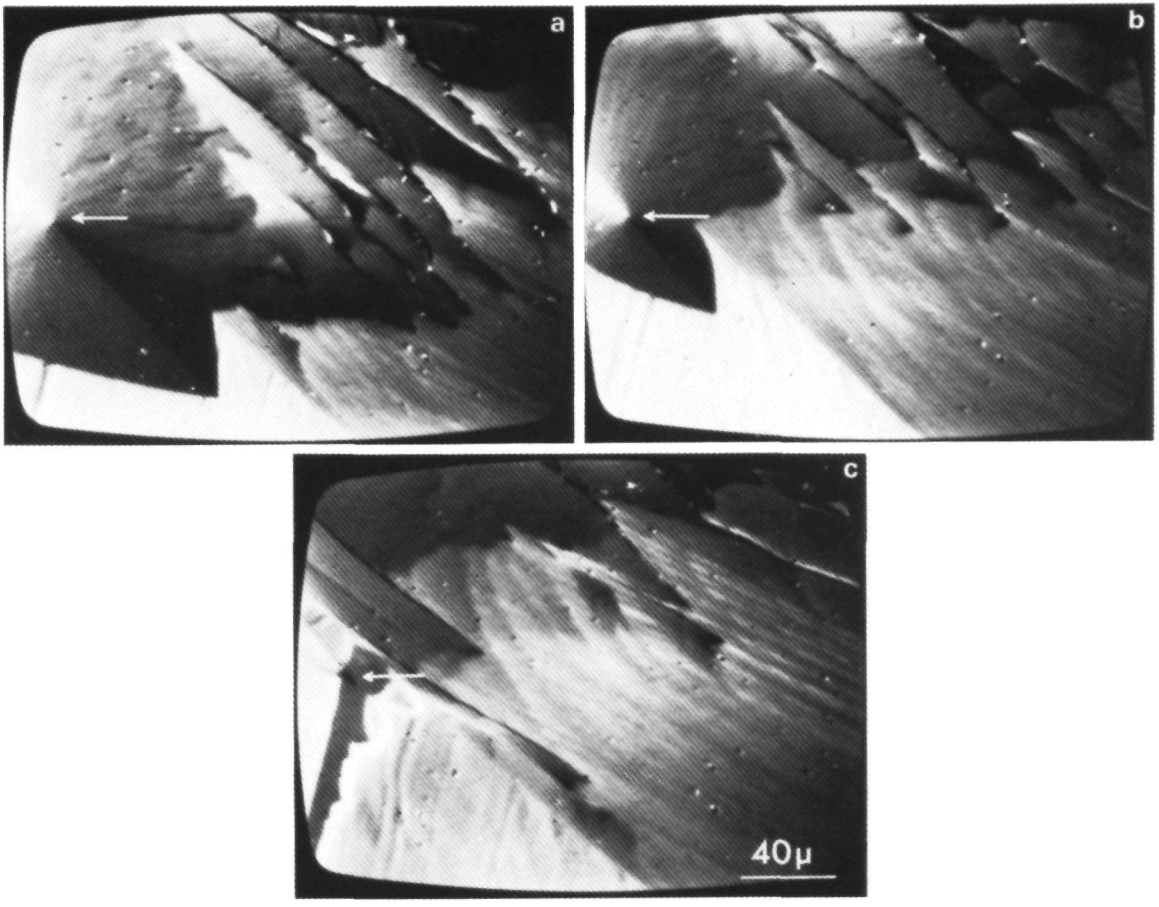

Fig. 1. Sequence of in-situ micrographs showing a growth hillock (the centre indicated by an arrow) on {100} overwhelmed by a step train originating from an other source (DICM): (a) $t = 0$ s; (b) $t = 20$ s; (c) $t = 30$ s.

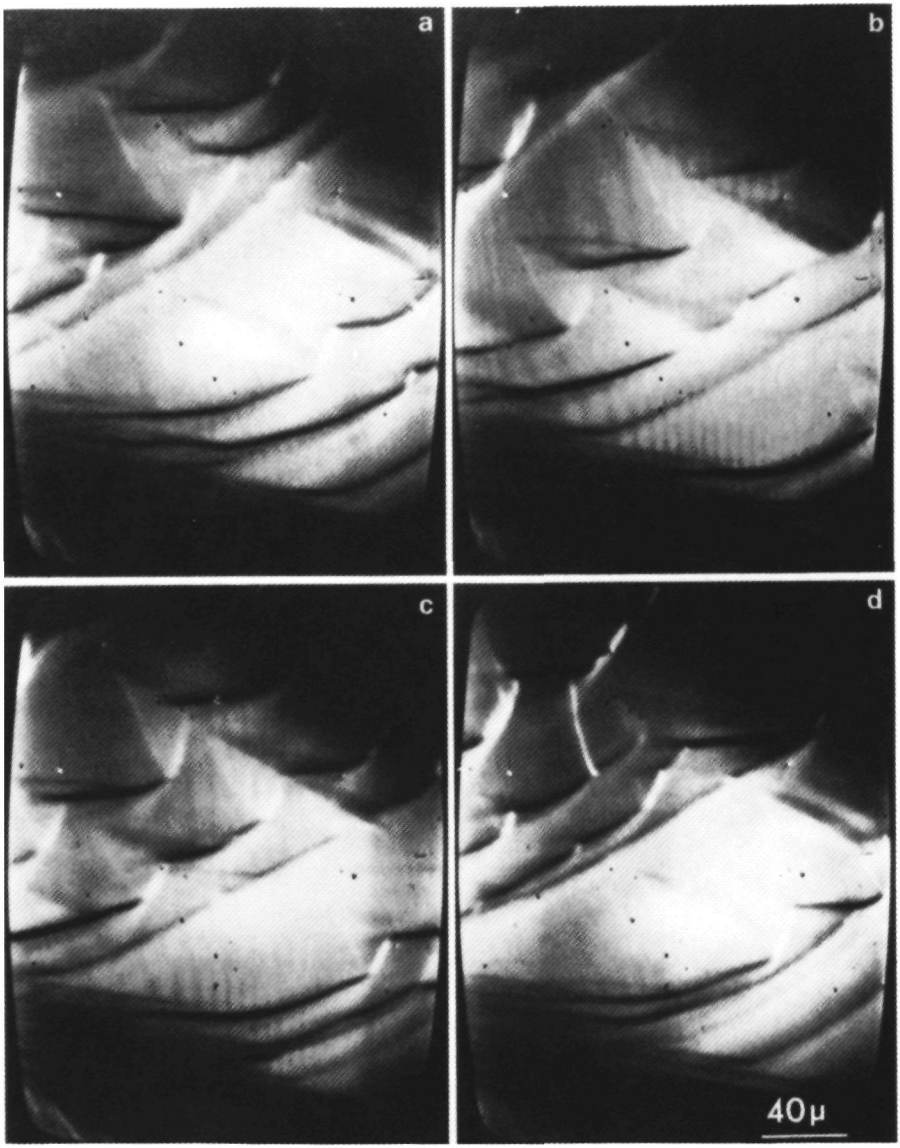

Fig. 2. Group of shallow growth hillocks on {100} periodically overgrown by passing macro-steps running from the lower right to the upper left corner: (a) $t = 0$ s; (b) $t = 2$ s; (c) $t = 3$ s; (b) $t = 4$ s (in situ oblique illumination).

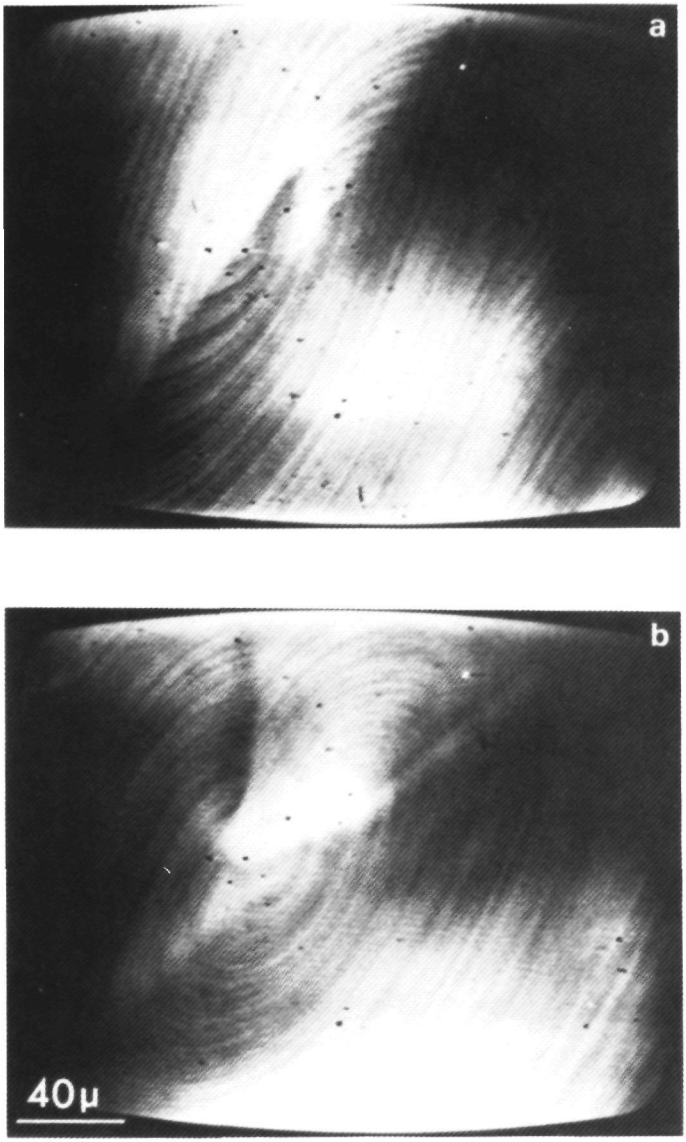

Fig. 3. Difference in spiral shape on the {100} surfaces of crystals grown in clean and contaminated solutions: (a) two pointed elliptical spirals growing in a clean solution; (b) the same spirals after addition of Cr^{3+} (in situ oblique illumination).

running along the edge with {101} are retarded This can be understood from the fact that in general volume diffusion is facilitated at crystal edges [11] However, the pyramidal faces of KDP grow much faster than the {100} faces This depletes the diffusion layer of {100} near the edge with {101} and explains the observed retardation

Secondly, kinematic waves [12] could be detected We saw large bunches absorbing and emitting small steps, which reflects the difference between individual step velocity and the so-called kinematic-wave velocity Normally these kinds of step patterns are described in terms of interacting surface diffusion fields However, volume diffusion can give rise to the same effects, only the interaction distance between the steps is much larger As we actually observe the retardation of small steps near large bunches, we think that the formation of kinematic waves arises from an overlap between volume diffusion fields

3 2 Growth hillock shape and Cr^{3+} addition

So far, we have not commented on the shape of the small hillocks shown in fig 2 The two-fold symmetry axis of this pointed ellipsoid agrees with the two-dimensional point group symmetry given [13] for the {100} faces of structures with a $\bar{4}2$ m three-dimensional point group symmetry Strangely enough this shape resembles the one found by Torgeson and Jackson (fig 5 in ref [5]) on ADP after Cr^{3+} impurity addition, though Davey and Mullin [3] observed only pure elliptical hillocks in normal as well as in impure solutions However, it must be noticed that these observations on ADP refer to very high steps in the order of μm The step heights we observed range from 80 to 1000 Å

Presently the relation between the hillock shape and the pH, impurity content and the supersaturation are being investigated As a first result we found that upon impurity addition (Cr^{3+}) at high supersaturation the pointed spiral hills are transformed into smooth ellipsoids as shown in figs 3a and 3b The step velocity does not change very much upon impurity addition but the hillocks seem to become more flat, which implies a reduction of the overall growth rate The flattening of the hillocks suggests an increase in edge free energy, γ, because for spiral growth the step spacing increases with increasing γ [14] The effect of impurity on γ is confirmed by the observation [15] that three-dimensional nucleation is inhibited in the presence of three-valent ionic impurities

In conventional impurity adsorption models [10,16], the edge free energy is usually assumed to be reduced However, in the case of KDP it is known that large quantities of metal ions [17] enter the lattice at K^+ positions [18] Now, steps in which M^{3+} ions are incorporated will have a higher edge free energy, as the broken bond energy [19] for each M^{3+} ion is three times higher than for a K^+ ion As we find a considerable increase in γ, this indicates that the density of metal ions at the step must be rather high

4. Growth patterns on {100} faces at low supersaturation

In previous works [20–22] it has been found that at low supersaturation (up to 5%) the growth velocity of the {100} face is zero This effect, the occurrence of a dead area, has been interpreted as being due to a two-dimensional nucleation barrier [20,21] However, also the adsorption of impurities could cause such an effect The latter mechanism is corroborated by our in situ observation that advancing spiral steps become blocked when we lower the supersaturation to about 2% The investigation discussed in this section concentrates on this region of supersaturation where the steps are seen to become inhibited

Decreasing the supersaturation from the fast growth regime to the inhibition point we generally observe an increase of the step spacing of the growth hillock Also very low steps ($\sim$ 100 Å) can now be seen Furthermore, the shape of the growth centres changes from pointed ellipsoids to rounded ellipses and steps become more irregularly shaped (fig 4)

It can be noticed that the orientational velocity dependence of the steps has diminished somewhat A height dependence of the step velocity still exists, though inverse as compared to the situation at high supersaturation Now, high steps generally move faster than lower ones Sometimes both high

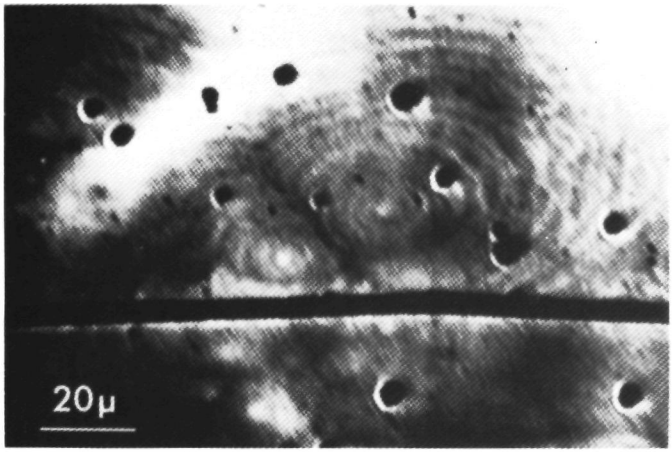

Fig. 4. Low (< 100 A), rounded steps at the critical supersaturation where growth just starts (in situ DICM).

and low steps are or become blocked, whereas others still move. In several cases it is observed that unblocking of steps occurs, when fresh steps overwhelm blocked ones. Similar phenomena were encountered in a previous study on potassium hydrogen phthalate [7,23].

These peculiar effects strongly point to the occurrence of time dependent impurity adsorption on the crystal surface. The nature of the impurity is still unclear. Addition of Cr^{3+} ions gives rise to the same effects and increases the dead area. However, other impurities might be involved as well. The time dependence of the impurity adsorption can be deduced from the observation that on a given surface area moving and blocked steps exists simultaneously. Whether a step moves or not depends on the previous history of a specific surface area and step front. This time dependence suggests that the impurity concentration in the liquid should be very low.

An impurity adsorption mechanism which predicts a dead area is the one given by Cabrera and Vermilyea [24]. In this model the surface is covered by a lattice of firmly attached impurities. Steps have to squeeze through and if the distance between the impurities is less than $2\rho_c$ (ρ_c being the critical radius of a two-dimensional nucleus) the steps are blocked. Since ρ_c is inversely proportional to the supersaturation this model predicts a supersaturation range where growth is inhibited. Secondly, the impurity action is essentially isotropic, which agrees with the observed reduction of anisotropy in the spiral shape. The irregular step pattern could result from partially blocked steps due to an inhomogeneous impurity distribution on the surface.

On the basis of averaged literature values for the surface free energy $\gamma'_{av} = 13 \pm 2.10^{-3}$ J/m^2 [25,26] the density of adsorbed impurities necessary to block the step advancement can be estimated from [14]:

$$\rho_c = \gamma' \Omega / \sigma_c RT.$$

Here Ω denotes the molar volume and σ_c the critical relative supersaturation necessary for step growth. For simplicity we have assumed in this formula a Kossel approximation where the edge free energy is equivalent to the surface free energy. For $\sigma_c = 2\%$ we find for the critical radius: $\rho_c = 120$ Å. This implies that an average surface coverages of about 1 in every 2000 growth units is enough to block step advancement (the length of one growth

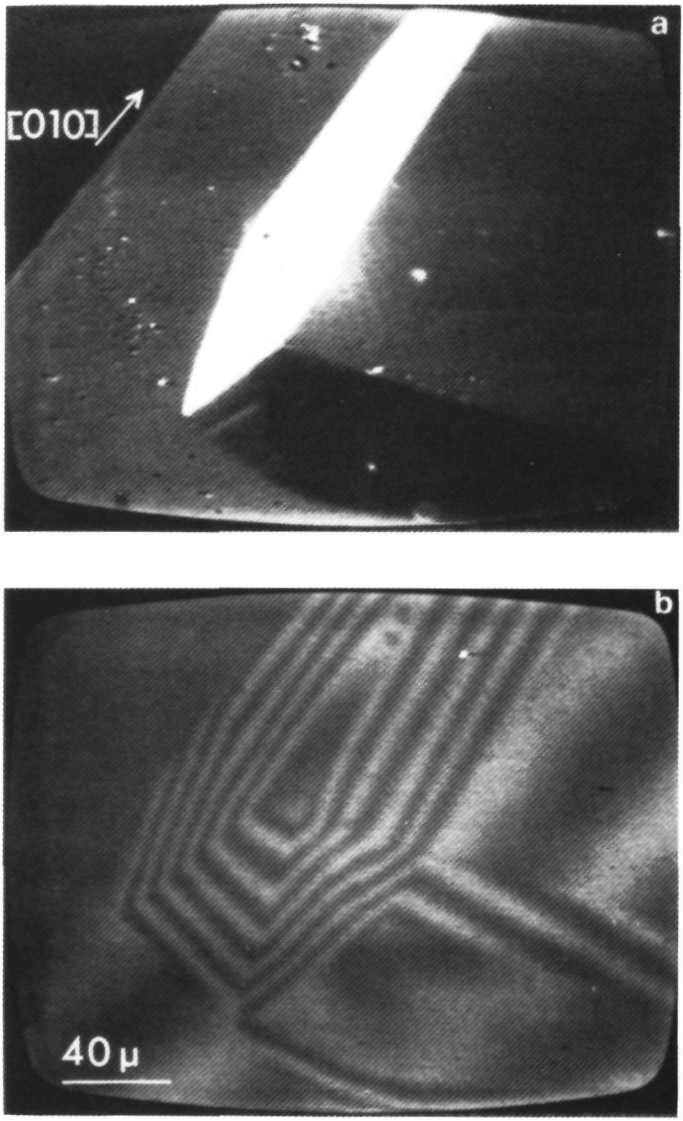

Fig. 5. In situ observation and measurement of very low steps on {101} KDP: (a) triangular growth hillock showing low steps at the largest of its side faces (DICM); (b) two-beam interferogram of (a). From this micrograph the height of the lower steps is determined to be 80 ± 20 Å ($\lambda = 5460$ Å and the refractive index of the solution $n \simeq 1.36$).'

unit being 5 Å). This is much larger than the ratio between the number of M^{3+} and solute ions in the liquid phase, which is at most $3:10^5$ and $3:10^7$ for normal and suprapur solutions, respectively. Still, as Belouet [27] found for three-valent metal ions very high segregation coefficients ($K \simeq 20$) at low supersaturation, these metal ions could be the species responsible for the blocking process. Currently work is in progress to examine more in detail the relation between M^{3+} impurity content and step movement [28].

5. Growth patterns on {101} faces

The present in-situ observation of the {101} surfaces has been concentrated mainly on the morphology of hillocks and the step patterns originating from their centres. A previous ex-situ study of {101} KDP [2] has already shown that the hillocks occurring on these faces are related to dislocations which generate the spiral steps.

An in-situ micrograph of such a triangular growth hillock is given in fig. 5a. On this hillock on the side face with the smallest inclination low steps can be detected. From the inclination of the steeper side face of the hillock, measured by two-beam interferometry (fig. 5b), the height of the low steps was deduced to be 80 ± 20 Å. This demonstrates the capability of the present in-situ method to detect very low steps.

From the literature it is known that the growth rate of {101} is several times higher than that of {100} [21]. The occurrence of a dead area at low supersaturation has never been reported. This is in accordance with the fact that during our in-situ studies on {101} we could not find a measurable range of supersaturation without step movement. Upon lowering the supersaturation from positive to negative values the steps simply reverse their advancement direction. Not even a change in the growth hillock morphology could be observed. Only after the addition of Cr^{3+} impurities the hillocks change and become more isotropic. As can be inferred from fig. 6 the $[\bar{1}\bar{1}1]$ and $[\bar{1}11]$ steps become more or less equivalent. The advancement rate ratio between steps parallel to [010] and those parallel to $[\bar{1}11]$ is reduced from 1 : 6 [2] to 1 : 2. Further we observed that the steps are more rounded.

The absence of a dead area, also after impurity (Cr^{3+}) addition, suggests that on {101} the Cabrera–Vermilyea description of impurity adsorption is not valid. As it has been found [27] that

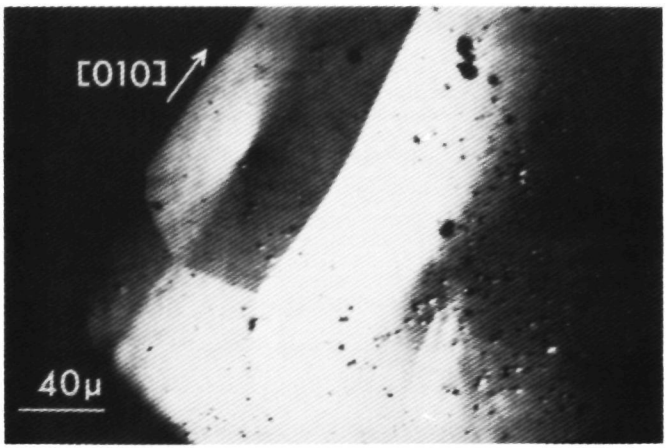

Fig. 6. Elliptically shaped growth hillocks on {101} faces formed after addition of Cr^{3+} ($\simeq 100$ ppm) impurity (in-situ DICM).

impurities hardly incorporate in the pyramidal growth sector, we assume that on {101} the lifetime of adsorbed impurities is very short For a more detailed description of the impurity adsorption on these faces quantitative measurements could give interesting results

6 Conclusion

From in situ microscopic observations of the {100} and {101} faces of KH_2PO_4 crystals it is found that crystal growth is a complicated, non-stationary process in which impurities play an important role

In agreement with recent Schlieren observations of stagnant solutions [29] it is found that on [100] KDP volume diffusion plays a minor, but significant role in the growth process Whether volume diffusion is followed by a direct kink integration or by a surface diffusion step is not quite clear yet

Within the supersaturation range ($0 < \sigma < 0.02$) the steps on {100} are completely blocked Comparison with growth phenomena in Cr^{3+} contaminated solutions lead to the conclusion that at low supersaturation an impurity adsorption after the mechanism of Cabrera and Vermilyea is active

For the occurrence of tapering of the {100} faces a blocking of steps on these faces seems to be required [30] We conclude that this inhibition is caused by impurity adsorption which is largely controlled by the supersaturation This gives a better understanding of Loiacono's [1] observation that tapering is the result of low supersaturation

On {101} no impurity effects were observed in normal, p a , solutions Cr^{3+} contaminated solutions showed a different step behaviour as compared to {100} Apparently an other impurity mechanism is active here, involving only loosely bonded impurities

The quality of the in-situ method is demonstrated by the observation of 80 Å steps

Generally we conclude that in-situ observation is a powerful tool for the investigation of growth mechanisms and impurity action

Acknowledgements

The authors are indebted to Prof Dr P Bennema and Dr J P van der Eerden for fruitful discussions and critical reading of the manuscript Also we thank J W van Kessel for technical assistance and F Polman for experimental contributions B Dam acknowledges financial support from the Netherlands Foundation for Pure Research (ZWO/SON)

References

[1] G M Loiacono J J Zola and G Kostecky J Crystal Growth 58 (1982) 495
[2] W J P van Enckevort R Janssen van Rosmalen and W H van der Linden J Crystal Growth 49 (1980) 502
[3] R J Davey and J W Mullin J Crystal Growth 26 (1974) 45
[4] R J Davey and J W Mullin J Crystal Growth 29 (1975) 45
[5] J L Torgeson and R W Jackson Science 148 (1965) 952
[6] K Tsukamoto J Crystal Growth 61 (1983) 199
[7] L A M J Jetten B van der Hoek and W J P van Enckevort J Crystal Growth 62 (1983) 603
[8] P Hartman Acta Cryst 9 (1956) 721
[9] P Bennema J Crystal Growth 5 (1969) 29
[10] A A Chernov Soviet Phys Usp 4 (1961) 116
[11] A Seeger Phil Mag 44 (1953) 1
[12] F C Frank in Growth and Perfection of Crystals Eds R H Doremus B W Roberts and D Turnbull (Wiley New York 1958) p 411
[13] International Tables for X Ray Crystallography Vol 1 Eds N F M Henry and K Lonsdale (Kynoch Birmingham 1969) p 40
[14] P Bennema and G H Gilmer in Crystal Growth An Introduction Ed P Hartman (North Holland Amsterdam 1973) p 263
[15] H Jaffe and R F Kjellgren Disc Faraday Soc 5 (1949) 319
[16] A A Chernov J Crystal Growth 42 (1977) 55
[17] C Belouet M Monnier and J C Verplanke J Crystal Growth 29 (1975) 109
[18] K Tsuchida and R Abe J Phys Soc Japan 46 (1979) 1225
[19] J P van der Eerden Dissertation University of Nijmegen (1979)
[20] J W Mullin A Amatavivadhana and M Chakraborty J Appl Chem 20 (1970) 153
[21] J Garside and R I Ristić J Crystal Growth 61 (1983) 215
[22] R Janssen-van Rosmalen Dissertation Technical University Delft (1977)

[23] L A M J Jetten, J C G Gardeniers and P Bennema, to be published
[24] N Cabrera and D A Vermilyea, in Growth and Perfection of Crystals, Eds R H Doremus, B W Roberts and D Turnbull (Wiley, New York, 1958) p 393
[25] O Söhnel, J Garside and S J Jančić, J Crystal Growth 39 (1977) 307
[26] O Söhnel, Kristall Tech 13 (1978) 1163
[27] C Belouet, E Dunia and J F Petroff, J Crystal Growth 23 (1974) 243
[28] B Dam, E Polman and W J P van Enckevort, in Industrial Crystallization 84, Eds S J Jančić and E J de Jong (North-Holland, Amsterdam, 1984) p 97
[29] W J P van Enckevort and M Matuchova, to be published
[30] B Dam and W J P van Enckevort, to be published

Industrial Crystallization 84, edited by S.J. Jančić and E.J de Jong
Elsevier Science Publishers B.V., Amsterdam, 1984 — Printed in The Netherlands

IN SITU OBSERVATION OF SURFACE PHENOMENA ON {100} KDP RELATED TO GROWTH KINETICS AND IMPURITY ACTION

B. Dam, E. Polman and W.J.P. van Enckevort

RIM, Laboratory of Solid State Chemistry,
Faculty of Science, Catholic University,
Toernooiveld, NL-6525 ED Nijmegen, The Netherlands.

SUMMARY

In situ observation of growth steps on {100} KH_2PO_4 by optical microscopy gives direct evidence for the role of M^{3+}-ions as growth inhibitors. These ions are found to be able to block growth completely below a certain critical supersaturation. Moreover they seem to be responsible for the formation of large, steep step bunches, which in turn produce inclusions parallel to {100}.

Additives such as EDTA, KCl and K_3PO_4 are found to be able to reduce the impurity action to a large extent.

The in situ observation of step patterns on growing or dissolving crystals proves to be a fast and direct method to determine the influence of impurities and additives relevant to the crystal growth proces.

1. INTRODUCTION

The isomorphous salts ammonium dihydrogen phosphate (ADP) and potassium dihydrogen phosphate (KDP) are two of the oldest crystals grown in large sizes for industrial purposes. Large numbers of ADP crystals have been produced because of its piezo-electrical properties [1]. Both crystals are well known model compounds to investigate the fundamental problems associated with crystallization processes.

Presently KDP is often used as a frequency doubler [2] in laser techniques. This application requires the growth of large, high quality single crystals. A bottleneck for the production of these crystals lies in the growth of the {100}-faces. These prismatic faces grow very slowly and are very sensitive to impurities and inclusion formation. Belouet et al. [3] were able to show that the segregation coefficient of Fe^{3+} and Cr^{3+}-ions in the prismatic sectors increases to K=20 at low supersaturation. From growth versus supersaturation measurements Mullin et al.[4] deduced that a certain minimum supersaturation is required for growth to take place on the {100} faces of ADP. Subsequently it was stated in Davey's in situ study on the kinetics of high macrosteps (in the order of microns) on {100} ADP [5], that below a certain supersaturation no macrosteps can be observed. These two observations pose an intriguing problem to anyone interested in crystal growth mechanisms. The question whether growth is really blocked below a certain supersaturation can only be answered by looking in situ at the behaviour of very low steps.

Recently it has become possible to do so by in situ microscopy, either in the transmission [6] or in the reflection mode [7]. Here, we will present the results of our in situ investigations of the step growth on {100}-KDP, concentrating mainly on the behaviour at low supersaturation and on the effect of three-valent metal impurities.

2. EXPERIMENTAL

The {100} surfaces of growing KDP crystals were observed by differential interference contrast microscopy (DICM) and by oblique illumination, both in reflection mode. The image was recorded on tape by means of a video camera which was connected to an analogue contrast amplifier. For (DICM) this method was calibrated [8] to be able to observe in situ 80 Å steps on {101}-KDP. Step heights of the same order of magnitude can be revealed by oblique illumination. Most experiments reported here were obtained using the latter microscopical method.

The crystal under observation was placed in a thermostated growth cell containing a stagnant solution.

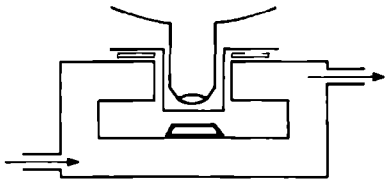

Fig.1. The thermostated growth cell

Saturated solutions were prepared at 25 °C from demi-water and Merck pro analyse (p.a.) or suprapur chemicals, in which the iron content is given as 3.10^{-3} and 3.10^{-5} mol % respectively (here mol % means the molecular % impurity relative to KDP solute).

The supersaturation region where growth is blocked was determined by the following procedure. First a small KDP crystal is placed in the slightly supersaturated solution of the growth cell. When the step growth is found to be stabilized, the temperature is decreased until all steps on the surface of observation are blocked, this temperature is called T(growth). The solution is then rapidly heated until etchpits are seen to be formed and cooled again until the dissolution steps stop advancing. This temperature corresponds to the saturation temperature T(sat), as it was found to be equal to T(sat) and T(growth) of the {101}-faces, where no blocking of steps can be detected. The difference between T(sat) and T(growth), ΔT, is the so-called 'dead area'; a supersaturation region where no step growth is observed.

3. GENERAL FEATURES

In a previous study [8] it was found that crystal growth is a highly non-stationary process even if external growth parameters are kept constant. Comparing the surface morphology of {100} and {101}-KDP, remarkable high and steep bunches on {100} are found. These bunches, which reflect instabilities in the growth process, are the main cause for inclusion formation [7,9]. *Therefore the {100}-faces are* particularly sensitive to inclusion formation.

Further the in situ observations gave positive evidence for a growth mechanism where volume diffusion of the growth unit is followed by direct kink integration in the step. Though until now these two steps are sufficient to explain all observed phenomena, it is not yet clear whether other factors (such as surface diffusion) definitely can be excluded from playing a role in the growth process. In order to study the growth mechanism in more detail, it is important to distinguish the effects caused by impurity adsorption. This is by no means trivial in the case of {100}-KDP, as in p.a. solutions impurities appeared to play an important role at low supersaturation. Impurity effects are observed when we reduce the supersaturation to about 1°C ($\sigma=\Delta c/c=1.5\%$), while growing in normal (p.a. Merck) solutions. The movement of the steps becomes very irregular: some are blocked, while others move fast over the same surface area in the same direction.

Upon further reduction of the supersaturation all steps become blocked and a supersaturation regime without growth (a dead area) is found [8].

As three-valent metal ions such as Cr^{3+} or Fe^{3+} are quite notorious as growth inhibitors on {100}-KDP [10], we think that these ions also play an important role in the normal crystal growth process, even if one uses p.a. chemicals.

The effect of adding these ions at high supersaturation is seen by a change in morphology of the growth hillocks. From pointed ellipsoids they transform into smooth ellipsoids.

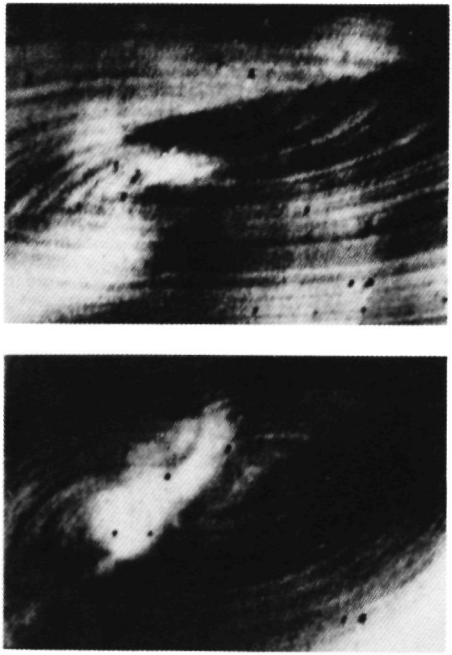

Fig.2a,b. Difference in spiral shape on {100} when grown in clean (a) or in contaminated solutions (b) at $\sigma=\Delta c/c=7\%$ (oblique illumination, 50x).

Therefore the nature of the impurities and the mechanism of their role as growth inhibitors were further investigated. Attention is also payed to possibilities to eliminate the role of these impurities.

4. THE DEAD AREA ON {100} KDP

The only impurity adsorption model predicting a critical supersaturation below which the advancement of steps is blocked, is the one given by Cabrera and Vermileya [11]. In this model the surface is covered by a 'lattice' of immobile impurities which act as pinning points for the advancing steps. The overall step movement is blocked when the average distance between the impurities is less than two times the radius of the two-dimensional critical nucleus. The impurity action is essentially isotropic, thus more rounded step patterns are to be expected after impurity addition.

As stated before, in p.a. solutions the effect of impurity adsorption can be observed at low supersaturation. By measuring the step advancement rate as a function of the supersaturation we found a dead area, ΔT, of 0.9 $\pm$0.2°C. The use of bi-dest instead of demi water did not change this result.

In order to find a relation between the impurity content of the solution and the critical supersaturation needed for step growth, controlled quantities of Cr^{3+}-ions were added to the solution. It turned out that small quantities of Cr^{3+} (0.05 mol % Cr^{3+} relative to KDP solute) cause an increase of the dead area to at least $\Delta T=3$°C. However, these experiments were far from reproduceable, as sometimes a ΔT of 8°C was found. Both the time the crystal was allowed to grow and the crystal itself appeared to influence the value of the critical supersaturation. Apparantly it is difficult to reach a steady state in this case.

A reduction of ΔT to 0°C is possible when one uses Merck suprapur KDP. Also a drastic change in the surface morphology can observed then. Whereas in normal

solutions often steep bunches are found, in suprapur solutions bunches are reduced in height and steepness. This implies that the probability for inclusion formation has decreased too. As the main difference between suprapur and p.a KDP is found in their iron content this again shows the possible role of iron as a growth inhibitor.

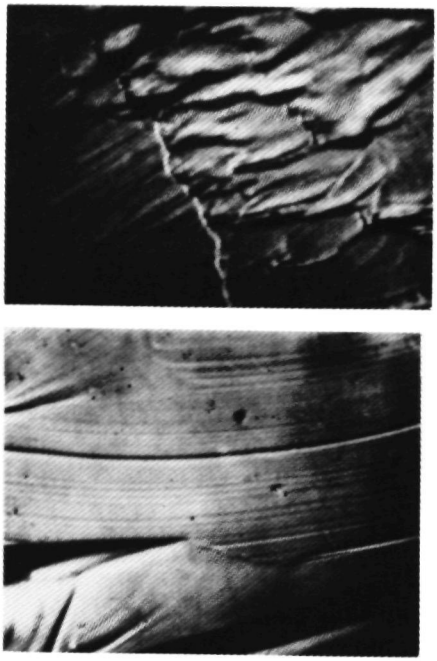

Fig.3. a) Crystal surface after Fe^{3+} addition at $\sigma \approx 7\%$); steps are completely blocked. b) The surface of the same crystal after subsequent EDTA addition. The step advancement is relatively unperturbed now (oblique illumination 25x).

As the use of suprapur chemicals will be not feasable for commercial use, we tried to reduce the activity of the M^{3+}-ions in another way. Two methods were indeed found. First the effect of the addition of trace amounts of EDTA (ethylene diamino-tetra-acetic acid), which is known as a strongly complexing reagent for M^{3+}-ions was investigated. It turned out that roughly 3.10^{-3} mol % EDTA is enough to reduce the dead area of crystals growing in a normal KDP solution to $\Delta T = 0°C$. The step bunches again loose a lot in steepness. This can be observed best by adding EDTA to a solution polluted with M^{3+}. A crystal surface completely covered by steep blocked bunches is regenerated in this way and step growth proceeds as in clean solutions (fig.3).

A second possibility to reduce the effect of M^{3+}-ions on step growth was found in the addition of extra potassium ions to the solution. This has been done in the form of KOH, K_3PO_4 and KCl addition. Addition of 7 mol % K_3PO_4 reduces the dead area to $\Delta T = 0.1°C$ whereas addition of 15 mol % KOH results in a decrease to $\Delta T = 0.6°C$. However in both cases the solubility and the pH increase, which hampers the interpretation of the observed effects. Solubility and pH are not seriously affected when we add KCl to the KDP solution. In order to decrease ΔT to 0°C at least 25 mol % of KCl is needed. In all three above mentioned cases the bunches remain rather steep, hence we suspect some action of impurities to be still present.

Finally it must be noted that paraffine, which is often used to cover growth solutions to prevent their evaporation, was found to increase the ΔT of suprapur solutions to 0.5°C. On the other hand mixing the KDP solution with very pure paraffine (Merck, Uvasol) did not result in any impurity effect. This again shows that great care should be taken to eliminate all possible impurity sources.

5.SOME CONSIDERATIONS REGARDING THE IMPURITY MODEL

As a starting point we have assumed that the Cabrera Vermileya mechanism is applicable to describe the observed effects of M^{3+}-impurities. In this model the impurities are adsorbed on the ledges between the steps and the adsorbed species are considered

to be immobile.

Indeed we think that adsorption at the ledge is the most plausible mechanism. Adsorption at kink positions would increase the polygonisation of the steps and rather the reverse is observed. Secondly, a step adsorption mechanism is not likely to give rise to the instable pattern of blocked and moving bunches. Careful observation of these bunches also showed that they are most likely to be retarded when the distance to next bunch moving in front of it is large. It is clear that the impurity adsorbtion between the steps can not be considered as a stationary process but is rather time dependent.

Regarding the nature of the adsorbed impurity a few remarks have to be made. In recent ESR studies it was found that Cr^{3+}-ions occupy both interstitial and K^+-sites in the KDP lattice [12]. For Fe^{3+} it was even possible to infer from the D-tensor that this substitutionally incorporated ion is surrounded by two H^+-vacancies [13]. Therefore any impurity model has to deal with at least the following three processes.

1) Adsorption of M^{3+} at the ledge at K^+-sites. This process will be competitive with K^+ adsorption, hence it will depend on the K^+ concentration.

2) Two $H_2PO_4^-$-groups have to be dehydrogenated. Either they are neighbouring groups present in the surface layer or dehydrogenation takes place in the solution and the HPO_4^{--} have to adsorb next to the M^{3+}-ion. In both cases this dehydrogenation will be favoured by a high solution pH, which could explain the observed increase in growth rate on {100} at higher pH's [4].

3) Incorporation of the adsorbed three-valent metal impurity in an advancing growth layer.

Considering these three steps, it is clear that impurity adsorption depends on many factors such as, supersaturation, K^+-concentration, impurity concentration, step velocity, step spacing, pH, etc. Hence it will be difficult to reach an equilibrium or a steady state in the process of impurity adsorption, especially as we have seen that crystal growth involves large fluctuations of these parameters.

Only at a relatively high or low supersaturation a steady state in impurity action can be expected. In the first case the impurities hardly get the chance to adsorb and are quickly overgrown by advancing fresh layers, whereas in the latter case step growth is completely blocked. At intermediate supersaturations the growth process will be very sensitive to any change of the mentioned parameters, especially because small variations tend to accumulate. For instance a local increase in the step spacing enhances the concentration of adsorbed impurities, which in turn reduces the step velocity. In this way a bunch of steps is created resulting in an even larger step spacing, etc.

The sensitivity of the {100}-orientation to inclusion formation for a large range of supersaturations becomes understandable in this way. The only method to prevent it seems to be to reduce the effect of impurities as good as possible.

6. CONCLUSION

In situ observation of step patterns on growing crystal surfaces prooves to be a powerful method to determine the effects of impurity adsorbtion on crystal growth.

Due to the presence of M^{3+}-impurities growth on {100}-KDP was found to become blocked below a certain supersaturation. The same impurities cause the formation of steep bunches and make the crystal growth process on the {100}-faces very sensitive to any change of the growth parameters. This promotes the formation of the commonly encountered inclusions parallel to these faces.

The effects of M^{3+} impurity adsorbtion can be circumvented by using suprapur solute material or by adding EDTA. Also the addition of KCl, KOH or K_3PO_4 improves the quality of the crystal surface. The

exact relation between these additives and the quality of large single crystals is presently being investigated.

The presently existing impurity models seem to be inadequate to account for all observed effects. Though the Cabrera-Vermileya model explains the dead area, a more sophiticated model should deal more explicitely with the mutual interaction between growth and adsorbtion processes.

ACKNOWLEDGEMENTS

We wish to thank Prof. Dr. P. Bennema and Prof. Dr. Wang Yaoshui for stimulating discussions. B. Dam acknowledges the financial support of the Netherlands Foundation for Pure Research (ZWO/SON).

REFERENCES

1) H. Jaffe and R.F. Kjellgren, Disc. Faraday Soc. 5 (1949) 319

2) G.M. Loiacono, J.J. Zola and G. Kostecky, J. Crystal Growth 62 (1983) 545

3) C. Belouet, E. Dunia and J.F. Petroff, J. Crystal Growth 23 (1974) 243

4) J.W. Mullin, A. Amatavivadhana and M. Chakraborty, J. Appl. Chem. 20

5) R.J. Davey and J.W. Mullin, J. Crystal Growth 29 (1975) 45

6) K. Tsukamoto, J. Crystal Growth 61 (1983) 199

7) L.A.M.J. Jetten, B. van der Hoek and W.J.P. van Enckevort, J. Crystal Growth 62 (1983) 603

8) B. Dam and W.J.P. van Enckevort, J. Crystal Growth to be published

9) R. Rodriguez, M. Aguilo and J. Tejada, J. Crystal Growth 47 (1979) 518

10) R.J. Davey and J.W Mullin, J. Crystal Growth 26 (1974) 45

11) N. Cabrera and D.A. Vermilyea, in: Growth and Perfection of Crystals, Eds. R.H. Doremus, B.W. Roberts and D. Turnbull (Wiley, New York, 1958) p.393

12) T. Kobayashi, J. Phys. Soc. Japan 35 (1973)

13) K. Tsuchida and R. Abe, J. Phys. Soc. Japan 46 (1979) 1225

THE GROWTH SPIRAL MORPHOLOGY ON {100} KDP RELATED TO IMPURITY EFFECTS AND STEP KINETICS

J.W. Noor and B. Dam

RIM, Laboratory of Solid State Chemistry,
Faculty of Sciene, Catholic University of Nijmegen,
Toernooiveld, NL-6525 ED Nijmegen, The Netherlands.

Abstract

The growth spiral shape of the {100} KH_2PO_4 surfaces has been a classical example to elucidate the importance of surface diffusion in the crystal growth process. We will show that this hypothesis is undermined by the pointed growth spiral shape actually observed. On the basis of a recent PBC analysis we propose a step growth mechanism in which direct integration of the growth unit at the kink site plays an important role. In addition, by in-situ microscopy a sharp transition is observed to a circular growth spiral shape upon lowering the supersaturation. This transition is interpreted as an effect of impurity adsorption. The equilibrium chemical composition of the mother liquid itself instead of M^{3+}-ions or other foreign species, is deduced to be responsible for this effect.

I Introduction

At equilibrium, the crystal form is determined by the minimisation of the total surface free energy. In the same way the surface forms (e.g. 2D-nuclei) at equilibrium will be determined by a minimisation of the edge free energy. Beyond equilibrium, diffusion and incorporation of the growth unit will become important factors and will influence crystal form and surface morphology. Also impurities influence the morphology. They may alter both the specific surface free energies and the step free energies and may interfere with the growth process.

The effect of impurities on crystal form has a famous example in the phenomenon of tapering on KDP [1,2]. Correspondingly, also the surface morphology of KDP is of interest. In-situ techniques recently allowed for a detailed study of the influence of three-valent metal ions (M^{3+}, M=Fe, Cr) on the step kinetics on {100} and {101} KDP surfaces [3,4]. Summarizing the results of these experiments, it appeared that M^{3+}-ions are able to block step advancement below a certain critical supersaturation. Only on crystals grown in a very pure solution step growth can be observed up to the equilibrium temperature without any visible blocking effect. At high supersaturation the effect of impurity adsorption is negligeable. Furthermore, crystal growth is found to exhibit memory effects. Growth is dependent on the growth history of a certain surface. Impurities enhance these effects. Steps become strongly dependent on the behaviour of preceding steps, when impurity adsorption is time dependent with respect to the step advancement. Blocking may thus be simultaneously accompanied by relatively unperturbed growth on other parts of the crystal surface with a different growth history.

Recently a theory is being developed by Van der Eerden and Müller-Krumbhaar [5], which takes this time dependence of impurity adsorption explicitely into account, applying an extended Cabrera Vermileya [6] type model.

Here, we will concentrate on the spiral morphology on {100} KDP and analyse it with respect to possible growth mechanisms and impurity models. Two modes of the growth spiral shape are found, a pointed and a circular one. The first will be related to an anisotropic kink integration growth model whereas the latter is interpreted as an impurity effect.

II Spiral shape

II-1 General

There exists an analogy between surface morphology and crystal shape. For crystal faces growing below their roughening temperature surface integration and step integration are assumed to be important rate limiting steps in the growth process. In a PBC-approach the growth velocity of an {hkl} face then is taken proportional to the attachment energy on this {hkl}-orientation [7]. Correspondingly, the advancement rate of a [uvw]-step would be proportional to the energy of those PBC's, which are not parallel to this step. An essential difference between a step and a crystal surface is however that a step is always microscopically rough (T_R=0) whereas a crystal face is flat,

i.e. in principle it grows below its roughening temperature ($T<T_R$). Neglecting for the moment macro-step formation, the modern approach [8] stresses that the kink density at the step will determine the kinetics and the shape of the growth spiral.

II-2 The PBC's at the KDP {100}-surface

One of the oldest considerations on step kinetics and surface morphology originates from the PBC-analysis of KDP by Hartman [9]. For KDP-type crystals the {100} and {101} orientations were found to be F-faces. Using a point charge approximation Hartman [9] calculated for the attachment energies of these faces that $|E_{att}\{100\}|<|E_{att}\{101\}|$. Thus the resulting crystal form was predicted to be elongated along the z-axis, which is actually often the case. Comparing the strength of the [010] and the [001] PBC's it was concluded that the spiral form on (010) should be elongated along the z-axis also. Experimentally the spiral shape is found to be elongated rather along [010] and Hartman [9] concluded surface diffusion to be responsible for this effect; the anisotropy being related to the existence of double rows of positive and negative ions along [010].

However the charge distribution of the H_2PO_4-ion is not a point-like one. Aguilo and Woensdregt [10] computed for several possible charge distributions the corresponding equilibrium growth form. Their drawings show that {101} could well be the most important growth form. This suggests that also the [010] PBC could be stronger than [001]. From these calculations it is clear that the hypothesis of surface diffusion is not a necessary one.

Apart from being elongated, the spirals on {100} are also found to be pointed, fig.1. The overall 2-fold axis of the growth figure agrees with the two-dimensional point group symmetry for the {100}-faces of crystals with a $\bar{4}2m$ space group symmetry.

II-3 Pointed spiral shape

The pointed spiral shape resembles the one found by Torgeson and Jackson [11] on ADP ($NH_4H_2PO_4$) after Cr^{3+}-impurity addition. Later this form was generally found on ADP [12] and KDP [3,4] without any impurities being added.

We do not think the pointed shape generally to be an impurity effect. In the first place, the pointed hillocks are not only found at high supersaturation (when the incorporation of impurities is known to be small [13]), but also during growth in solutions prepared from Merck suprapur chemicals. Secondly, etch pits formed after

dissolution in undersaturated solutions or in pure water, show the same kind of shape as the hillocks. Even if we etch an {100}-plate cut from the pyramidal {101} sectors, which have a very small impurity content [13], the same pointed shape is achieved. Therefore we conclude that the pointed shape is not caused by some impurity effect but reflects the properties of the crystalline surface structure.

Hence special attention was paid to the spiral shape in our in-situ experiments. The most intriguing result was that upon lowering the supersaturation a sudden transition occurs to a circular spiral shape. In the next section we will describe this effect in more detail. On the basis of our observations, in section IV arguments will be supplied for the hypothesis that the pointed shape reflects the rate limiting importance of kink integration in the growth process, whereas the circular shape at low supersaturation reflects an impurity adsorption effect.

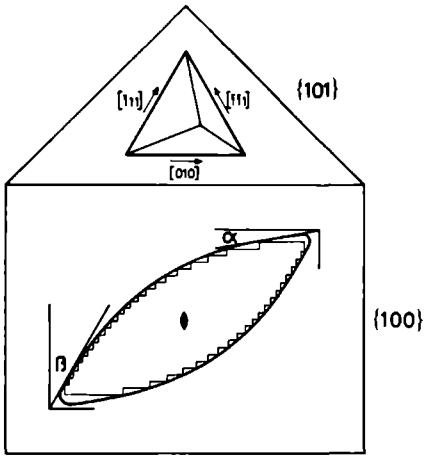

Fig.1
Sketch of the geometry of the growth figures on the {100} and {101} faces of KDP. On {100} the presupposed kink geometry is enscribed. The growth figures transform according to the crystal pointgroup symmetry.

III Observational

III-1 Experimental

The {100} surfaces of growing KDP crystals were observed by in-situ reflection microscopy using oblique illumination with closed aperture diaphragm [14]. The image was recorded on tape by means of a videocamera which was connected to an analogue contrast amplifier. With this method we are able to observe steps in the order of 100 Å [3].

The crystal under investigation was placed in a thermostated growth cell [4] containing a stagnant solution. Saturated solutions were prepared from demi-water and Merck pro analyse (p.a.) or suprapur chemicals in which the iron content is given as 3.10^{-3} mol-% and 3.10^{-5} mol-% respectively.

Most of the experiments were carried out at 35 °C. The saturation temperature and the relative supersaturation were calculated from the solubility-curve given by Janssen-van Rosmalen [15]: $c = a_o + a_1.T(°C)$ ($a_o = 0.1068$ and $a_1 = 0.3616.10^{-2}$). The supersaturation is defined as $\sigma = \Delta c/c_{eq}$. In this paper the supersaturation will be expressed in $\Delta T(°C)$. The relation between $\Delta T(°C)$ and σ is, for low supersaturations, a linear one, due to the linearity in the solubility-curve: $\Delta T = T_{eq} - T = 1$ °C corresponds to $\sigma = 1.6\%$.

For accurate temperature control a plastificated copper-constantane thermocouple was used, placed just above the crystal surface. In this way the temperature could be controlled within ± 0.03 °C.

III-2 General

The reflection mode enabled us to observe the influence of the supersaturation and the impurity-content on the behaviour of high and low steps on the prismatic {100} faces of KDP. Whereas Davey and Mullin [16] as well as Torgeson and Jackson [11] observed only very high steps in the order of µm, the step heights we observe range from 100 to 1000 Å. The spiral form on crystal surfaces in normal solutions with characteristic pH does not depend on the step height. Small hillocks consisting of very low steps have the same global structure as large hillocks consisting of large bunches.

A most peculiar aspect of the pointed spiral shape is the fact that the hillocks are not bounded by the only two PBC's given [9] for the (100) slice: [010] and [100]. The steps deviate from these PBC's by an angle α and β varying around 10 ° and 40 ° respectively. These angles are not constant, not even within one hillock (fig. 2).

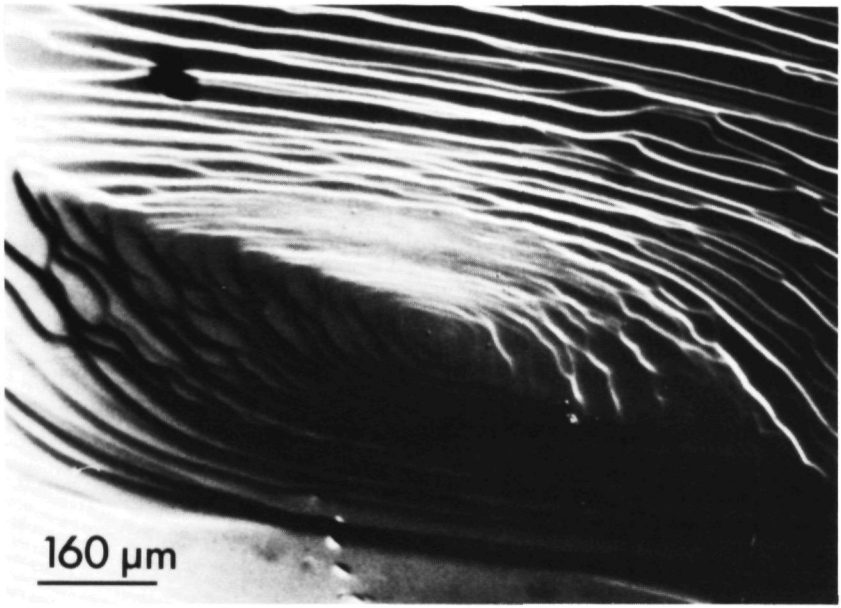

Fig.2
Growth spiral on {100}-KDP showing irregularly shaped bunches. Ex-situ differential interference contrast microscopy.

A (as we will see in section IV-1) related phenomenon is the behaviour of step perturbations. Steps moving approximately in the [001] direction, i.e. $\alpha \sim 0$, sometimes show perturbations which move fastly sideways to [010] or $[0\bar{1}0]$. We found the remarkable effect that the velocity of the perturbations moving in the [010] direction is different from the velocity of perturbations moving in the opposite $[0\bar{1}0]$ direction.

Upon lowering the supersaturation of a p.a. solution blocking of steps is observed. In p.a. solutions the supersaturation region where no visible step is observed anymore, the so-called dead area, is $\Delta T = 0.9 \pm 0.2$ °C. In suprapur solutions no blocking of steps could be detected, thus allowing for a study of the spiral morphology in the low supersaturation region.

III-3 Transition in growth spiral shape

In suprapur solutions upon lowering the supersaturation the shape of the growth spirals changes from pointed ellipsoids to circles. Careful in-situ observations revealed the following features of this change in spiral shape.

1)Upon lowering the supersaturation by increasing the solution temperature with a rate of about 0.02°C/min at a certain critical supersaturation the growth centre starts to emit circular steps. The transition is rather sudden. The overall step velocity of the rounded step is somewhat lower than the step velocity of the preceding pointed steps. Generally a small increase in the step spacing of the growth hillock is observed. The transition occurs mainly in the centre of the growth hillock. The advancing circular steps gradually cover the whole crystal surface. The other steps of the same spiral remain pointed, although sometimes also these pointed spiral steps become somewhat more circular. The transition process can not always be followed so easily. Steps may loose their coherency at the transition making it impossibe to follow any intermediate stages.

The above mentioned observations suggest that around the critical supersaturation at which the transition occurs, there are two possible growth modes: one with circular steps and a low step advancement and the other with pointed steps and a higher step advancement.

2)By decreasing the temperature the reverse transition is achieved. In this proces two stages can be distinguished. The first stage shows a loss of coherency in the rounded steps in the direction which will become the pointed direction of the growth spiral. Small parts of bunches seem to escape from the circular bunches and the spiral becomes partly pointed. The loss of coherence proceeds gradually to the centre of the growth spiral. In the second stage the growth centre itself emits pointed steps and the whole spiral becomes pointed again. Sometimes only the second stage is observed. Due to the higher step velocity of the pointed steps, in that case the pointed steps will overwhelm the rounded steps. In fig. 3 this kind of transition is shown.

3)An important aspect is the fact that a hysteresis is observed. The transition from a pointed ellipsoid to a circular one occurs at a higher critical temperature than the reverse transition. The difference in $\Delta T_{critical}$ is about 0.1 to 0.2 °C, where ΔT_{crit} is defined as $\Delta T_{crit} = T_{eq} - T_{crit}$. Even at very slow temperature changes this hysterese was observed, which makes it improbable that it is due to difficulties in reaching an equilibrium state.

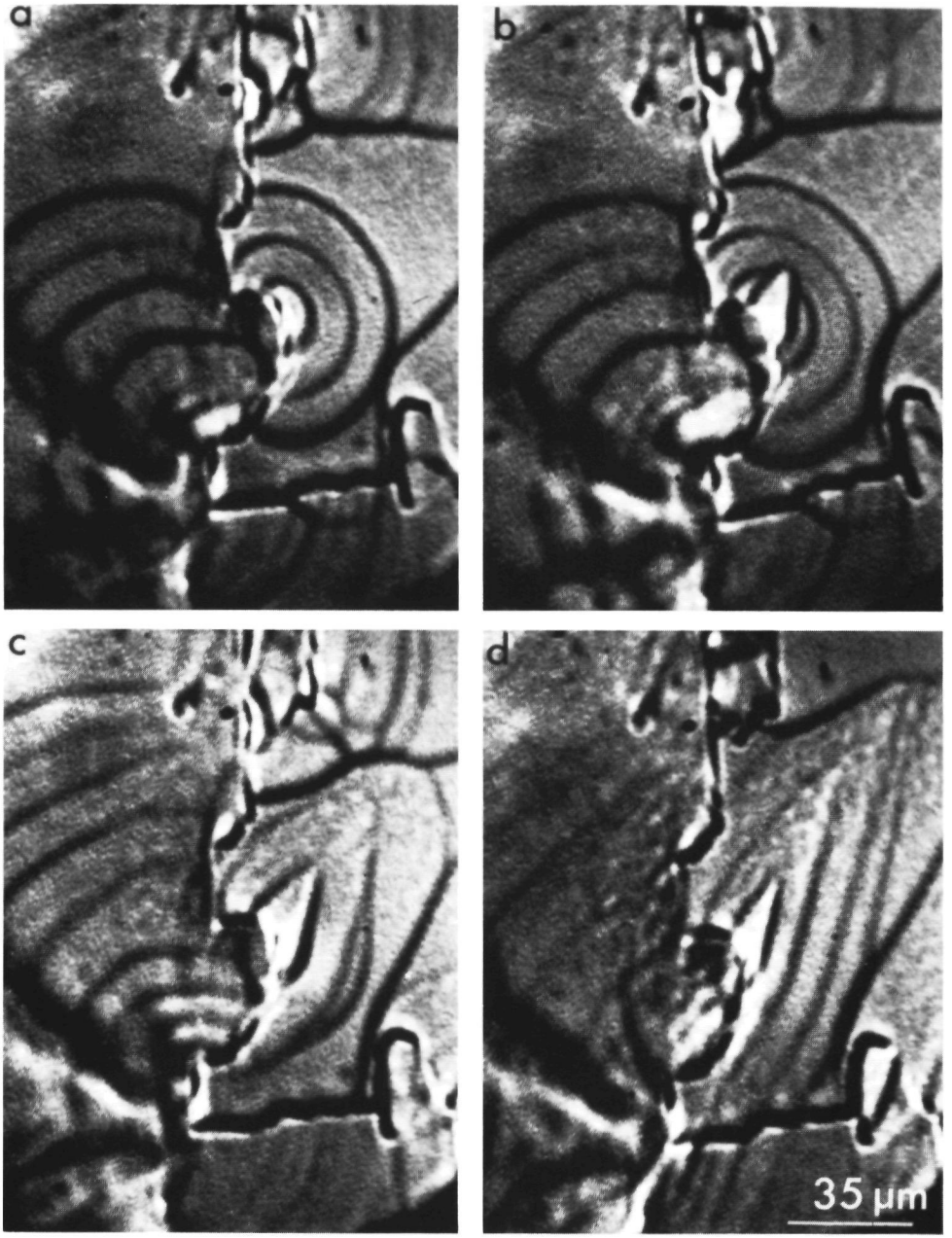

Fig.3
Sequence of the transition from a circular spiral shape a) to a pointed one d). Note, that the pointed steps have a higher advancement rate than the circular ones.

4)Apart from the small hysteresis, the critical temperature of one spiral is reproduceable. There is however a wide variation in ΔT_{crit} for different growth spirals on one crystal surface: 1 °C<ΔT_{crit}<3 °C. This variation could not be related to any step property such as step height or step spacing. A serious problem in determining ΔT_{crit} arises from the continuous competition between different growth centres. E.g. pointed growth spirals with a high step velocity easily overwhelm circular growth spirals, which have a lower step velocity.

Summarising, the retardation of steps, the hysteresis in the spiral shape transition and the observation of different growth modes suggest an impurity effect to be responsible for the transition to the circular spiral shape, despite the use of suprapur chemicals. To exclude the possibility that the small M^{3+}-content still present in these suprapur solutions is the cause for the transition in spiral shape, we added up to 10^{-4}-weight % Fe^{3+} relative to KDP solute to the solution. Although this concentration is already high enough to cause a blocking of step advancement before the equilibrium temperature is reached, no clear change in T_{crit} was measured. Of course many other species present in the mother phase may act as impurities as well. As the effect of mono-valent and two-valent cationic impurities is usually small compared to the three-valent ones (see e.g. Hottenhuis et al. [17]), we shortly tried the effect of an anionic impurity, H_2SO_4. Due to the KDP buffer action the pH remains constant upon addition of small quantities of acid and any effect of adding sulphuric acid can be savely attributed to the activity of the sulphate ions. Rather a large amount of H_2SO_4 was needed to observe any effect on the step behaviour. Only when adding the acid up to a concentration of 10^{-2} mol/litre the ΔT_{crit} was increased to 4.6°C.

IV Discusion

IV-1 The pointed growth spiral.

As explained in section II we believe the pointed spiral shape to be an effect not caused by impurities. As no other PBC's than [001] and [010] can be found in the (100) slice [9], we turn to the stability of kinks within one step along such a PBC.

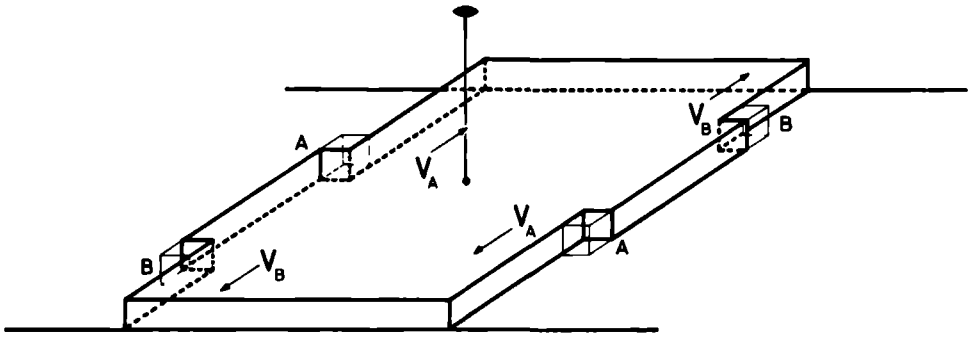

fig.4
Arrangement of kinks on the {100} surface of KDP. The electrostatic interaction of kink A is different from kink B as only a two-fold axis is present on the crystal surface. The advancement of kink A will thus be different from kink B as soon as kink intergration is one of the rate determining steps of the growth process.

As can be inferred from fig.4 it is clear that the symmetry in principle allows for two different bonding geometries in opposite kinks of each step. The bonding geometry of kink A is not symmetry related to the geometry of kink B. We propose then that an anisotropic integration of the growth units at these two kink positions is responsible for the pointed spiral shape. The anisotropy might be due to a difference in kink integration energy and/or a difference in the activation energy needed to enter the kink site. Anyhow the effective concentration of kinks A will be different from the concentration of kinks B. In this way the microscopic kink configuration as sketched in fig.1 results in the pointed spiral shape.

In principle, the anionic and cationic building units could behave in opposite fashions, thus canceling the anisotropy effect. However, recently Nielsen [18] concluded that for a whole series of electrolyte solutions (amongst it KDP) the dehydratation of the cation is much slower than that of the anion. This implies that the dehydration of

the cation will be the rate limiting step in the growth process. In that case also the kink integration will be limited by the cations and the avancement of kinks at a given step will depend entirely on the integration of the cationic building unit.

In fact what we propose is more or less analogeous to the difference in surface energies of opposite faces on non-polar crystals. Along the same line of thought we deduce that the 2-fold axis on {100}-KDP allows for a difference in edge free energy between directions deviating from <010> or <001> in the positive sense and those deviating in the negative sense.

Kinetically, the anisotropic kink integration effect is exactly what we observe on a large scale in the behaviour of perturbations in steps, moving at different velocities in opposite directions (see III-2). Such a macroscopic perturbation will consist of a giant number of kinks, and its velocity will depend on the velocity of the invidual kinks. Indeed the fast perturbations move towards the point of the growth spiral, taking the proper step advancement direction into account.

It would be interesting to compare the pointed spiral form with the equilibrium surface form to separate kinetical and thermodynamical effects. However at low supersaturations the influence of impurities is generally more pronounced. Near equilibrium we found the {100} growth spiral to become circular, which we do not think is the equilibrium growth form.

IV-2 The circular growth spiral

It was reported before [3] that at high supersaturation the pointed growth spirals become rounded somewhat upon M^{3+}-impurity addition. At low supersaturation we have now observed the sudden transition to a circular growth spiral, combined with a slowing down of the step velocity. Nevertheless this transition could not be related to the concentration of Fe^{3+}-impurities.

Still many features of the transition can be interpreted in an impurity adsorption model in which the adsorption is time dependent with respect to the step velocity [5]. The hysteresis in the transition reflects the non-linearity of the adsorption process. If a step is in a certain mode, i.e. suffers from impurity adsorption or not, it will stick to that mode. On one hand a critical supersaturation is necessary to break through the adsorbed layer, on the other hand once a step is in the high velocity mode, impurities will have less time to adsorb and low supersaturations can be achieved before impurities controll the step advancement. The different

critical supersaturation of spirals on the same crystal surface could origin from the difference in number of cooporating dislocations or from the size of the dislocation Burgers vectors, both factors inducing different step kinetics of the resulting growth spiral.

Excluding the M^{3+}-ions, the nature of the impurity responsible for the circular step behaviour remains an open question. Sulphate-ions were found to influence the transition temperature but these ions are of course not present in large quantities in KDP-solutions. Here, we want to mention the possible influence of the chemical composition of the mother phase itself. Apart from poly-phosphates usually present in highly concentrated phospate solutions, the two- and three-valent phosphate ions in equilibrium with $H_2PO_4^-$ could adsorb on $H_2PO_4^-$-sites as well, thus acting as impurity. The concentration of the two-valent phosphate ions (approximately 10^{-3} mol/litre) is only one order of magnitude lower than the concentration of sulphate-ions, which had a large effect on the transition temperature. The HPO_4^{2-} and PO_4^{3-} activity is expected to be less dramatic than that of the three-valent cations. Their hydration energy is lower and they will easily either desorb from the surface or gain one or two H^+-ions from the solution to be incorporated as a normal H_2PO_4-ion. However, as long as these two-valent anions are adsorbed on the surface they will hinder step advancement. Again, as in the case of the three-valent metal ions, at lower supersaturation the density of these ions will become higher and higher until they control the step advancement completely. Contrary to the case of adsorbed M^{3+}-ions the anion-impurities should have a residence time small enough to allow for a visible step advancement. As long as the impurity adsorption is isotropic, this step advancement will be isotropic too. The growth regime with circular growth spiral can thus be compared with the regime of step blockment in the case of M^{3+}-impurities. The difference being that the latter do not allow for any noticeable step advancement, when controlling step advancement. The anion impurities in our model control step advancement without blocking it. Assuming that the step blocking mechanism is the same whether cationic or anionic impurities are involved, this implies that the time needed for incorporation or desorption is considerably shorter for anionic than for the three-valent cationic impurities.

V Conclusion

The spiral shape on {100} KDP is a pointed ellipsoid, elongated along <010>. The elongation along <010> was initially proposed to be a surface diffusion effect [7]. We deduce however that kink integration of cations is one of the most important rate determining factors.

From symmetry considerations we conclude that the anisotropy of the kink integration is responsible for the fact that the spiral shape is a pointed one.

At low supersaturation a sharp transition occurs from the pointed growth spiral shape to a circular one. In-situ observation of the step kinetics showed that the circular spiral shape reflects an impurity adsorption effect. The retardation of circular steps with respect to the pointed ones, the hysteresis in the spiral shape and the existence of different growth modes at the same temperature, all suggest an impurity adsorption mechanism in which the adsorption is time dependent with respect to the step velocity, to be responsible for the observed change in growth spiral shape.

In this way the growth spiral shape reveals two growth mechanisms. In the circular growth regime the advancement of steps is controlled by the density of adsorbed impurities. The step advancement is isotropic as long as the density of adsorbed impurities is isotropic. Above a certain critical supersaturation a transition to another growth regime occurs in which kink integration is a rate limiting factor.

The nature of the impurity responsible for the isotropic step advancement is not quite clear yet. Foreign species, such as M^{3+}-ions, quite notorious as a retarding factor, are not responsible for the circular spiral shape. Possibly the mother liquid itself plays an important role in the growth process at low supersaturation. The HPO_4^{2-} ions may act as impurities causing the transformation to the circular growth spiral shape. Also other constituents of the mother phase such as poly-phosphates can not be excluded as growth inhibitors.

Acknowledgements

We would like to acknowledge experimental contributions of W.J.P. van Enckevort and E. Polman and critical reading of the manuscript by J. P. van der Eerden. Part of this work was financially supported by ZWO/SON.

References

1) H.J. Kolb and J.J. Comer, J. Am. Chem. Soc. 67 (1945) 894.

2) B. Dam, P. Bennema and W.J.P. van Enckevort, J. Crystal Growth (1986) to be published.

3) B. Dam and W.J.P. van Enckevort, J. Crystal Growth 69 (1984) 306.

4) B. Dam, E. Polman and W.J.P. van Enckevort in: Industrial Crystallization 84, Eds. S.J. Jancic and E.J. de Jong (North-Holland, Amsterdam, 1984) p97.

5) J.P. van der Eerden and H. Müller-Krumbhaar, Electrochimica Acta, to be published.

6) N. Cabrera and D.A. Vermilyea, in: Growth and Perfection of Crystals, Eds. R.H. Doremus, B.W. Roberts and D. Turnbull (Wiley, New York, 1958) p.393.

7) P. Hartman and P. Bennema, J. Crystal Growth 49 (1980) 145-156.

8) I. Sunagawa and P. Bennema, in: Preparation and Properties of Solid State Materials, Vol.7 (Dekker, New York, 1982) p.1.

9) P. Hartman, Acta Cryst. 9 (1956) 721.

10) M. Aguilo and C.F. Woensdregt, Abstracts of the VIIth International Conference on Crystal Growth, Stuttgart 1983, p2.37.

11) J.L. Torgeson and R.W. Jackson, Science 148 (1965) 952.

12) R.I. Ristic, J. Garside and B. Zizic, J. Crystal Growth 69 (1984) 442.

13) C. Belouet, E. Dunia and J.F. Petroff, J. Crystal Growth 23 (1974) 243.

14) W.J.P. van Enckevort, Progr. in Crystal Growth and Characterization, 9 (1984) 1.

15) R. Janssen-Van Rosmalen, Thesis (Technical University of Delft, 1977).

16) R.J. Davey and J.W. Mullin, J. Crystal Growth 26 (1974) 45; R.J. Davey and J.W. Mullin, J. Crystal Growth 29 (1975) 45.

17) M.H.J. Hottenhuis and C.B. Lucasius, submitted to J. Crystal Growth.

18) A. E. Nielson, J. Crystal Growth 67 (1984) 289.

Journal of Crystal Growth 74 (1986)
North-Holland, Amsterdam

THE MECHANISM OF TAPERING ON KDP-TYPE CRYSTALS

B. DAM, P. BENNEMA and W.J.P. VAN ENCKEVORT

RIM Laboratory of Solid State Chemistry, Faculty of Science Catholic University, Toernooiveld NL-6525 ED Nijmegen, The Netherlands

Received 15 May 1985, manuscript received in final form 28 October 1985

The anomalous wedge-like shape of KH_2PO_4-type single crystals, also called tapering, is reconsidered. A reformulation of the problem is given on the basis of a detailed observation of the boundary between prismatic and pyramidal growth sectors by means of transmitted light polarization microscopy. A narrowing of both pyramidal and prismatic sectors can be identified to constitute tapering. The first being due to an overall retardation of prismatic growth layers caused by impurity adsorption whereas the narrowing of the pyramidal sectors is due to the inability of pyramidal growth layers to reach the prismatic crystal edge. The retardation of pyramidal growth layers can be explained in terms of a change in electrostatic parameters near the crystal edge or by assuming a fundamental roughness of the crystal edge. A connected net analysis shows the presence of two equally stable {022} nets parallel to the pyramidal faces. In a polar environment this equality is broken, favouring a {011} double layer growth mechanism which can also explain in principle the low segregation coefficient for three-valent positive metal ions in the pyramidal growth sector.

1. Introduction

The phenomenon of tapering of {010} faces of KDP-type crystals is a classical example of habit modification [1]. Whereas the ideal morphology consists of prismatic {010} and pyramidal {011} faces (point group $\bar{4}2m$, fig. 1b), in reality often high index {0kl} orientations are observed on KDP crystals (fig. 1a). Also naturally grown quartz crystals sometimes show tapered prismatic faces.

Originally the occurrence of these anomalous high-index faces has been related to the adsorption of metal impurities. However many other growth parameters such as pH, supersaturation and hydrodynamics have been recognized to affect the occurrence and the degree of tapering on KDP-type crystals. In a recent review Loiacono et al. [2] showed that of all these parameters only the supersaturation is really important. This statement must be reinterpreted a bit after recent in-situ studies on step growth phenomena on {010} KDP [3]. It was observed that the action of three-valent M^{3+} metal impurities is strongly coupled to the supersaturation. In solutions made from Merck p.a. chemicals step growth is inhibited in the supersaturation range between 0 and 1%. Between 1 and 3% growth is partially blocked, some growth layers advance, whereas others are completely blocked. At higher supersaturations no blocking effects were observed, unless after adding Cr^{3+} or other three-valent metal impurities to the solution. As also the other growth parameters affect the impurity adsorption, it can be concluded that small quantities of impurities seriously retard growth on {010}, which is probably the main cause for tapering. Indeed, it was observed that the addition of 10^{-3}% EDTA per mol KDP not only reduces the step-blocking effects on growing crystal surfaces, but it also results in virtually untapered crystals [4].

Neither the exact nature of the curved, irregular faces, nor the mechanism by which they are formed is clearly understood. From literature at least three possible views on the nature of tapering can be extracted:

(1) Because of impurity adsorption on {010}, which extends its influence to the pyramidal faces, pyramidal growth layers are retarded at the crystal edge (Kolb and Comer [5]). This is the oldest statement regarding the mechanism of tapering.

(2) Prismatic growth layers are retarded by impur-

0022-0248/86/$03.50

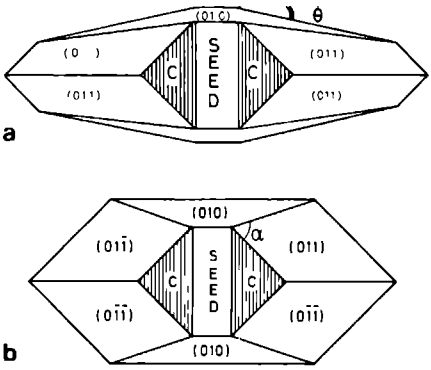

Fig 1 Schematic representation of the growth sectors and the boundaries between them in a (100) projection C is the capping region (a) A tapered crystal (b) An ideally behaving crystal The tapering angle is denoted by θ the ideal behaviour of the sector boundary is characterized by $45° < \alpha < 180°$

ity adsorption The tapering results from the high concentration of growth centres at the centre of the {010} faces resulting in a pile up of bunched growth layers there, which constitutes the tapered surface (Byteva [6], Fontcuberta et al [7])
(3) Due to impurity adsorption surface PBC's are formed stabilizing the high index faces as F-faces (Davey and Mullin [8])

These opinions on tapering will be reconsidered on the basis of published experimental results and new microscopic observations of the boundary between prismatic and pyramidal growth sectors The trajectory of the sector boundary has not been studied in great detail until now Here we will show that it offers a wealth of information on the nature of tapering From the observation of the sector boundary we learn that the problem of tapering can be reformulated as the impossibility of prismatic and pyramidal growth layers to reach the edge between these faces

In section 4 a connected net analysis is presented which shows the structural differences between prismatic and pyramidal growth layers Conditions and possible causes for the tapering effect are then discussed in section 5

2. Experimental

Tapering can be observed best on large ($3 \times 3 \times 10$ cm^3) single crystals For our experiments such crystals were grown in a three-vessel system using polished {001} plates as seeds in the same way as described in ref [9] The temperatures in the system can be kept constant within ± 0.01°C The supersaturation $\sigma = \Delta c / c_{eq}$ is fixed at 1 7% at a growth temperature of 29 50°C Here, Δc is the difference between the actual concentration and the saturation concentration c_{eq}, expressing the concentrations as mass fractions At the beginning of the growth process, the {001} seed surface is covered with small {112}-oriented "roofs", the (crystallographically inequivalent) {$\bar{1}$12} orientations being absent [10] Upon further growth inclusions are formed between the "roofs" until small {101} pyramids are formed which gradually coalesce into one single pyramidal top The region full of inclusions is usually called the capping region (region C in fig 1) As soon as the natural pyramidal top faces are formed, the growth proceeds flawlessly and clear single crystals can be obtained The crystals show only a weak tapering ($\theta \approx 0$–5°C) The tapering angle is not constant and the crystal shape is usually somewhat curved

The same applies to crystals grown by the temperature decrease method Seed crystals were mounted on plastic rods, which rotate in a stirred and thermostated saturated solution Starting at a temperature of about 40°C, the crystals were grown by cooling the solution at a rate of 0 1°C/day Now the supersaturation is not well known but again tapered crystals are obtained When using the same solution several times (by adding some KDP solute after each growth run) the average tapering angle increases, sometimes up to 10–15° (fig 1a)

In both growth methods the solution was at its own pH and Merck p a chemicals were used (containing up to 0 001 wt% Fe) The use of sawn {101} seeds or as-grown pyramidal caps was not found to be of any influence on the tapering behaviour

Surface observations were carried out using an optical reflection differential interference contrast microscope Transmitted light polarization mi-

croscopy was used to study the internal structure of the crystal sector boundaries and the growth bands

3. Observations

3.1 Surface morphology

The surface morphology of the {0*kl*} faces appeared to be completely different from {010} and {011} The difference is most clearly seen if one places untapered seed crystals (simply obtained at room temperature from a p a solution saturated at 30°C) in Cr^{3} -contaminated supersaturated solutions After growth a sharp morphological discontinuity is found then between the original slightly grown {010} surface and the newly formed {0*kl*} surface The tapered surface is rather rough and apart from striations no coherent step patterns were found On {0*kl*} hillocks can be seen but they do not emit steps and their nature is unclear (fig 2a) On the other hand, on the {010} faces lots of spiral centres bounded by irregular macro-steps can be observed (fig 2b)

3.2 The sector boundary

Due to the preferential absorption of metal impurities in the prismatic sector, in a large tapered crystal these sectors can be recognized as greenish crystal regions [11] From visual inspection two important features of tapering can be distinguished in this way

(1) The thickness of the prismatic sectors decreases from seed to top

(2) The cross section of the top of the crystal is always smaller than the original seed (fig 1a)

Apparently the first effect, "prismatic tapering", is the kind of tapering as has been described first by Byteva [6] The second effect, however, has not been explicitly noted by him Yet the anomalous narrowing of the pyramidal growth sector, "pyramidal tapering", can be seen also on Lang topographs (see, e g , ref [12]) and on etched {010} plates [13]

This pyramidal tapering can only be understood if one supposes that the pyramidal growth layers do not reach the edge with the prismatic faces At most, if $v_{(100)} = 0$ a horizontal sector boundary is expected ($\alpha = 45°$ in fig 1b) Increasing the ratio $v_{(100)}/v_{(101)}$, the pyramidal sectors should widen, reaching a maximum at $\alpha = 180°$, when $v_{(101)} = 0$ The growth velocities of the (*hkl*) faces here being indicated by $v_{(hkl)}$

3.3 Microscopic observation of the sector boundary

Detailed f tures of the trajectories of the prismatic-pyramidal sector boundary can be studied by transmitted light microscopy Best results are obtained when the crystal is placed between crossed polarizers in a near-extinction position Using this technique, both sector boundaries and growth bands become visible In fig 3 the different orientations of the growth bands within the prismatic sectors are shown The {0*kl*} orientations tend to become gradually more parallel to {010} upon growth No preferential orientation of these bands could be discerned However, compared to the sector boundary the growth bands are remarkably straight

A priori growth parallel to prismatic faces and growth on tapered orientations need not be of the same nature In principle, one should distinguish between prismatic and taper growth sectors However, neither by Lang topography nor by the present microscopical method a boundary between these two sectors was found Therefore growth on tapered faces is called prismatic growth

The orientation of the sector boundary is not constant On many crystals the pyramidal tapering is strongest at the seed and decreases towards the pyramidal top of the crystal Surprisingly sometimes also a kind of climb of the sector boundaries can be found (see also fig 3) Here the pyramidal sector suddenly widens, which is in fact its expected behaviour, though in a more gradual manner These inclinations of the sector boundary are irregularly spaced and are sometimes related to growth bands Such observations suggest a relation between prismatic and pyramidal growth velocities, and sector tapering This hypothesis was tested by interrupting a growth run A crystal growing under standard conditions (section 2) was taken out of the three-vessel system to scratch its pyra-

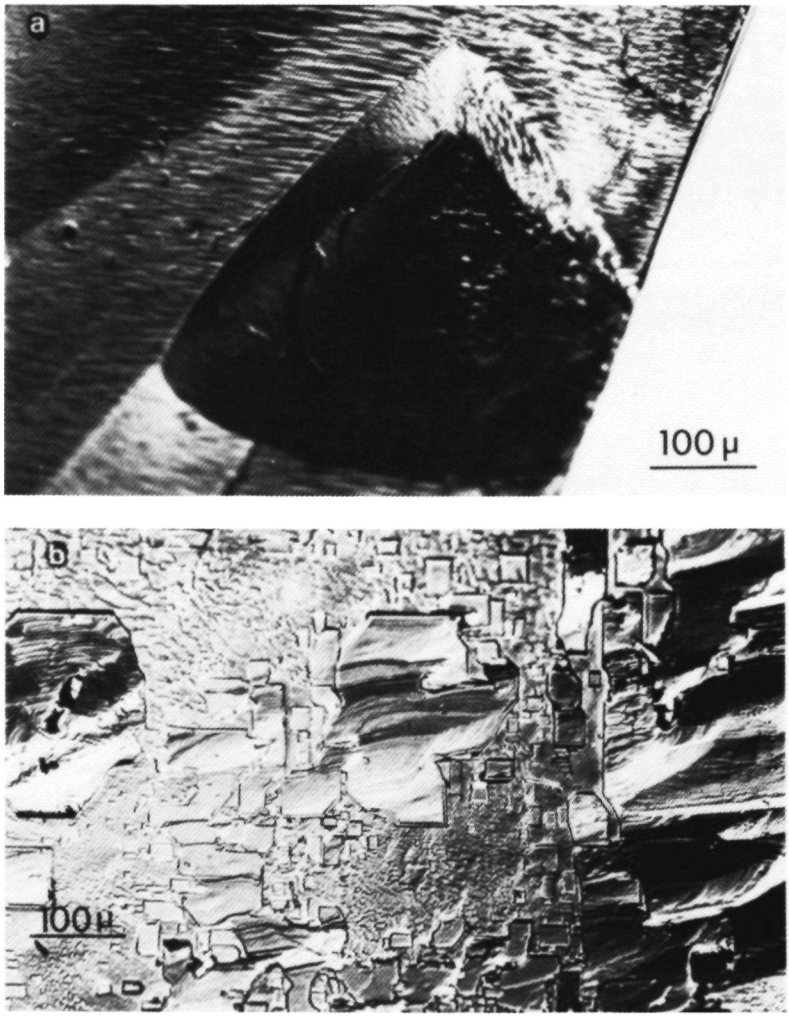

Fig. 2. A differential interference contrast micrograph (DICM) of the surface morphology of (a) an {0*kl*} tapered surface showing striations and a hillock (b) an {010} surface after growing in a Cr^{3+}-contaminated solution, showing irregularly shaped macro steps and numerous growth spirals. Growth by temperature decrease, after adding 15 ppm Cr^{3+} ions per mol KDP.

midal faces. Upon initiating growth, lots of inclusions are formed which in turn produce dislocation bundles and hereby an increase of the growth rate. This relation between inclusion formation and growth rate being found earlier by a surface morphological [14] and Lang topographical study [15].

The result of this experiment is as follows. After re-initiating growth, the tapering of the sector

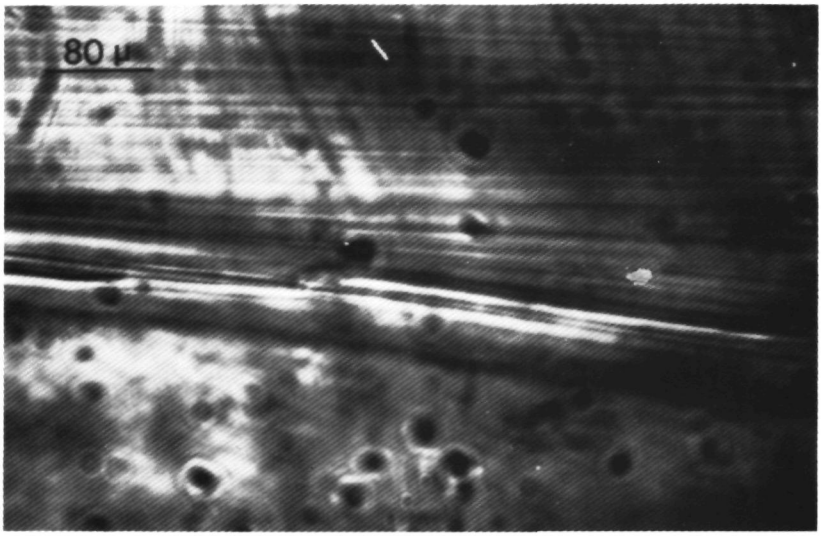

Fig. 3. Transmitted light polarization micrograph (TPM) of a pyramidal-prismatic sector boundary of KDP. In the upper part the prismatic growth bands are shown; the top of the crystal is at the right side of the picture.

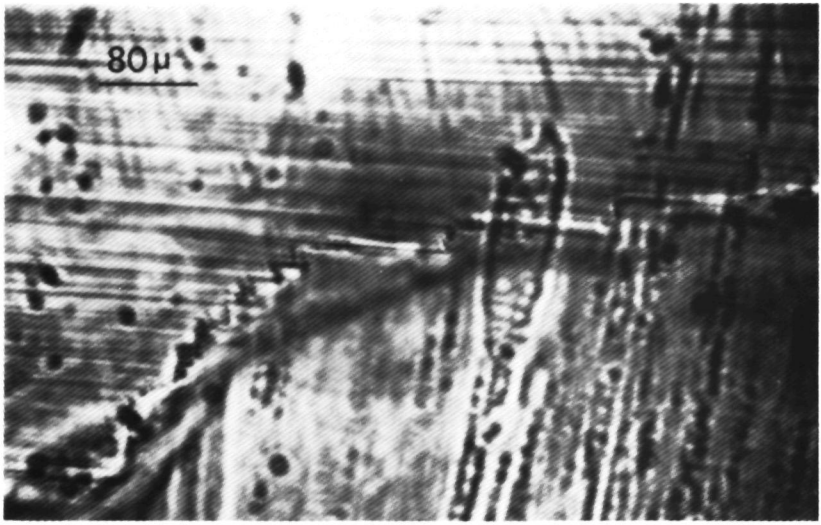

Fig. 4. Sudden stepwise widening of the pyramidal sector after an interruption of the growth run (TPM); the top of the crystal is at the right side of the picture.

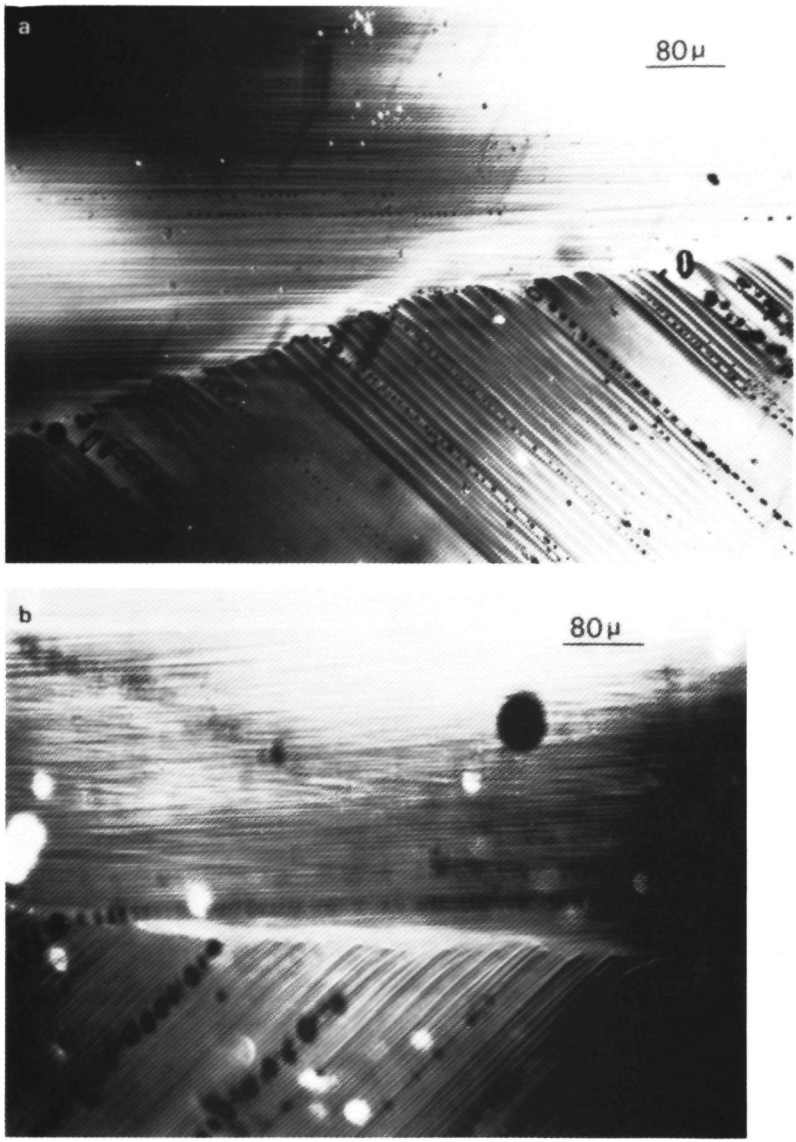

Fig. 5. Sector boundary of an untapered crystal grown at high supersaturation. Both in the prismatic and in the pyramidal sector (lower part of the photograph) one can observe growth bands, sometimes decorated by inclusions. (a) Note the curvature of the line of inclusions near the sector boundary (the crystal top is at the right). (b) In this case a definite sector boundary is absent. A curvature of the growth bands near the intersection of the different growth bands can be seen (crystal top at the left).

boundaries first increases in the same way as already noted to occur near the crystal seed After about 1 mm, a stepwise widening of the pyramidal sector is observed (fig 4) The steps of the widening sector boundary have the form of inverted z's their sharp angle varying between 45 and 90°

Apparently, the dislocations produced upon scratching generate a relative increase in the flux of pyramidal steps arriving at the prismatic crystal edge, thus resulting in the enhanced pyramidal tapering The following stepwise widening of the pyramidal sector can only result from a relative increase of the number of arriving prismatic steps We have no explanation for the latter effect the external growth conditions being kept constant The sector boundary trajectory reveals however that sector tapering is governed by a subtle competition between arriving pyramidal steps and prismatic growth of the resulting stepped crystal edge

3 4 Confrontation with existing views on tapering

From the three views on tapering the third one is inconsistent with our observations as far as it concerns the F-face character of the {0*kl*} orientations We find no preferential direction for either the growth bands or the sector boundary The tapered surfaces of almost all crystals are curved Hence, the stabilization of the {0*kl*} planes to F-faces, specified by Davey and Mullin [8] seems unrealistic since in that case the faces should be strictly planar Moreover we would expect then the presence of well-defined growth centres The {0*kl*} surfaces behave more like impurity stabilized S-faces, showing the typical unidirectional striated surface patterns (see, e g , p 37 in ref [16]) However, the existence of an adsorbed layer of impurities is in itself not impossible

Retardation of prismatic growth layers (Byteva [6]) clearly plays a role in the tapering process However, these retarded layers alone do not fully constitute tapering, because this cannot explain the decrease in width of the pyramidal sectors Besides, no relation between the growth spirals on {010} and growth on the tapered faces was found Growth on tapered surfaces seems to originate largely from the stepped sector boundary Roughly the local thickness of this growth sector depends on the time passed since the crystal edge was formed

As is shown by the trajectories of the sector boundary, pyramidal tapering depends on both prismatic and pyramidal growth velocities If prismatic growth is fast, sector tapering will only play a role on a small scale without affecting the crystal form Any pyramidal tapering will be masked by high prismatic growth rates and the decline of the sector boundary will be compensated by small inclinating steps Such a sector boundary is shown in fig 5a and is typical for untapered crystals grown at high supersaturation Thus for pyramidal tapering to be important for the final crystal form, a low prismatic growth rate is a necessary condition More precise necessary is a (partial) blocking of prismatic steps as found by in situ observations [4]

However this condition is not sufficient The narrowing of the pyramidal growth sector can only result from the inability of pyramidal growth layers to reach the crystal edge It seems that the pyramidal steps stop before reaching the edge The resulting stepped edge interface grows prismatically, i e with a high impurity content In order to consider the reason for the complex phenomenon tapering appears to be we will evaluate the {010} and {011} surface structures in the next section In section 5 the behaviour of growth layers near the intersection of different planes will be discussed

4. Structure and impurity sensitivity of the KDP faces

4 1 The connected nets in {011} and {010} planes

According to recent theories, the crystal growth form will be dominated by crystal faces which are parallel to so-called connected nets, or F-slices [17,18] Connected nets are determined from crystal graphs according to certain crystallographic rules, which will be explained briefly

A crystal graph is an infinite set of points, which are connected to each other according to certain relations (bonds) The crystal graph has the symmetry of one of the 230 space groups The points of the crystal graph correspond to the

"centres of gravity" of the growth units Due to this reduction the symmetry of the graph may be higher than that of the electron density structure

In the case of KDP we will consider a graph consisting of potassium and phosphate ions as points and the first nearest neighbour attractive bonds as the relations connecting the points The physical requirement for a 2D-connected net to be stable (so that an F-face parallel to it can be formed), is that for all directions the edge free energy is larger than zero Hence the following criteria for the determination of connected nets have been derived [17]

(1) The whole crystal graph must be partitioned unambiguously in parallel stacks of equal connected nets, which have no essential points in common

(2) Those symmetry elements of the space group, which leave the reciprocal vector $\boldsymbol{k}\{hkl\}$ normal to the connected net $\{hkl\}$ invariant, apart from the sign, must be able to transform the nets into themselves and into each other without assigning simultaneously essential points to two different symmetry related slices

The thickness of a 2D-connected net $\{hkl\}$ is determined by the minimal distance between two identical surface free energies, i e the maximal slice thickness equals the lattice plane distance $d\{hkl\}$ The distance between identical lattice planes can be reduced further by the non-primitive translational elements of the space group Hence systematic extinctions have to be taken into account when determining the slice thickness (Donnay and Harker [19])

This is illustrated by the [100] projection of KDP as presented in fig 6 The [100] PBC's are connected along [001] and [111] Due to criterium (2), the slices have to be bounded by planes containing the two-fold axes and screw axes Without looking at the crystal graph, it is then clear from the stacking of two-fold axes and screw axes normal to the plane that, in principle, for {020} and {011} two "empty" slices are allowed ({010} being space group forbidden) For {020} one easily sees that only the slice containing fully the 2D bond structure is the physically relevant one in constituting the {020} F-face In the $\{020\}_1$ net an unambiguous assignment of points and bonds to a

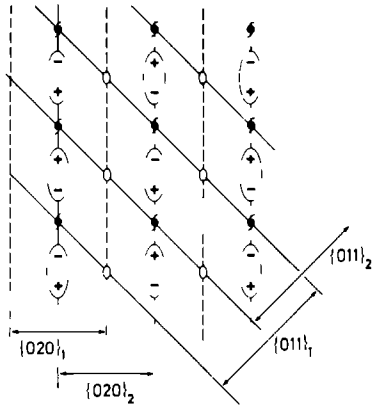

Fig 6 KDP structure projected on the (100) plane Ellipses denote the [100] PBC s which are zigzag chains of potassium and phosphate ions lying $^1/_2a$ above each other

certain net or its neighbour is impossible For {011} the situation is more complex Both $\{011\}_1$ and $\{011\}_2$ slices are allowed Moreover each slice contains two 2D-connected nets, with equal slice energies The two connected nets are related by two-fold (screw) axes laying between the nets Here we encounter a reduction of the distance between equivalent bond structures This is the result of the higher symmetry of the crystal graph with respect to the electron density structure, a situation first noticed by Donnay and Donnay [20]

In such a situation the question arises whether growth kinetics is determined by one double layer {011} or by two single {022} layers As noted by Hartman and Heijnen [21], this will be determined by the difference in surface free energy of the two sub-layers Fig 6 shows that the {022} layers are strongly polar One connected net has phosphate ions on top (which will be denoted as layer A) whereas the other one (layer B) has potassium as outer ions The difference in polarity of the layers and especially the differences in size and polarizability of the ions will result in a difference in the surface free energy

Also the surface morphology points in this direction The etch pits and growth hillocks on

{011} KDP have a triangular shape without symmetry [14], in accordance with the crystal's $\bar{4}2m$ points group symmetry If the polarity of the surface layers did not play a role in the step kinetics, the surface figures would result from an interplay of steps of both layers A and B As the connected nets A and B, which have an asymmetric {111}ZnS-type structure, are related by a two-fold axis lying ‖ [100] between the two nets, the inverse of each step direction should be present in that case As the thus resulting, hexagonally shaped, surface figures have not been observed, the surface is bounded by only one type of polar A or B layers A monolayer step mechanism thus seems unlikely for solution-grown KDP crystals

The question remains, which of the two alternative {011} double layers is rate determining, i e has the lowest surface free energy This is not easy to say as the properties of the solid–liquid interface are still poorly understood Hence, we will attack the problem from another side

4 2 Impurity action and attachment energy on {011} surfaces

It is known that the impurity caption of M^{3+} ions in the pyramidal sectors is very low With respect to the prismatic sectors the segregation coefficient of the pyramidal growth sector can be a factor 50 less [22], depending on the supersaturation The difference is also seen when studying the surfaces with in-situ microscopy Contrary to the prismatic surfaces the pyramidal ones do not show excessive bunching and, most important do not show a so-called dead area a supersaturation range where growth is completely blocked due to adsorption of three-valent metal ions (present as trace impurities in p a chemicals [4]) Upon adding extra metal impurities to the solution, we found that the growth hillocks on {011} loose much of their anisotropy and get a rounded character This points to an impurity mechanism where the M^{3+} ions absorb on the terraces between the steps The impurities will be distributed randomly on the surface causing an isotropic behaviour of the steps as soon as the step velocity is determined by density of adsorbed impurities [3] On the prismatic {010} surfaces the same mechanism is active In order to explain the difference in segregation coefficients, one is forced to assume then that the attachment of cations on pyramidal terraces is less favourable than on prismatic terraces Hence, in a consistent description the {011} top layer is the one whereupon it is difficult for positive ions to attach

In order to calculate the electrostatic interactions, we red' ' the potassium and phosphate ions to point charges Following the Madelung procedure [23], the electrostatic potential of an ion attached to an {011} face is obtained by adding the contributions of the underlying layers, which are in turn calculated by summing over the contributions of the constituting [100] chains The KDP lattice parameters are $a = 7\,444$ Å and $c = 6\,945$ Å [24], the phosphor and potassium positions being (space group $I\bar{4}2d$)

P 0, 0, 0, 1/2, 0, 1/4, 1/2, 1/2, 1/2,
0, 1/2, 3/4,

K 0, 0, 1/2, 1/2, 0, 3/4, 1/2, 1/2, 0,
0, 1/2, 1/4

In the point charge approximation the attachment energy of K^+ on {011} then appears to be positive on layer B and negative on layer A The attachment energy of the phosphate ions compensates this, leading for each layer to a total negative attachment energy per molecule, the latter being in reasonable agreement with literature [25] (table 1) The slice energy for pyramidal ions refers to the total slice energy and not to the usually given half slice energy Moreover, this energy here refers to a {022} slice It is clear now that the attachment

Table 1
Attachment and slice energies expressed in e^2 Å^{-1} units of K^+ and H_2PO_4 ions on {011} pyramidal and {010} prismatic faces the summed ionic energies give the molecular values which are compared with those obtained by Hartman [25] the slice energies E_{slice} represent the total energy of an ion with a slice the crystallization energy equals $E_{slice} + E_{att}$

	F_{slice} (e^2 Å^{-1})	F_{att} (e^2 Å^{-1})	E_{att} [25] (e^2 Å^{-1})
Pyramidal positive ion	−0 3338	0 1238	
Pyramidal negative ion	−0 3338	−0 2085	
Pyramidal molecule	−0 6676	−0 0847	−0 0851
Prismatic molecule	−0 7934	−0 0216	0 0208

at the terrace between two steps of single K^+ ions will be severely hindered on layer B. This implies that, if layer B is indeed the prominent outer growth layer, M^{3+} impurity adsorption is even less plausible. Hence, in the point charge assumption, the impurity distribution in the crystal is consistent with a double layer growth model with layer B as top layer. Note that in a single layer growth mechanism the attachment energy, averaged over layer A and B, would favour impurity adsorption on the pyramidal face.

5. The tapering mechanism

We have seen in the preceding section how different prismatic and pyramidal growth are. Prismatic tapering can be explained as an impurity effect. But what causes the pyramidal tapering, i.e. the retardation of pyramidal growth layers close to the edge? Here, two suggestions will be discussed shortly.

On the basis of attachment energies of cations on the alternative {011} layers, we have argued that only on one of the two double layers M^{3+} impurity adsorption is difficult. The attachment energy on ionic crystals deals however with long-range forces. It follows that for special positions of the crystal surface the relevant energies have to be recalculated. For NaCl such calculations have been done by Piela and Andzelm [26]. In our case such calculations are very cumbersome due to the low symmetry of the ionic configuration. Moreover in such subtle calculations the reduction to point charges is a severe limitation. Not to speak of the negligence of surface relaxation effects in these calculations. Hence, we can only say that in principle at the crystal edge the attachment energies could change in such a way that impurity adsorption is promoted compared to the rest of the pyramidal surface. Then pyramidal steps can become blocked, causing the observed tapering effect.

Apart from an energetical change in adsorption conditions, on the other hand, the step behaviour near the crystal edge could influence the rate of impurity adsorption. Already Herring [27] showed that in the equilibrium growth form the edge between two crystal faces can be rough or rounded depending on the shape of the Wulff plot. During growth the same could happen. Moreover, microscopically steps are rough by nature (their roughening temperature is $T = 0$ K), hence crystal edges are bound to be rough as well. This roughness would usually be masked by the subsequent growth layers of each plane resulting in the ideal sector boundary behaviour depicted in fig. 1b. But as soon as growth on one of the intersecting planes is blocked, the crystal edge is not so easily formed. Instead, the filling up of the crystal edge will be a stochastic process, slower than the initial growth rate. As soon as the growth rate is retarded, the chances for impurity adsorption will increase.

Already Jaffe and Kjellgren [11] observed that the greenish colour of the prismatic sector is strongest near the sector boundary! Hence, the observation of sector boundaries by etching [13] and Lang topography [12] may be partly due to the enhanced impurity adsorption at the sector boundary. Also the visibility of sector boundaries between adjacent pyramidal sectors (in the absence of growth bands [22]) can be understood in this way. There too, a small rough edge preferentially adsorbing impurities might exist.

With the above given two models we have dealt with the problem of pyramidal sector tapering. In both cases we arrive at a stepped crystal edge with a high concentration of adsorped impurities. How does such an edge configuration develop?

From the blocking of steps on the prismatic surfaces [3,4], one can conclude that impurity desorption is a relatively slow process. As soon as crystal growth is severely retarded by impurity adsorption, a very high supersaturation is needed to reanimate crystal growth again. Thus showing the non-linearity of crystal growth, when it is perturbed by relatively slowly desorbing impurities. From the high impurity content of the tapered prismatic sector, it seems obvious that the blocked crystal edges grow in a prismatic way. Growth will be essentially determined then by the incorporation or desorption of impurities. It follows that once a stepped {0*kl*} surface with a high concentration of adsorbed impurities is formed, this will be a relatively stable configuration.

6 Conclusion

Transmission polarization microscopy beautifully shows the irregular trajectory of the prismatic pyramidal sector boundary of KH_2PO_4 shedding a new light on the phenomenon of tapering A detailed observation of this boundary enables one to distinguish between prismatic and pyramidal tapering Prismatic tapering is due to an inhomogeneous distribution of the growth centres combined with the effect of metal M^{3+} impurities retarding the resulting growth layers Pyramidal tapering is an edge effect and only influences crystal morphology when prismatic growth is too slow to fill up the distorted edge configuration Hence the trajectory of the sector boundary is found to be a function of the velocity of prismatic and pyramidal growth

A connected net analysis shows that in principle both {022} and {011} growth layers might occur The pyramidal surface morphology and the low segregation coefficient for three-valent metal ions point however to a growth mechanism involving {011} double layers with K atoms on top Near the crystal edge the situation will be more complicated

On geometrical grounds one could argue that the electrostatics of the pyramidal growth layer changes drastically near the crystal edge in such a way that there M^{1+} ions have a negative attachment energy and retard the pyramidal growth layers On the other hand also a fundamental roughness of the crystal edge at low supersaturation could result in tapering as long as prismatic growth is blocked

As this retardation could not yet be observed by in situ microscopy [3], the edge effects should occur at distances less than 1 μm A detailed scan of the impurity concentration several μm around the sector boundary would therefore be an interesting experiment

Acknowledgements

We are indebted to W H van der Linden for growing many beautiful crystals Part of this work was supported by The Netherlands Foundation for Pure Research (ZWO/SON)

References

[1] H E Buckley Crystal Growth (Wiley New York 1951) p 339
[2] G M Loiacono J J Zola and G Kostecky J Crystal Growth 58 (1982) 495
[3] B Dam and W J P van Enckevort J Crystal Growth 69 (1984) 306
[4] B Dam E Polman and W J P van Enckevort in Industrial Crystallization 84 Eds S J Jančic and F J de Jong (Elsevier Amsterdam 1984) p 97
[5] H J Kolb and J J Comer J Am Chem Soc 67 (1945) 894
[6] I M Byteva in Growth of Crystals Vol IV Eds A V Shubnikov and N N Sheftal (Consultants Bureau New York 1966) p 16
[7] J Fontcuberta R Rodriguez and J Tejada J Crystal Growth 44 (1978) 593
[8] R J Davey and J W Mullin Kristall Tech 11 (1976) 229
[9] R Janssen van Rosmalen W H van der Linden E Dobbinga and D Visser Kristall Tech 13 (1978) 17
[10] M Elwenspoek and P Bennema in Industrial Crystallization 84 Eds S J Jančic and E J de Jong (Elsevier Amsterdam 1984) p 267
[11] H Jaffe and R F Kjellgren Disc Faraday Soc 5 (1949) 319
[12] v G Lutsau Y M Fishman and I S Res Kristall Tech 5 (1970) 445
Y M Fishman and V G Lutsau Phys Status Solidi (a) 3 (1970) 829
[13] B Dam and W J P van Enckevort J Crystal Growth 51 (1981) 607
[14] W J P van Enckevort R Janssen van Rosmalen and W H van der Linden J Crystal Growth 49 (1980) 502
[15] W J P van Enckevort R Janssen van Rosmalen W H van der Linden and H Klapper J Crystal Growth 60 (1982) 67
[16] P Bennema and I Sunagawa in Preparation and Properties of Solid State Materials Vol VII Ed W R Wilcox (Dekker New York 1982) p 1
[17] P Bennema and J P van der Eerden to be published in a book on crystal morphology edited by I Sunagawa
[18] J J M Rijpkema H J F Knops P Bennema and J P van der Eerden J Crystal Growth 61 (1982) 295
[19] G D H Donnay and D Harker Am Mineralogist 22 (1937) 446
[20] J D H Donnay and G Donnay Compt Rend (Paris) 252 (1961) 908
[21] P Hartman and W M M Heijnen J Crystal Growth 63 (1983) 261
[22] C Belouet E Dunia and J F Petroff J Crystal Growth 23 (1974) 243
[23] F Madelung Physik Z 19 (1918) 524
[24] A R Ubbelohde and I Woodward Proc Roy Soc (London) A188 (1947) 358
[25] P Hartman Acta Cryst 9 (1956) 721
[26] L Piela and J Andzelm Surface Sci 84 (1979) 179
[27] C Herring Phys Rev 82 (1951) 87

3.Layer growth on reconstructed silicon surfaces

Journal of Crystal Growth 67 (1984) 400–403
North-Holland, Amsterdam

PRIORITY COMMUNICATION

A "ROUGH HEART" MODEL FOR "EDGE" DISLOCATIONS WHICH ACT AS PERSISTENT GROWTH SOURCES

L.J. GILING and B. DAM

RIM, Laboratory of Solid State Physics and Chemistry, Faculty of Science, Catholic University of Nijmegen, Toernooiveld, 6525 ED Nijmegen, The Netherlands

Received 2 April 1984

The reason why "edge" dislocations can act as persistent growth sources on Si and GaAs surfaces is thought to be due to the absence of surface reconstruction at a dislocation outcrop This locally creates a rough surface area where the nucleation rate and growth rate are much higher than on the surrounding surface. In this way a growth hill will develop. When the hill is large enough and stretches beyond the influence sphere of the stress field of the dislocation, its rim will be subject again to reconstruction generating in this way new steps Thus mechanism will be especially operative on {001} surfaces of Si and GaAs, although a similar mechanism might also be present on the {111} and {110} faces of these and other crystals belonging to the zincblende structure

So far in crystal growth theories the only possibility for a persistent step source was the screw dislocation which emerges at a crystal surface emitting growth spirals. Recently Bauser and Strunk [1] have presented convincing experimental evidence that also the outcrop of an "edge" dislocation, that is a dislocation with its Burgers vector parallel to the surface, can act as a point of repeated nucleation. In this way growth hillocks with concentric steps are formed on the {001} surfaces of GaAs.

That such "edge" dislocations are able to function as persistent step sources has also been observed on NaCl and KCl by Keller [2]. This phenomenon is important for all crystal growers, because it gives a fundamental extension to the possibilities for crystal growth.

The question is how to understand its mechanism. Bauser and Strunk give an explanation in which the "edge" dislocation splits into two partial dislocations, generating in this way a stacking fault with compensating components of the Burgers vector normal to the surface. This certainly is a possibility and careful examination of the dislocation and the surrounding step pattern might give more evidence for this mechanism. However, it is not clear why the dislocations should split up and whether this is a main phenomenon for "edge" type dislocations. In our opinion this explanation is worthwhile to consider but deserves further experimental attention.

Frank, as the father of the growth spiral, has put forward the idea [3] that nucleation is facilitated on one of both stressed sides of the "edge" dislocation, viz. on that side (compressive or repulsive) where the lattice spacing of the nucleus fits best with the local surface spacing. The disadvantage of this possibility is that effectively the action of such a source can only be discerned in a very narrow supersaturation region. The preferential nucleation can only be observed between the $\Delta\mu$ value for the local optimal condition of nucleation and the critical $\Delta\mu_{\text{normal}}$ value for the normal two-dimensional nucleation on the common surface around the dislocations. For, when $\Delta\mu \gtrsim \Delta\mu_{\text{normal}}$ the majority of the growth nuclei will be due to two-dimensional nucleation and these will largely outnumber the nuclei formed on "edge" dislocations. As the reported "edge" sources seem to be quite common and not critical to supersaturation, Frank's suggestion seems to be questionable.

Fruitful discussions on this subject during the 1983 School on Crystal Growth (ISSCG-5) in

Davos stimulated the idea that a logical explanation of this problem could be given if surface reconstruction is taken into account For surface scientists who are familiar with surface reconstruction and crystal growth theory the explanation is straightforward and even quite simple

Surfaces in general constitute a special phase of the solid and from surface detection techniques it is known that the atomic arrangement in the surface top layer can deviate rather drastically from the bulk positions A special reconstruction exists for the {001} surface of Si, Ge, diamond and most of the III–V's including GaAs, which all crystallize in the zincblende or diamond structure

If such a crystal is cleaved along a {001} face and one does not allow (hypothetically) for an atomic readjustment in the top layer, the surface will look like the one pictured in fig 1 Every atom on the surface has two dangling bonds and such a surface is in essence a rough surface [4] Each position offers a kink place and every growth unit (e g a Si atom) that arrives from the gas phase immediately finds a half crystal place (or a kink position) on the surface and is incorporated in the solid without the necessity to diffuse over the surface to a step or to a kink position in a step In other words, on such a surface full of kinks a normal growth mechanism is active

In reality, relaxation of the surface will occur as is always observed for Si, GaAs and related compounds during growth by molecular beam epitaxy (MBE) [5] The reconstruction on the {001} surface is characterized by the dimer formation between adjacent side lobes This is called a (2×1) reconstruction as the unit surface cell now consists of 2 atoms (fig 2) This bond formation is rather stable and is observed both for silicon and gallium arsenide up to the growth temperatures (1160 and 620 °C, respectively) [5,6] For GaAs the dimers are formed by the dangling bonds of the As atoms Therefore, the presence of the reconstruction also depends on the partial pressure of mono-atomic arsenic, higher pressures stabilize the 2×1 dimer formation to higher temperatures An important point is that the reconstructions are only detectable so far by vacuum techniques (electron microscopy, RHEED, LEED etc) Adsorption processes, which can destroy the dimerization, play a minor role in such a high vacuum because of the low concentration of background impurities Under normal crystal growth conditions adsorption processes can be more severe because of the high partial vapour pressures However, it appears that at the growth temperature the adsorption, even at 1 bar, is strongly reduced due to the $T\Delta S$ term in the Gibbs free energy associated with adsorption [7] Indeed there are positive reasons to believe that also under normal growth conditions of silicon and GaAs by CVD and MOCVD and of GaAs by LPE, adsorption is so small that the (2×1) reconstruction is present at the surface

The main argument to support this idea is the experimentally observed F-character of the {001} face, i e the {001} face is a stable or flat face On this surface steps can be found by microscopic methods and even square hillocks and etch pits

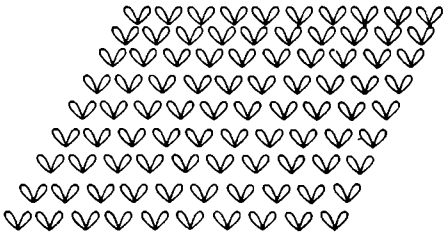

Fig 1 Unreconstructed {100} surface of zincblende type crystals Each surface site has two dangling bonds In terms of crystal growth theories such a surface is rough with a corresponding high growth rate

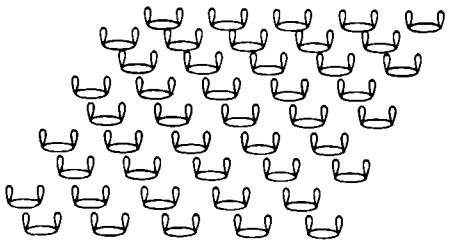

Fig 2 (2×1) reconstructed {100} surface of zincblende type crystals The alternating reconstruction pattern creates an extra periodic bond chain in the surface In this way the surface is stabilized and growth will occur by a step mechanism

have been observed Also in the plot of the growth rate versus the orientation a cusp occurs in the {001} direction [8], showing that this direction has a lower growth rate than adjacent orientations This is in contrast with what one would expect for an unreconstructed {001} surface Such a face is not flat at all, it is a rough (stepped/kinked (S/K)) face and no steps should be present at all Instead of square hillocks and pits only a rough surface should be visible This is in sharp contrast with all experimental observations and gives a strong indication that the {001} surface is stabilized by some mechanism The (2×1) surface reconstruction offers this possibility because it creates an extra periodic bond chain to the one which already exists In this way it can change the S/K character of the face into an F-one This idea, which has been presented at the 1983 International Conference on Crystal Growth (ICCG-7) in Stuttgart will be the subject of two forthcoming papers [9,10]

When one accepts that the {001} surface of diamond-like crystals is reconstructed under normal crystal growth conditions, the explanation that "edge" dislocations can act as growth sources for concentric steps is rather simple

When an "edge" dislocation emerges at a {001} surface the stress field around the dislocation will locally destroy the (2×1) reconstruction, probably on the repulsive side Thus at this side of the dislocation a rough area, "a rough heart", will be created, surrounded by a flat stabilized area (fig 3) Such a local rough area has a higher growth rate than the flat reconstructed surface around the dislocation, and so it will start to grow out normal to the surface After a few atomic layers it will also spread laterally because the rim also offers kink sites The centre of the nucleus will remain rough under the stress field of the dislocation, but as soon as the lateral spreading is far enough away from the centre, reconstruction of the atoms of the newly formed {001} layers will set in again and steps will be formed

This mechanism will be operative already at low $\Delta\mu$ because the critical nucleus size is one atom on such a rough surface The essential difference with Frank's model is that now nucleation is not a rate determining step

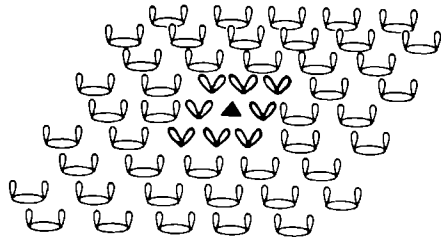

Fig 3 Schematical idea of the rough heart model Around the dislocation outcrop (▲) the dimer formation is broken creating a local rough spot on an otherwise flat reconstructed surface Locally the growth rate will be higher which gives rise to a persistent step source

Proof of the reconstruction mechanism should be obtained by looking more closely at the exact centre of the growth hillocks where no steps should be present From the photographs as published by Bauser and Strunk [1] an indication in this direction can be obtained because in the centre of the growth hill no steps can be discerned However, the decoration technique could fail to reveal steps there because of the smaller step distance So a direct proof is still missing, but this must not be too difficult to obtain

The above mentioned mechanism is not restricted to the {001} surface, in fact all surfaces which reconstruct ((2×1)-{111}, (7×7)-{111}, etc) will provide local spots where the reconstruction is destroyed resulting in a higher growth rate Because of the lack of knowledge about the precise atomic structure of these reconstructions, it is not clear up to now whether here also rough areas will be formed where a critical nucleus of one atom exists If not, then we end up with the same situation as sketched in the stress model of Frank, viz that only in a very narrow $\Delta\mu$ range the effect will be observable

The investigations were supported in part by the Netherlands Foundation for Chemical Research (SON) with financial aid from the Netherlands Organization for the Advancement of Pure Research (ZWO)

References

[1] E Bauser and H Strunk J Crystal Growth 51 (1981) 362

[2] K W Keller, in Abstracts Proc ICCG-7, Stuttgart, 1983, SY1-9

[3] F C Frank, J Crystal Growth 51 (1981) 367

[4] J P van der Eerden, P Bennema and T A Cherepanova, Progr Crystal Growth Characterization 1 (1978) 219

[5] K Ploog, in Crystals Growth, Properties and Applications, Vol 3, III–V Semiconductors, Ed H C Freyhardt (Springer, Berlin, 1980) p 113

[6] B Z Ol'shanetskii, A V Rzhanov and F L Edel'man, Soviet Phys -Semicond 7 (1974) 1538

[7] L J Giling and A A Saaman, in Proc 4th European Conf on CVD, Eindhoven, 1983, Eds J Bloem, G Verspui and L R Wolff, p 280

[8] L Hollan and C Schiller, J Crystal Growth 13/14 (1972) 319

[9] L.J Giling and W.J P van Enckevort, J Crystal Growth, to be published

[10] W J P van Enckevort and L J Giling, Surface Sci , to be published

4.The morphology of modulated K2SO4-type structures

Observation of Bands of Faces on Incommensurate Rb_2ZnBr_4 Single Crystals

B. Dam, A. Janner, P. Bennema, W. H. v. d. Linden, and Th. Rasing [(a)]
Faculty of Science, Catholic University of Nijmegen, Toernooiveld, 6525 ED Nijmegen, The Netherlands
(Received 29 September 1982)

The macroscopic consequences of displacive modulation on the morphology of incommensurate single crystals are confirmed. Bands of faces in the neighborhood of stable normal crystal faces have been observed on spherically shaped Rb_2ZnBr_4 crystals. An interpretation is given in terms of classical morphological theory extended to include (four-dimensional) superspace group symmetry. This leads to the view that the formation of these bands involves, at least partly, so-called satellite faces and gives a simple explanation of why the set of bands has a lower point-group symmetry than the set of normal faces.

PACS numbers: 61.50.Em, 61.50.Cj

As observed first by de Wolff and collaborators,[1] incommensurate single crystals of Rb_2ZnBr_4 and Rb_2ZnCl_4 grown in an aqueous solution show morphological features due to their modulation in the form of so-called satellite faces. These satellite faces could be interpreted[2] by extension of the classical geometrical theories of Bravais,[3] Friedel,[4] and Donnay and Harker.[5]

On the basis of the Bravais-Friedel-Donnay-Harker law, a fairly large number of satellite faces is expected to have about the same morphological importance. Their simultaneous appearance is favored by use of spherically shaped single crystals as the initial growth form. Indeed, as reported below, with this technique a number of growth bands could be made visible in addition to the normal faces. A normal face appears as a depression on the growing sphere. Satellite faces appear within a strip of ledged faces forming a kind of staircase, which will here be called a "staircase band" (or simply a "band") of faces, the faces being called "steps." Bands of this kind have also been observed on a number of inorganic single crystals like ADP ($NH_4H_2PO_4$) and KDP (KH_2PO_4)[6,7] (see Fig. 1), and on crystalline metals like cadmium and zinc.[8]

For the sphere experiments two large, transparent, single crystals of Rb_2ZnBr_4 were selected and polished into half spheres of about 1 cm diam with poles along the ⟨101⟩ and ⟨110⟩ directions, respectively. Because of inversion symmetry half a sphere already contains all relevant information. After growth for about 1 h in a slightly supersaturated solution at about 30 °C, beautiful faces and bands could be observed. Goniometer measurements allowed the faces to be indexed as (100), (001), (201), (111), (110), and (310). These are normally expected crystal faces in crystals of the K_2SO_4 structure type.[9] As far as the observations allowed us to conclude, all these faces obey the *mmm* point-group symmetry of the average crystal structure (space group *Pcmn*).

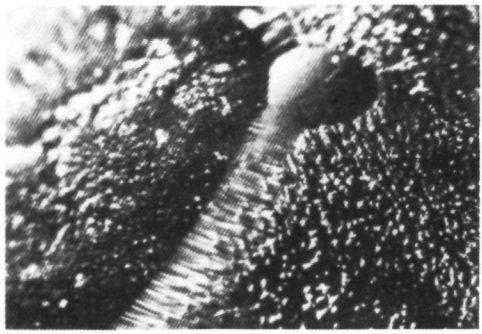

FIG. 1. Growth process on a single-crystal sphere of KDP showing the appearance of a normal crystal face and of a staircase band of faces.

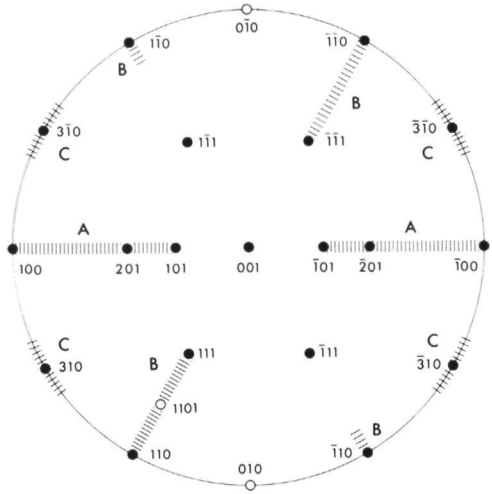

FIG. 2. Stereogram of a single-crystal sphere of Rb_2ZnBr_4 showing the location of observed (solid circles) and expected (open circles) normal faces and staircase bands of faces (hatched areas). The morphologically important satellite face (1101) is also indicated.

In contrast to these faces, the bands have point-group symmetry 222 only. These bands produce vague reflections with varying orientations along well-defined zones (Fig. 2). Thus goniometric reflections definitely exclude the possibility of staircase bands with steps built up from normal faces only.

The most important set of bands (A) appears in the [010] zone in the region comprised between the faces (101) and (10$\bar{1}$) and includes the main faces (100) and (201). This band consists of about a hundred steps. A second set of bands (B) is found in the [1$\bar{1}$0] zone. It clearly shows a 222 point-group symmetry. On the first sphere grown, only small bands formed asymmetrically around (110). The second experiment, however, revealed a band which started at (111) and contained (110) without reaching (11$\bar{1}$). The number of steps in this band is much smaller than in the case of band A. This second band contains, in particular, the satellite face (1101) already observed on other single crystals.[2] (The four-index symbols are explained further on.) The third and weakest set of bands (C) is located around (310) in the [001] zone. These bands do not end in a normal low-index face and upon growing they decrease and disappear rapidly.

In the modulated phase (at room temperature) the crystal of Rb_2ZnBr_4 has a (3+1)-dimensional superspace symmetry group[2] possibly given by $Pcmn(00\gamma)(ss\bar{1})$, or alternatively $Pc2_1n(00\gamma)(s\bar{1}\bar{1})$, implying an orthohombic average structure with space-group $Pcmn$ (or $Pc2_1n$) with unit cell parameters $a = 13.33$ Å, $b = 7.656$ Å, and $c = 9.707$ Å. The modulation wave vector is $\vec{q} = \gamma\vec{c}^* = 0.3\vec{c}^*$. Despite the fact that γ is only approximately 0.3 at 30 °C, that value has been adopted in what follows. The Fourier wave vectors of the matter distribution of the crystal have the general form $\vec{k} = (hklm) = h\vec{a}^* + k\vec{b}^* + l\vec{c}^* + m\vec{q}$ with h, k, l, m integers. The superspace group symmetry given above implies restrictions on the set of possible combinations (systematic extinction rules), but these restrictions have been disregarded here, because the experimental data so far available do not allow their detailed verification. (See Janner and co-workers[10] for more details on the superspace approach.) The interpretation of the bands is based on the following extension of the Bravais-Friedel-Donnay-Harker law:

(1) Crystal faces correspond in the three-dimensional space to fronts of Fourier matter waves. The intersection between real space and lattice hyperplanes with indices ($hklm$) in four-dimensional superspace corresponds to crystal faces normal to Fourier wave vectors $\vec{k} = (hklm)$.[3]

(2) The morphological importance of a given set of symmetry-related faces is greater for smaller values $|\vec{k}|$ of the wave vectors involved.[4] For normal faces ($m = 0$), this means that the indices should be small. The corresponding condition implying that the morphological importance of satellite faces decreases for increasing values

of m does not follow directly from the Friedel law, but is plausible if interpreted in terms of magnitude of the Fourier components.

(3) Reflections forbidden by superspace (four-dimensional) symmetry imply vanishing of those Fourier components and also low morphological importance of the corresponding faces.[5]

Faces with $m=0$ are labeled as usual by (hkl) only, and are called normal faces, whereas those with $m\neq 0$ are denoted as satellite faces. The wave vectors of satellite faces deviate only slightly in length from those of the nearby main faces. Thus, bands of satellite faces around morphologically important normal faces are expected, especially in the zones parallel to a strong periodic bond chain.[11] In particular for Rb_2ZnBr_4, in the approximation given by $\gamma=0.3$, there are (disregarding possible extinction rules) nine different satellite faces between (hkl) and $(hk\,l+1)$ with m values varying between -5 and $+5$

$l\,m$	00	$1\bar{7}$	$1\bar{4}$	01	$1\bar{2}$	$1\bar{5}$	02	$1\bar{1}$	$2\bar{4}$	$0\bar{3}$	10
$l+,\,n$	0.0	0.1	0.2	0.3	0.4	0.5	0.6	0.7	0.8	0.9	1.0

We call such a set of satellite faces a family, labeled by the two limiting normal faces. In general a band is thought to consist of the union of several such families of satellite faces. Even if a detailed identification of the individual satellite faces within a band is very difficult and has not yet been made, to recognize globally the families involved is fairly straightforward. In Table I an example is given of how band A can be built up from two kinds of families having $h=1$ and 2, respectively i.e., (100)–(101), (200)–(201), and (201)–(202). It can be seen that a whole band of faces can be constructed in this way, even if we restrict ourselves to m values lower than 4. A number of satellite faces occurring in these bands have also been observed in naturally shaped single crystals of Rb_2ZnBr_4 and of Rb_2ZnCl_4.[12] From the plot of the $|\vec{k}|$ values (Fig. 3) it can be recognized that the morphological importance of faces diminishes fairly strong from (101) to (001).

TABLE I Expected low-index satellite faces in the zone [010] as a function of their angle ρ with respect to the face (001).

ρ	$hklm$	$hklm$	ρ	$hklm$	$hklm$
90.0	100	200	55.5	$10\bar{1}5$	201
86.1	···	$201\bar{3}$	52.9	···	2023
82.2	1013	$201\bar{4}$	50.5	1002	2004
78.4	···	2001	48.2	···	2011
74.6	$10\bar{1}4$	$201\bar{2}$	46.1	$101\bar{1}$	$202\bar{2}$
71.0	···	$201\bar{5}$	44 2	···	2005
67.6	1001	2002	42 3	$102\bar{4}$	2012
64.3	···	$201\bar{1}$	40 6	···	$202\bar{1}$
61.2	$101\bar{2}$	$202\bar{4}$	39.0	1003	$203\bar{4}$
58.2	···	2003	37.5	···	2013
			36.1	101	202

Band B is probably made up from two kinds of families having $h-k=1$ and $h=k=2$, though the $|\vec{k}|$ values are a bit high in the latter case. The reduction of symmetry in this band cannot be explained on the basis of $|\vec{k}|$ values only, but admits a simple interpretation in terms of superspace-group symmetry. According to the superspace-group approach, what one can see macroscopically is a point group (conventionally denoted by K_E and representing the so-called external part of the superspace point group K_S), which in general is a subgroup of the point group K_0 of the average structure. In terms of modulation, one gets such a symmetry reduction in particular when modulation waves with the same wave vector $\vec{q}$ but different relative phases coexist in the crystal.[13] This interpretation still has to be verified by a better fit of the diffraction data available for Rb_2ZnBr_4 crystals, under the assumption of a superspace group having (external) point-group symmetry 222 instead of mmm or $m2m$, as considered until now.[2] Let us remark that this inter-

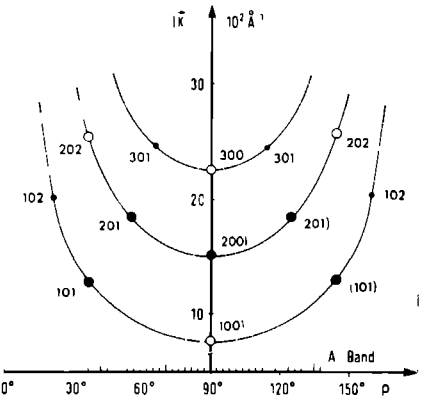

FIG. 3. Variation in wave-vector length for various families of satellite faces expected to build up the observed A band. Large black circles indicate observed normal faces, small black circles the expected faces, and open circles the forbidden ones

pretation is consistent with the observed *mmm* point symmetry of the normal faces. These indeed reflect the symmetry of the average structure even in the modulated case, whereas this is not so, in general, for the satellite faces.

Band *C* cannot be explained on the basis of the present theory without the assumption of an additional small-amplitude modulation in the $\vec{a}^*$ axis.

Concluding, it is amazing how much can be said on the basis of the purely geometrical Bravais-Friedel-Donnay-Harker law only, even concerning such subtle properties as superspace symmetry elements, as implied by the point-group symmetry of the configuration of band *B*. Probably also the abrupt ending of the bands at (101) and (111) can be explained by structural arguments. If we consider the satellite faces as being stabilized by the presence of two faces with high morphological importance, and not by only one, then clearly the situation at either side of (111) and of (101), respectively, is different and may explain the ending.

This analysis applies both to incommensurate and to commensurate (long-period) modulated crystals. This means that the precise role of incommensurability in the morphology has to be elucidated further. We even expect that under favorable conditions (e.g., near edges formed by normal faces) bands of satellite faces should appear in naturally grown incommensurate single crystals, as suggested by the experiments of Uyeda.[14]

It has to be stressed that the interpretation given here of the new morphological features observed in incommensurate Rb_2ZnBr_4, though consistent, need not to be the whole truth of the story. No satisfactory explanation for the bands on ADP and KDP, nor on cadmium or zinc crystals, could be given, as all those crystals are not known to be modulated, and no such periodic lattice distortion could yet be established from x-ray diffraction experiments. In any case, crystal-sphere experiments seem to be of importance for the further investigation of structural properties.

Part of this work has been supported by the Netherlands Foundation for Pure Research (ZWO/FOM-SON).

---

[a]Present address: Physics Department, University of California, Berkeley, Cal. 94720.

[1]P. M. de Wolff, private communication.

[2]A Janner, Th. Rasing, P. Bennema, and W. H. van der Linden, Phys. Rev Lett. 45, 1700 (1980).

[3]A. Bravais, J. Ec. Polytech (Paris) 19, 1 (1850).

[4]G. Friedel, Bull Soc. Fr. Mineral. 30, 326 (1907).

[5]G. D. H. Donnay and D. Harker, Am. Mineral. 22, 446 (1937).

[6]P. Bennema, Z. Kristallogr. 121, 312 (1965).

[7]B. Dam, P. Bennema, W J. P. van Enckevort, and A. Janner, in Extended Abstracts of the Proceedings of the International Conference on Crystal Growth, Moscow, 1980 (unpublished), Vol. 4, p 18.

[8]S. Budurov and N. Stoichev, in *Growth of Crystals*, edited by N. N. Sheftal (Consultants Bureau, New York, 1968), Vol 5A, p. 110.

[9]P. Groth, *Chemische Kristallographie* (W. Engelmann, Leipzig, 1906), Vol. 2, pp. 337–358.

[10]A. Janner and T. Janssen, Acta Crystallogr. Sec. A 36, 399, 408 (1980); P M. de Wolff, T. Janssen, and A. Janner, Acta Crystallogr. Sec. A 37, 625 (1981).

[11]P. Hartman and W. G. Perdok, Acta Crystallogr. 8, 42, 521 (1955).

[12]Th. Rasing, thesis, University of Nijmegen, 1982 (unpublished).

[13]A. Janner and B. W. v. Beest, in Proceedings of the Eleventh International Colloquium on Group Theoretical Methods in Physics, Istanbul, 23–28 August 1982 (to be published)

[14]R. Uyeda, in Collected Abstracts of the Proceedings of the Twelfth International Congress of Crystallography, Ottawa, Canada, August 1981 (to be published).

Zeitschrift fur Kristallographie 165, 247–254 (1983)

Morphological determination of modulated-cell parameters of Rb_2ZnBr_4

B Dam and A. Janner

RIM Laboratory of Solid State Chemistry and Institute for Theoretical Physics,
Faculty of Science, Catholic University of Nijmegen,
Toernooiveld, NI-6525 ED Nijmegen, The Netherlands

Received April 18, 1983

Morphology / Growth Sphere / Superspace Groups / Rb_2ZnBr_4 / Symmetry / Satellite face

Abstract. The morphology of Rb_2ZnBr_4 single crystals as observed in growth sphere experiments is analyzed on the basis of geometrical morphological laws extended to take into account the incommensurate modulated nature of these crystals

Especially in the past, identification of crystals faces (*hkl*) on the basis of these classical morphological laws has been a powerful tool in the determination of 3-dimensional cell parameters In analogy, the relative magnitude of the modulation wave vector (the fourth lattice constant in the language of the superspace approach) can be deduced now from the identification of satellite faces described by four low rational indices (*hklm*).

Introduction

Nowadays the determination of crystal structure is possible without considering the crystal morphology. Still, the morphological laws of Steno and Hauy [see (Burke, 1966) for an historical review] have laid the foundation of the science of crystallography and of the laws of symmetry. This science could only develop after the recognition that similar faces on different crystals of the same mineral, form identical angles. Thus the relative dimensions of the crystals faces were excluded from having any structural meaning. Secondly, cleavage experiments lead to the opinion that crystals are built up from identical basic units. A regular stacking of these building blocks limits the number of possible crystal faces. Accordingly, it was stated that for every crystal face a rational indexing (*hkl*) should be possible.

Considering the symmetry of the crystal form as well, it became possible in this way to group crystals into classes From these crystal classes, later the 32

point groups have evolved This class determination often proved to be correct when more structural information became available through the introduction of X-ray diffraction techniques

X-ray results have also been used to modify the morphological laws of Bravais and Friedel Based on the assumption that densest lattice planes grow slowest, Bravais had postulated that the Morphological Importance (MI) of a crystal face is proportional to its atom density and therefore also (Friedel) to the interplanar spacing However, estimations of interplanar distances were purely based on the ratios of the unit-cell dimensions Knowledge of symmetry transformations involving non-primitive translations (due to screw axes or glide planes) revealed the existence of equivalent reticular densities having smaller interplanar distances than is possible if one considers lattice planes only This considerably improved the predictive power of the Bravais-Friedel law (Donnay-Harker) Of course, for the definite classification of crystals into the 230 space groups diffraction techniques are essential

Presently, the situation is completely reversed and morphological predictions are explicitly based on crystal structure For example, the strength of Periodic Bond Chains or PBC s (Hartman et al , 1955) and the roughening temperature of two dimensional networks (Rijpkema et al , 1983) allow a fairly accurate prediction of the MI of crystal faces

The evident relation between structure and morphology suggests to investigate the effects of (incommensurate) modulation on crystal form It has already been shown that some macroscopic morphological aspects of Rb_2ZnBr_4 incommensurate single crystals can be related to their displacive modulated nature Apart from a change in the MI of the normal crystal faces in the modulated phase (Rasing 1982), new features have been found

Indeed, on single crystals of Rb_2ZnBr_4 high index faces have been found, which could be characterized by four low indices h,k,l,m (so-called satellite faces, Janner et al , 1982) Furthermore, on grown spheres, staircase bands of faces have been observed between morphologically important faces in zones parallel to strong PBC's (Dam et al , 1983) Such bands were also found on spheres of KH_2PO_4 and $NH_4H_2PO_4$ crystals (Dam et al , 1980), which are not known to be modulated

Though the exact characterization of these bands is not yet possible, goniometer measurements reveal that in the bands of Rb_2ZnBr_4 satellite faces are at least partly involved In fact vague reflections with varying orientations along well defined zones were found Some of these goniometer reflections are relatively strong and allow to be measured separately and to be identified as satellite faces

In this paper it is shown how the relative magnitude of the modulation wave vector $\vec{q}$ (in fact the ratio of this fourth lattice parameter with respect to the three other ones) can be derived from these satellite reflections, using a properly extended Bravais-Friedel-Donnay-Harker (BFDH) law

Experiment

Growth sphere experiments have always been a very sensitive means for the determination of crystal forms, as it offers an equal opportunity to any growth direction to manifest itself. Numerous examples of this technique are given by Honigmann (1958)

For the present sphere experiments large transparent single crystals of Rb_2ZnBr_4 were selected After machining and polishing into half spheres, the crystals were grown for about two hours in a slightly supersaturated solution at 30 °C Beautiful faces and bands were observed (Fig 1) though compared with previous observations (Dam et al., 1983) one of the bands (the so-called band A) was less pronounced and the band around (310) could not be seen As an example, band B is shown in Figure 2 Though the band is not so well developed as those on KH_2PO_4 and $NH_4H_2PO_4$ (Dam et al , 1980) clearly the typical staircase structure can be recognized between the two main faces (111) and (110)

Using an optical goniometer strong single satellite reflections were obtained in band A around $(\bar{2}01)$ and (201) and in band B between (110) and (111) Satellites were not found between $(\bar{1}10)$ and $(\bar{1}11)$, which again stresses

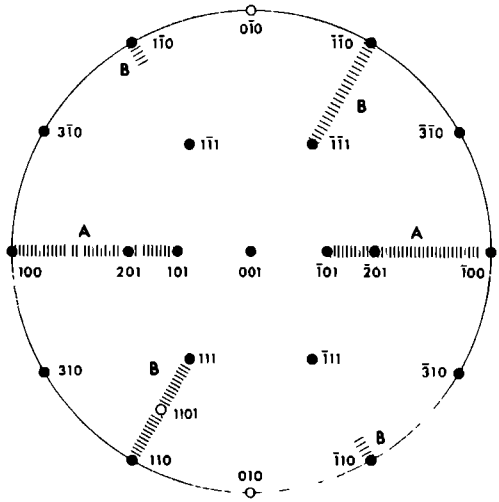

Fig. 1. Stereogram of a single-crystal-sphere of Rb_2ZnBr_4 showing the location of observed (●) and expected (○) normal faces and staircase bands of faces (≡) The morphologically important satellite face (1101) is also indicated

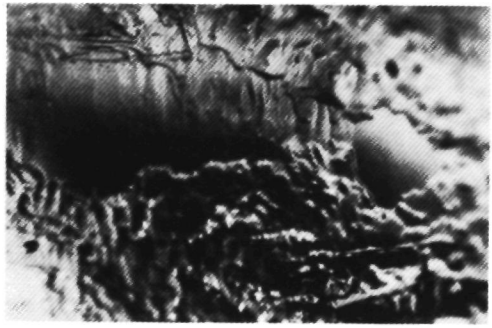

Fig. 2. Band structure on Rb_2ZnBr_4 between the two main faces (111) and (110) (band B in Fig. 1). Goniometer measurements reveal satellite reflections within this band

the point group symmetry reduction to 222, as it also appears from the general configuration of the bands.

Results and discussion

In Table 1 the averaged angles of the observed satellite reflections with respect to (001) are given (the data were collected from two spheres). Let us now interpret these reflections as due to normal crystal faces. The morphological laws of rational indexing applied to these faces restrict the angles ϕ_1 and ϕ_2 according to the possible ratios between ha^* and lc^* and between $|h(\vec{a}^* + \vec{b}^*)|$ and lc^* respectively:

$$\tan \phi_1 = ha^*/lc^* \tag{1}$$

$$\tan \phi_2 = h|\vec{a}^* + \vec{b}^*|/lc^* \tag{2}$$

The lowest possible indices found in this way (indicated in column three of Table 1) still imply very small interplanar distances, in fact incompatible with the spirit of the classical BFDH-laws. Furthermore, even such high indices represent a poor fit of the angles measured for the satellite reflections, as one can see comparing columns one and four of the same table. (Note that for the observed angles an average value has been used; the measured angles are indicated in Table 3). This situation is not surprising if one knows that the morphological laws, when applied to (incommensurate) modulated crystals, have to be extended to take into account superspace group symmetry.

Table 1. Averaged angles of the observed satellite faces with respect to (001) The angles are interpreted classically according to Eqs (1) and (2), after having approximated their value (ϕ_{cal}) in terms of normal indices h and l

	ϕ^{av}_{obs}	l/h	hkl	ϕ_{cal}	zone
ϕ_1	51 27	0 584	503	50 51	[010]
	60 36	0 415	502	61 22	[010]
ϕ_2	64 00	0 713	332	65 48	[1$\bar{1}$0]
	78 87	0 288	331	77 17	[1$\bar{1}$0]
	83 50	0 167	661	83 48	[1$\bar{1}$0]

Even if the crystal structure of Rb_2ZnBr_4 in its incommensurate phase is not yet fully clarified (Hogervorst et al., 1983), one knows from preliminary X-ray and neutron experiments (de Pater, 1979; de Pater et al., 1978 and 1979) that the modulated phase of Rb_2ZnBr_4 is characterized by a basic structure with space group *Pcmn* and a displacive modulation having an incommensurate wave vector $\vec{q} \simeq 0.3\vec{c} = \gamma\vec{c}^*$, with respect to the average lattice parameters $a = 13.33$ Å, $b = 7.656$ Å and $c = 9.707$ Å.

In the case of a (3 + 1)-dimensional incommensurate structure, there is no 3-dimensional lattice periodicity. Still, Fourier wave vectors $\vec{K}$ of the crystal can be expressed as integral linear combinations of (3 + 1) basis vectors; accordingly, they can be brought in a one-to-one correspondence with the vectors of a 4-dimensional reciprocal lattice Σ^* in a so called superspace, and in such a way that by orthogonal projection onto the 3-dimensional real space one gets back the original Fourier wave vectors (see e g. de Wolff, 1974 and 1977, Janner et al , 1977 and 1980). This construction allows a natural generalization of the laws of Bravais and Friedel, once one admits that crystal faces correspond to fronts of Fourier matter waves having wave vectors $\vec{k}$ giving rise to strong diffraction spots. Indeed, making then use of the superspace description mentioned above one has:

1) Crystal faces normal to Fourier wave vectors $\vec{K} = (hklm)$ correspond to the intersection with the real space of lattice hyperplanes having indices $(hklm)$ in the four dimensional superspace (Bravais)

2) The MI of a crystal face is greater for smaller values of $|\vec{K}|$ of the wave vectors involved, implying that not only h,k and l but also m has to be small (Friedel).

Note that in this generalization the original laws are contained as special case. Therefore, even for incommensurate crystals the morphological identification of the normal faces ($m = 0$) allows the determination of the 3-dimensional cell parameters (their ratio actually) as has been done during the last century and at the beginning of the present one. These cell parameters are in fact those of the basic structure which one has by disregarding

Table 2. Possible values for γ giving allowed $(hklm)$-indices according to Eqs (3) and (4) The corresponding standard deviation σ is also given for each set of values

ϕ^{av}_{obs}	γ	$hklm$	γ	$hklm$	γ	$hklm$	γ	$hklm$
51 27	0 105	$101\bar{4}$	0 292	1002	0 418	$101\bar{1}$	0 146	1004
60 36	0 104	1004	0 293	$101\bar{2}$	0 416	1001	0 146	1014
64 00	0 096	$111\bar{3}$	0 287	$111\bar{1}$	0 427	$11\bar{1}4$	0 142	$111\bar{2}$
78 87	0 096	1103	0 288	1101	0.429	$11\bar{1}3$	0 144	1102
83 50	0 084	1102	0 292	$11\bar{1}4$	0 416	$111\bar{2}$	0 167	1101
σ 10^3	8 4		2 7		6.3		10 2	

modulation, or those of the average structure. (These two structures need not to be identical but share the value of their unit-cell parameters.)

In the present case this preliminary work has not been repeated and the 3-dimensional cell parameters have been taken from the results of diffraction experiments. Also the knowledge of the direction of the modulation wave vector has been used, even though we think that it is possible to derive it from crystal sphere morphology, if a sufficient large number of measured satellite reflection data is available.

Based on the superspace adapted morphological laws and taking into account the starting point explained above, a strategy for the identification of satellite faces can be formulated as follows:

1) Substitution in Eqs. (1) and (2) of lc^* by $(l+m\gamma)c^*$ determines for integral values of h, l and m the set of allowed angles ϕ_1 and ϕ_2 as a function of γ.

$$\tan \phi_1 = ha^*/(l+m\gamma)c^* \tag{3}$$

$$\tan \phi_2 = h|\vec{a}^* + \vec{b}^*|/(l+m\gamma)c^* \tag{4}$$

2) The expected value of γ follows from the consistency with a four indices indexing $(hklm)$ with minimal values for the indices as well as for the length of the corresponding $\vec{k}$-vectors.

Given the orthorhombic cell parameters a^*, b^* and c^* and the knowledge that $\vec{q}$ is along the c-axis, possible values for m and l were considered following condition 1). In order to fulfil condition 2) only $h=1$, $l=0, \pm 1$ and $m=\pm 1, \pm 2, \pm 3, \pm 4$ have been considered. From the values of γ found in this way, the most consistent ones were collected in Table 2. One can see that for $\gamma \simeq 0.29$ the standard deviation is smallest giving thus the largest probability to the corresponding indexing.

On the basis of a given superspace group for the crystal in question, extinction conditions could discriminate even better between these possibilities by generalizing Donnay-Harker law as well as already discussed by Janner et al. (1980). In the present analysis the data available were not

Table 3. Identification of observed satellite faces according to the most probable indexing giving the corresponding computed values for γ One finds $\gamma_{av} = 0\ 291$

	ϕ_{obs}	l/h	$hklm$	γ	zone
ϕ_1	36 00	1 002	1010	—	[010]
	51 16	0 580	1002	0 290	[010]
	51 25	0 584	1002	0 292	[010]
	51 40	0 581	1002	0 291	[010]
	55 67	0 497	2010	—	[010]
	60 32	0 415	$10\bar{1}2$	0 293	[010]
	60 80	0 407	$10\bar{1}2$	0 296	[010]
	60 32	0 415	$10\bar{1}2$	0 293	[010]
	60 00	0 420	$10\bar{1}2$	0 290	[010]
ϕ_2	55 50	1 005	1110	—	$[1\bar{1}0]$
	64 00	0 713	$111\bar{1}$	0 287	$[1\bar{1}0]$
	78 87	0 288	1101	0 288	$[1\bar{1}0]$
	83 50	0 167	$11\bar{1}4$	0 292	$[1\bar{1}0]$

considered sufficient for allowing a critical discussion of superspace group symmetry on the basis of the morphology of the crystalline growth spheres

In Table 3 the angles the observed satellite faces make with (001) are given together with the values of some relevant normal faces Adopting now the indexing which was found in Table 2 to be the most probable one, the corresponding values for γ are computed An average of $\gamma = 0\ 291$ is found, which compares well with the neutron diffraction result $\gamma = 0\ 293$ (Gesi et al , 1978)

Concluding it can be said that crystal morphology can be applied successfully in determining modulation parameters Ratios and relative orientation of 4-dimensional cell-constants can in principle be derived macroscopically from morphological observation It is expected that morphology also will allow the determination of the superspace point group, which (we recall) need not be the same as the 3-dimensional point group of the average structure

Acknowledgements We wish to thank W H van der Linden for growing large single crystals and H W van Brakel for making the crystal spheres Also we thank Dr P Bennema and Dr W J P van Enckevort for critical reading of the manuscript Part of this work was supported by the Netherlands Foundation for Pure Research (ZWO/SON)

References

Burke, J G *Origins of the science of crystals* Berkely and Los Angeles University of California Press 1966

Dam, B , Bennema, P , Van Enckevort, W J P , Janner, A On the occurrence of growth bands on spheres of single crystals of KH_2PO_4 and $NH_4H_2PO_4$ Extended abstracts of the International Conference on crystal growth, Vol IV, 18 – 21, Moscow (1980)

Dam, B , Janner, A , Bennema, P , Van der Linden, W H , Rasing, Th Observation of bands of faces on incommensurate Rb_2ZnBr_4 single crystals Phys Rev Lett **50**, 849 – 852 (1983)

Gesi, K , Iizumi, M Neutron scattering study on the incommensurate phases in Rb_2ZnBr_4 J Phys Soc Japan, **45**, 1777 – 1780 (1978)

Hartman, P , Perdok, W G On the relation between structure and morphology of crystals I, II and III Acta Crystallogr **8**, 49 – 52, 521 – 524 and 524 – 529 (1955)

Hogervorst, A C R , Wolff, P M , de private communication

Honigmann, B *Gleichgewichts- und Wachstumsformen von Kristallen* Darmstadt Steinkopff Verlag 1958

Janner, A , Janssen, T Symmetry of periodically modulated crystals Phys Rev **B15**, 643 – 658 (1977)

Janner, A , Janssen, T Symmetry of incommensurate crystal phases, I and II Acta Crystallogr **A36**, 399 – 408, 408 – 415 (1980)

Janner A , Rasing, Th , Bennema, P , Van der Linden, W H Identification of satellite faces on single crystals of the incommensurate structures Rb_2ZnBr_4 and Rb_2ZnCl_4 Phys Rev Lett **45**, 1700 – 1702 (1980)

Pater, C J , de Average structure of Rb_2ZnBr_4 Acta Crystallogr **B35**, 299 – 302 (1979)

Pater, C J , de, Van Dijk, C Neutron scattering study of the incommensurate phase transition of Rb_2ZnBr_4 Phys Rev **B18**, 1281 – 1293 (1978)

Pater, C J , de, Axe, J D , Currat, R Neutron scattering study of the incommensurate-commensurate phase transition of Rb_2ZnBr_4 Phys Rev **B19**, 4684 – 4690 (1979)

Rasing, Th Experimental investigation of 4-dimensional superspace crystals Ph D Thesis, University of Nijmegen (1982)

Rijpkema, J J M , Knops H J F , Bennema, P , Van der Eerden, J P Determination of the Ising critical temperature of F-slices with an application to garnet J Crystal Growth, **61**, 295 – 306 (1983)

Wolff, P M , de The pseudo symmetry of modulated crystal structures Acta Crystallogr **A30**, 777 – 785 (1974)

Wolff, P M , de Symmetry operations for displacively modulated structures Acta Crystallogr **A33**, 493 497 (1977)

Acta Cryst (1986) B42, 69-77

A Superspace Approach to the Structure and Morphology of Tetramethylammonium Tetrachlorozincate, $2C_4H_{12}N^+ . ZnCl_4^{2-}$

BY B DAM AND A JANNER

RIM Laboratory of Solid State Chemistry and Institute for Theoretical Physics, Faculty of Science, Catholic University of Nijmegen, Toernooiveld, NL-6525 ED Nijmegen, The Netherlands

(*Received* 18 *February* 1985, *accepted* 17 *July* 1985)

Abstract

It is shown that the modulated phases of tetramethylammonium tetrachlorozincate, $[(CH_3)_4N]_2ZnCl_4$, can be described by one superspace group $Pcmn(00\gamma)(1s\bar{1})$ This group is consistent not only with the properties of the diffraction pattern of the commensurate and incommensurate phases (and in particular with the corresponding space-group assignments found in the literature) but also with the crystal morphology, the latter being studied here by growth sphere experiments The description of the morphology in terms of main and satellite faces, analogous to the description of the diffraction pattern, reveals a simple order in the crystal morphology of the different phases Whereas the main faces remain relatively unperturbed, the position and appearance of satellite faces are directly related to the modulation wave In fact, the evolution of the modulation wave vector can be monitored from the position of the satellite faces with respect to the main faces Morphological extinction conditions even show compatibility with the proposed superspace group Though the bonding structure of the satellite faces is not quite understood yet, a preliminary explanation is given in terms of a stabilized step structure

1. Introduction

In the past, identification of crystal faces $\{hkl\}$ on the basis of geometrical morphological laws served as an important tool in the determination of relative unit-cell parameters and the derivation of both point-group and possibly space-group symmetry

After the introduction by de Wolff (1977) of the superspace description for one-dimensionally modulated structures, attempts have been made to characterize the morphology of these modulated crystals by extending the standard geometrical laws to include superspace-group symmetry Indeed, from the morphology of Rb_2ZnBr_4 and Rb_2ZnCl_4, which at room temperature are displacively modulated β-K_2SO_4-type structures, extra so-called satellite faces related to the modulation wave vector could be determined (Janner, Rasing, Bennema & van der Linden, 1980, Rasing, 1982) In subsequent growth sphere experiments only for Rb_2ZnBr_4 were a few of the reported satellite faces found However, it appeared to be possible to determine from the orientation of these satellite faces the relative length of the modulation wave with respect to the average unit-cell parameters (Dam & Janner, 1983)

Although this shows that the extended geometrical laws can be successfully applied to incommensurately modulated structures, the thermodynamic and structural reasons for their success is not clear In this respect the microscopic nature of the satellite faces is still an open question, they can possibly be considered as *F* faces, *i e* as faces with a non-zero edge free energy (van der Eerden, 1979)

To study this problem in more detail the morphology of $[(CH_3)_4N]_2ZnCl_4$ (here denoted TMA-ZC) was investigated Special attention was paid to the relation between the morphological importance (MI) of the satellite faces and the symmetry and periodicity of the modulation wave

The basic structure of $[(CH_3)_4N]_2ZnCl_4$ is of the same type as that of Rb_2ZnBr_4 (Hogervorst, 1983) and has space-group symmetry *Pcmn* The modulation vector $\mathbf{q} = \gamma\mathbf{c}^*$ has the same orientation as in Rb_2ZnBr_4 (along the c^* axis) but in TMA-ZC it can attain several values and five modulated phases have been found, as shown in Table 1 (Tanisaki & Mashiyama, 1980, Almairac, Ribet, Ribet & Bziouet, 1980)

TMA-ZC transforms below $T = 293$K from the para phase I (*Pcmn*) into phase II, which is incommensurate Incommensurability arises because γ is temperature dependent within the same phase II, and therefore it cannot be expressed in terms of a given rational number, even if one does so at fixed temperature values (*e g* at about 290K one has $\gamma \sim 0.42$)

The other four low-temperature phases are commensurate Phase III shows a small ferroelectric effect (Sawada, Shiroishi, Yamamoto, Takashige & Matsuo, 1978) and is modulated with $\gamma = 2/5$, while in phases IV and VI $\gamma = 1/3$ The data known so far for phase V support the idea of $\gamma = 2$ Such a modulation, while keeping the same orthorhombic lattice, lowers the original space-group symmetry by changing the atomic positions within the same unit cell without,

0108-7681/86/010069-09$01 50

Table 1. *Description of the structural changes occurring in* $[(CH_3)_4N]_2ZnCl_4$ *below* 300 K

The wave vector **q** is taken along the pseudo-hexagonal c axis, the polarization being along the shortest axis b

The various phases of $[(CH_3)_4N]_2ZnCl_4$					
VI	V	IV	III	II	I
$q = 1/3c^*$	$q = 2c^*$	$q = 1/3c^*$	$q = 2/5c^*$	$q = 0.42c^*$	para
$T < 161$ K	$T > 161$ K	$T > 181$ K	$T > 276.5$ K	$T > 279$ K	$T > 293$ K
$P2_12_12_1$	$P2_1/c11$	$P112_1/n$	$Pc2_1n$	?	*Pcmn*
—	$\alpha = 90.02°$	$\gamma = 90.3°$	—	—	—

however, giving rise to additional satellite reflections. Note that only the room-temperature (average?) structure has been solved (Wiesner, Srivastava, Kennard, DiVaira & Lingafelter, 1967).

All these cases can be described in terms of a single periodic distortion wave (the modulation) of a basic crystal structure. The Fourier wave vectors **k** of its electron density distribution (which label the Bragg spots of the corresponding diffraction pattern and the crystal growth faces as well) are integral linear combinations of $\mathbf{a}^*$, $\mathbf{b}^*$, $\mathbf{c}^*$ and $\mathbf{q} = \gamma\mathbf{c}^*$. The first three vectors span the orthorhombic reciprocal lattice Λ^* of the undistorted basic structure (essentially that of phase I with space group *Pcmn*).

While the morphological consequences of the incommensurability for phase II, the undistorted phase I and the other two modulated phases III and IV are considered experimentally, the theoretical investigation given below also includes the two low-temperature phases V and VI.

The main result is that it is convenient to adopt the same description (structurally and morphologically) for all the different phases I to VI of TMA-ZC. This is possible on the basis of a (3+1)-dimensional superspace-group characterization. Indeed, phases II to VI can be viewed (within a very good approximation) as one-dimensional modulations of *orthorhombic* basic structures having the same undistorted space-group symmetry *Pcmn* as phase I.

All the structural information available at present is compatible with a single superspace-group assignment

$$Pcmn(00\gamma)(1s\bar{1}) = \text{No } 62.c.9.4 \qquad (1)$$

characteristic for most of the incommensurate phases of compounds isostructural with K_2SO_4. The meaning of the superspace-group symbol will become clear below; the right-hand number is that adopted in a full classification list of (3+1)-dimensional superspace groups by de Wolff, Janssen & Janner (1981). Note that such a unique assignment is not in conflict with the change in space-group symmetry for these six phases. On the contrary, it supports the assignments made on the basis of diffraction data [not yet supported by detailed structure determinations] (Tanisaki & Mashiyama, 1980).

This result also fits with a more general analysis performed by Hogervorst (1985) on a large number of β-K_2SO_4-type crystal structures. He discusses the relevance of this same superspace group for most of the modulate phases of these compounds. Analogous ideas, but now formulated in terms of representations of the space group *Pcmn* and within the framework of Landau's theory for second-order phase transitions, have been expressed by Plesko, Kind & Arend (1980) and by Muralt, Arend, Altermatt & Chapuis (1984).

In this work we will first give a superspace analysis of the TMA-ZC structure. Then the classical geometrical morphological laws and their physical meaning are briefly discussed before extending them to include the superspace description of modulated crystals. These new laws and the proposed superspace group will then be tested on the morphology of TMA-ZC.

The main result of our morphological study of phases I to IV of TMA-ZC by growth sphere experiments reveals that the space group *Pcmn* of the average structure is reflected in the so-called main faces that are practically unaffected by the phase transitions. Only the so-called satellite faces are dependent on the crystal phase. Their position is directly related to the wave vector **q** and their appearance allows a superspace-group determination as discussed below. In addition, also from a morphological point of view, all the four investigated phases appear to share the same crystallographic symmetry in four dimensions indicated above.

2. The superspace description

The superspace is, in general, a $(3+d)$-dimensional Euclidean space, which has been introduced to recover the crystallographic symmetry of incommensurate modulated crystal phases. It is, however, a useful concept even if the modulation is commensurate and gives rise to a superstructure. To elucidate this, a few key concepts appearing in the superspace approach have to be presented and applied to TMA-ZC, the reader being referred to other papers for more details (Janner & Janssen, 1980; Janner, 1983).

As already said, Fourier wave vectors of TMA-ZC can be labelled by four integers (indices) h, k, l and m:

$$\mathbf{k} = h\mathbf{a}^* + k\mathbf{b}^* + l\mathbf{c}^* + m\mathbf{q} \in M^* \qquad (2)$$

with $\mathbf{a}^*$, $\mathbf{b}^*$, $\mathbf{c}^*$ orthorhombic and $\mathbf{q} = \gamma\mathbf{c}^*$.

In the *para phase* (I), $\gamma = 0$, thus $m = 0$ and the indices $\{hkl0\} = \{hkl\}$ describe the normal Bragg reflections (and the normal crystal growth faces denoted as main faces) submitted to the systematic extinction rules one finds in *International Tables for*

Crystallography (1983). For the space group *Pcmn*, the conditions for reflection are:

$$hkl\text{: no conditions; } hk0\text{: } h+k \text{ even; } 0kl\text{: } l \text{ even.} \quad (3)$$

The atomic equivalent positions at x, y, z with

$$x=\mathbf{ra}^*, \quad y=\mathbf{rb}^* \quad \text{and} \quad z=\mathbf{rc}^* \quad (4)$$

are defined modulo integers n_1, n_2, n_3 as a consequence of the orthorhombic lattice translational symmetry $\mathbf{n}=n_1\mathbf{a}+n_2\mathbf{b}+n_3\mathbf{c}$ of the structure ($\mathbf{a}^*$, $\mathbf{b}^*$, $\mathbf{c}^*$ span Λ^* and are reciprocal to $\mathbf{a}$, $\mathbf{b}$, $\mathbf{c}$). Accordingly, as is well known, in the Fourier phase factor $\exp(2\pi i\mathbf{kr})$ the scalar product $\mathbf{kr}$ is expressible as an integral linear combination of these unit-cell coordinates x, y, z.

2.1. *The incommensurate phase*

In the incommensurate phase (II), $\gamma\sim0{\cdot}42$ is considered irrational and thus $\mathbf{q}$ incommensurate with respect to Λ^*. Looking at (2), one sees that in order to keep the same property as above for the scalar product $\mathbf{kr}$ one needs *four coordinates*:

$$x=\mathbf{ra}^*, \quad y=\mathbf{rb}^*, \quad z=\mathbf{rc}^* \quad \text{and} \quad t=\mathbf{rq} \quad (5)$$

now defined four modulo integers n_1 to n_4. The additional coordinate t is of course not independent of x, y, z, but can be made so by considering the family of structures one gets through shift of the phase of the modulation wave, and representing the whole by plotting the t coordinate along a fourth axis $\mathbf{d}$ perpendicular to $\mathbf{a}$, $\mathbf{b}$, $\mathbf{c}$ (and thus to $\mathbf{a}^*$, $\mathbf{b}^*$, $\mathbf{c}^*$). It is convenient to choose $|\mathbf{d}|=\lambda$, the modulation wavelength (Fig. 1*a*). All the various three-dimensional modulated crystals then appear as sections for constant t of that pattern, which is called a *superspace embedding* of the modulated crystal. Note that as a result of such an embedding a four-dimensional lattice translational symmetry is obtained and a four-dimensional space-group symmetry is then the result.

In the present context it is convenient to take as a basis in the four-dimensional space the orthorhombic basis set spanned by $\mathbf{a}$, $\mathbf{b}$, $\mathbf{c}$, $\mathbf{d}$ even though it is not a basis for the four-dimensional lattice of symmetry translations in superspace. These lattice translations can be expressed in terms of the following set of equilvalent positions:

$$(x', y', z', t')=(x+n_1, y+n_2, z+n_3, t-\gamma n_3+n_4) \quad (6)$$

for any integer n_1, n_2, n_3, n_4. For M^* as in (2) a projection of a four-dimensional reciprocal lattice Σ^* spanned by $\mathbf{a}^*$, $\mathbf{b}^*$, $\mathbf{c}^*$ and $\mathbf{d}^*=\mathbf{q}+\mathbf{d}/\lambda^2$, the above coordinates are the components of vectors n_s of the corresponding direct lattice Σ (with origin at x, y, z, t).

In addition, one has the following set of equivalent positions associated with the point-group generators of the superspace group indicated in (1), the origin being at the inversion centre.

$$\begin{aligned}
g_s^1&=(1,1)\text{:} && x, y, z, t\\
g_s^2&=(c,1)_x\text{:} && \tfrac{1}{2}-x, y, \tfrac{1}{2}+z, t-\tfrac{1}{2}\gamma\\
g_s^3&=(m,s)_y\text{:} && x, \tfrac{1}{2}-y, z, t+\tfrac{1}{2}\\
g_s^4&=(n,\bar{1}s)_z\text{:} && \tfrac{1}{2}+x, \tfrac{1}{2}+y, \tfrac{1}{2}-z, -t-\tfrac{1}{2}\gamma+\tfrac{1}{2}\\
g_s^5&=(\bar{1},\bar{1})\text{:} && -x, -y, -z, -t\\
g_s^6&=(2_1,\bar{1})_x\text{:} && \tfrac{1}{2}+x, -y, \tfrac{1}{2}-z, -t-\tfrac{1}{2}\gamma\\
g_s^7&=(2_1,\bar{1}s)_y\text{:} && -x, \tfrac{1}{2}+y, -z, -t+\tfrac{1}{2}\\
g_s^8&=(2_1,s)_z\text{:} && \tfrac{1}{2}-x, \tfrac{1}{2}-y, \tfrac{1}{2}+z, t-\tfrac{1}{2}\gamma+\tfrac{1}{2}.
\end{aligned} \quad (7)$$

For γ irrational any $t=$ constant section describes with arbitrary precision the same crystal structure in space, because the set of phases of the modulation wave occurring for a given atom in the undistorted structure is dense in the interval 0 to 2π.

2.2. *The commensurate phases*

In a good approximation all the phases II to VI have the same superspace-group symmetry given

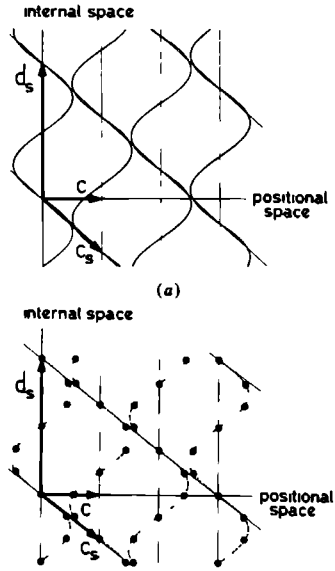

Fig 1 (*a*) Supercrystal plot in the point-atom approximation for the incommensurate case. Each section perpendicular to the internal direction gives the same modulated structure, only differing in a choice of origin. The amplitude of the modulation wave is strongly exaggerated. (*b*) Corresponding supercrystal plot in the commensurate case ($\gamma=1/6$). Only sections at $t=0$, $\pm1/6$, $\pm2/6$, give modulated crystals with $P112_1/n$ space-group symmetry.

Table 2. *Conditions for superspace-group elements to induce 3D Euclidean symmetry in a given section t = constant, as a function of t and of the modulation wavelength $\lambda = c/\gamma$*

The integers m and n express translational symmetry, whereas the relative prime integers r and s occur in the commensurate modulated case only

	Conditions for 3D Euclidean symmetry			
$\gamma = r/s$	$(c, 1)_x$ $2n/(1+2m)$	$(m, s)_y$ $(1+2n)/2m$	$(2_1, s)_z$ $(1+2n)/(1+2m)$	
$t' = t$	$(n, \bar{1}s)_z$ $(1+2n)/4-(1+2m)\gamma/4$	$(\bar{1}, \bar{1})$ $n/2-m\gamma/2$	$(2_1, \bar{1})_x$ $n/2-(1+2m)\gamma/4$	$(2_1, \bar{1}s)_y$ $(1+2n)/4-m\gamma/2$

above and can thus also be described in terms of the equivalent positions of (7).

The commensurability is expressed by the condition

$$\gamma = r/s \in Q, \tag{8}$$

with r, s relatively prime integers. For phases III and VI one has $\gamma = \frac{1}{3}$ and for phase IV $\gamma = \frac{2}{5}$. The three-dimensional Euclidean symmetry of the crystal structure (which is now a 3D space group) depends on r, s *and* the t value of the section t = constant. The condition for an element g_s of the superspace group G_s to induce a three-dimensional Euclidean symmetry in space is to leave such a section invariant.

Let us now discuss those conditions on r, s and t for the generators of the superspace group of TMA-ZC indicated in (7), each combined with the four-dimensional lattice translations of (6).

Consider first $g_s^2 = (c, 1)_x$. Combined with a lattice translation n_s it transforms the position x, y, z, t to

$$(x', y', z', t') = (\tfrac{1}{2} - x + n_1, y + n_2, \tfrac{1}{2} + z + n_3, t - \tfrac{1}{2}\gamma - n_3\gamma + n_4). \tag{9}$$

Accordingly the condition $t = t'$ requires

$$\gamma = r/s = 2n_4/(1+2n_3), \tag{10}$$

implying that $(c)_x$ is a symmetry element compatible with a modulated structure having $\gamma = \frac{2}{5}$ but not with one having $\gamma = \frac{1}{3}$.

In the same way, and now considering $g_s^3 = (m, s)_y$, one finds that $t = t'$ implies

$$\gamma = r/s = (1+2n_4)/2n_3, \tag{11}$$

so that m_y cannot be a symmetry element for a modulated structure with $\gamma = \frac{1}{3}$ or for one having $\gamma = \frac{2}{5}$.

The situation is different for the generator $g_s^4 = (n, \bar{1}s)_z$, again combined with lattice translations. The condition $t = t'$ now yields

$$-(1+2n_3)r + (2n_4+1)s = 4st. \tag{12}$$

For any integers r, s there is a solution (rational γ does not lead to restrictions) but only for discrete values of t. This simply reflects the fact that in a given (commensurate) modulated structure (superstructure) only a finite number of different phases of the modulation wave occur: which one occurs depends on the structure and on its space-group symmetry. Equation (12) implies, in particular, that in order to have $n_z = \{m_z|\frac{1}{2}, \frac{1}{2}, \frac{1}{2}\}$ as a symmetry element for the t = constant section the following conditions have to be satisfied:

$$\begin{aligned} &\text{for } \gamma = \tfrac{1}{3}: \quad t = \nu/6, \\ &\text{for } \gamma = \tfrac{2}{5}: \quad t = (2\nu+1)/20, \end{aligned} \tag{13}$$

for ν any integer (Fig. 1*b*).

This analysis can be completed by considering all other generators of the superspace group given in (7). The resulting conditions for the generators of *Pcmn* to be symmetry elements for the various modulated phases are indicated in Table 2 (see also Janssen, 1985). One sees, as already recognized in previous publications by other authors (Tanisaki & Mashiyama, 1980; Plesko, Kind & Arend, 1980; Muralt, Arend, Altermatt & Chapuis, 1984; Iizumi, Axe & Shirane, 1977), that the following space groups can occur for the **q** vectors involved:

$$\begin{aligned} &P2_12_12_1 \quad Pc2_1n \quad P(2_1/n)_z \\ &P(2_1/c)_x \quad Pc_x \quad \text{and} \quad P(2_1)_z, \end{aligned} \tag{14}$$

lower symmetries being of course possible but not expected.

The space groups assigned to phases III to VI by Tanisaki & Mashiyama (1980) are in full agreement with the present analysis. The corresponding values for γ and for equivalent sections at t are summarized in Table 3. In particular, for phase V the unusual value for the modulation $\gamma = 2$ is the smallest one for compatibility between the assigned space group and the common superspace group.

Note, however, that the non-orthorhombic phases still have (in the present approximation) a (pseudo-)orthorhombic lattice. The label pseudo indicates that the lattice symmetry is higher than that required by the (three-dimensional) space group. That lattice symmetry is, however, imposed by the superspace group.

The small deviations of β and α from 90° in phases IV and V, respectively, must be seen as symmetry breaking. The same possibly applies to the small ferroelectric effect observed in phase III. The 3D space-group assignment $Pc2_1n$ for this phase allows, in itself, ferroelectricity, *i.e.* a non-zero total electric moment within the fivefold supercell (with respect to the paraelectric phase I). The proposed superspace-group symmetry, however, implies in the incom-

Table 3 *Compatibility relations between 3D space-group and superspace-group symmetry in the commensurately modulated cases*

The space groups indicated are Euclidean symmetry groups for each of the sections t = constant indicated, whereas the superspace group leaves the set of equivalent sections labelled by an integer ν invariant

	Space group compatibility with $Pcmn(00\gamma)(1s\bar{1})$					
Phases	VI	V	IV	III	II	I
Space group	$P2_12_12_1$	$P2_1/c11$	$P112_1/n$	$Pc2_1n$	Incommensurate	$Pcmn$
γ	1/3	2	1/3	2/5	Irrational	0
t	$(1+2\nu)/12$	$\nu/2$	$\nu/6$	$(1+2\nu)/20$	Dense	Arbitrary

mensurate case a zero ferroelectric effect For the commensurate case one needs more structural details in order to draw the same conclusion

The high-temperature hexagonal K_2SO_4 structure lies beyond this discussion, as it is a *disordered* type *Pcmn* structure (Unruh, 1981)

2 3 *Extinction rules*

The property that all phases I to VI of TMA ZC share the same superspace group symmetry implies the same conditions for occurrence of Fourier components, once a common four-indices labelling (h, k, l, m) as in (2) has been adopted Then the group $Pcmn(00\gamma)(1s\bar{1})$ leads to the following conditions for reflection (de Wolff, Janssen & Janner, 1981)

$$\begin{aligned} &hklm \text{ no conditions}, \quad hk00 \ h+k \text{ even}, \\ &h0lm \ m \text{ even}, \quad 0klm \ l \text{ even} \end{aligned} \tag{15}$$

The extinction rules for the space groups of the commensurate phases are normally expressed in terms of three indices (called here HKL), which refer to different bases, but have to be compatible with the above one as these space groups are subgroups of the same superspace group For $\gamma = r/s$ with r, s relatively prime integers the reciprocal-lattice vectors $\mathbf{k}$ can be written as

$$\mathbf{k} = H\mathbf{A}^* + K\mathbf{B}^* + L\mathbf{C}^* \tag{16}$$

with $A^* = a^*$, $B^* = b^*$ and $C^* = c^*/s$ Accordingly we simply have

$$(h, k, l, m) = (h, k, sl + rm) = (H, K, L) \tag{17}$$

and one easily verifies that indeed the extinction rules for the various space groups given in (14) are compatible with (15)

Most remarkable is the fact that none of these space groups imply conditions for $H0L$ reflections The $h0lm$, $m = 2n$ condition thus seems typical for the superspace group

3. Modulated structures and morphology

3 1 *Classical geometrical laws and their physical interpretation*

According to the classical morphological laws of Bravais, Friedel, Donnay and Harker (BFDH), the larger the distance between equivalent lattice planes $\{hkl\}$, the larger the morphological importance (MI) of the crystal face parallel to these planes, this implies that h, k and l are small integers It follows that $\{hkl\}$ faces related through point-group symmetry will all have the same MI The non-primitive translational components of the space group manifest themselves by bisecting, trisecting *etc* the distance between equivalent lattice planes, thus reducing the MI of such orientations Evidently, both the definition of a three dimensional (3D) space group and the applicability of the BFDH laws depend on the existence of lattice translational symmetry In fact, lattice translational symmetry was derived from crystal morphology as it is implicit in the law of rational indices of Hauy (Friedel, 1911)

Thermodynamically, the equilibrium form of a crystal is determined by the minimalization of the surface free energy (Herring, 1951) Flat crystal faces of finite size can develop along planes that have a minimal edge free energy larger than zero This energy γ generally decreases with increasing temperature and vanishes at the roughening temperature $T_R\{hkl\}$ (van der Eerden, Bennema & Cherepanova, 1978) Abstracting from the crystal growth parameters, one may say that in general MI$\{hkl\}$ increases with increasing γ and hence with increasing $(T_R\{hkl\} - T)$

Structurally, a non-zero edge free energy is obtained when a 2D network of strong bonds can be constructed within the $\{hkl\}$ slice The roughening temperature of such a bond network has been shown to be dependent on the strength and the geometry of the bond structure (Rijpkema, Knops, Bennema & van der Eerden, 1982) It must be noted that the distance between equivalent (or almost equivalent) bond structures is sometimes smaller than that of the equivalent lattice planes Correspondingly, the MI of such orientations is lower than expected on the basis of BFDH [see Donnay & Donnay (1961) or Hartman (1968)]

In summary, it appears that the success of the geometrical laws of Bravais, Friedel, Donnay and Harker originates from a correspondence between the distance $d\{hkl\}$ and the strength of the 2D bond structure contained in the corresponding $\{hkl\}$ slice In other words, the Fourier transform of electron densities usually resembles that of the bond densities

3 2 *Extended morphological laws and their physical interpretation*

A direct generalization of the classical geometrical laws is possible if one considers crystal faces (and crystal planes) as wave fronts of Fourier density waves For both commensurate and incommensurate modulations the BFDH laws then have to be applied to wave vectors $\mathbf{k} = h\mathbf{a}^* + k\mathbf{b}^* + l\mathbf{c}^* + m\mathbf{q}$ lying normal to crystal faces $\{hklm\}$ Corresponding to the classical case we assume that the MI of such a face will increase with increasing $d\{hklm\}$ the distance between neighbouring wave fronts, assuming h, k, l and m to be small integers Furthermore, superspace symmetry relating $\mathbf{k}$ and $\mathbf{k}'$ will result in the relation $MI(\mathbf{k}) = MI(\mathbf{k}')$, whereas systematic extinctions of the superspace group for $\mathbf{k}''$ will make $MI(\mathbf{k}'') = 0$

Note that $\mathbf{k}$ is defined in 3D space Therefore, the condition h, k, l *and* m small does not follow directly from the requirement that $d\{hklm\}$ has to be large, but it is required for the corresponding lattice hyper planes in 4D space

Indeed, the vector $\mathbf{k}$ is the projection of a reciprocal-lattice vector k_s, which is a Fourier wave vector of the crystal embedded in superspace As the latter does have lattice periodicity, an extension of the classical morphological laws to superspace is expected to be in complete analogy with the 3D case However, at present, the absence of a description of the bond structure in superspace prevents this Hence a physical interpretation of these extended laws when applied to a modulated 3D crystal as a cross section of the 4D supercrystal is not yet possible

Anyhow, a fruitful approach to this problem is to distinguish between main $\{hkl0\}$ and satellite $\{hklm\}$ faces, though now defined in 3D space, just as one does for the diffraction pattern in terms of main and satellite reflections Lattice planes are discussed for the commensurate modulation case (superstructure) while treating incommensurability as a limiting case At phase transitions characterized by a change of $\mathbf{q}$ it is evident that $d\{hklm\}$ changes only when $m \neq 0$ Indeed, it is easily seen that some orientations of superstructures have this property (Fig 2) For example, in s-fold superstructures along c, $\{h'k'l'\}^s$ faces, where h', k' and l' are the indices of the s-fold superstructure, can be identified as main $\{hkl0\}$ faces

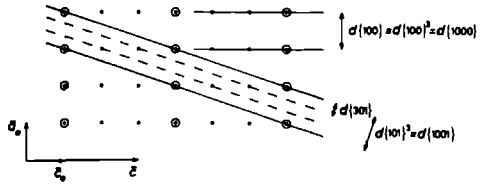

Fig 2 The changes occurring in lattice planes after a modulation triples the c axis

Table 4 *Comparitive morphology of* $[(CH_3)_4N]_2ZnCl_4$, *as far as main faces are concerned*

For commensurate superstructures the present faces are described in the classical three index notation $\{HKL\}$ For the incommensurate case the use of the four index notation with $\mathbf{a}^*$, $\mathbf{b}^*$, $\mathbf{c}^*$ and $\mathbf{q}$ as basis vectors is inevitable This notation can in fact be used to describe the morphology in all phases (column 1)

	The main faces of $[(CH_3)_4N]_2ZnCl_4$			
Phases	IV	III	II	I
$\{hklm\}$	$q = 1/3c^*$	$q = 2/5c^*$	$q = 0\,42c^*$	Para
{2000}	{200}	{200}	{2000}	{200}
{2010}	{203}	{205}	{2010}	{201}
{1010}	{103}	{105}	{1010}	{101}
{1020}	{106}	{1 0 10}	{1020}	{102}
{0020}	{006}	{0 0 10}	{0020}	{002}
{1100}	{110}	{110}	{1100}	{110}
{1110}	{113}	{115}	{1110}	{111}
{0200}	{020}	{020}	{0200}	{020}
{0120}	{016}	{0 1 $\bar{10}$}	{0120}	{012}

if $l' = zs$ (z integer and h, k, l indices of the basic structure) The action of a modulation wave $\mathbf{q} = \gamma\mathbf{c}^*$ upon these orientations will only affect the periodicity of the 2D bond structure parallel to this orientation, *i e* the $\{hkl0\}$ bond structure unit is made up from modulated $\{hkl\}$ units The distance between the lattice planes is left unperturbed As long as the structural changes involved by the modulation wave are small, its effect on the MI of $\{hkl0\}$ planes will be small, *i e* $MI\{hkl\} \sim MI\{hkl0\}$

On the other hand, a satellite slice $\{hklm\}$ of a crystal in its modulated phase will contain 's' (if $\gamma = r/s$) lattice planes, which have become inequivalent through the action of the modulation Clearly, the increased distance between equivalent lattice planes opens the possibility for the formation of new bond structures and hence an enhancing of the MI of these orientations On the other hand, it may happen that in each of these lattice planes a stable 2D bond structure is already present Then, one has the case described by Donnay & Donnay (1961), which shows the difference between the crystal described in terms of bonds or in terms of electron densities The MI of such an orientation will only slightly change when going into that modulated phase, the strongest of the 's' inequivalent bond structures present will determine the MI The existence of pseudo-translations cannot be determined from the geometry of the diffraction pattern only, as it is typically a property of the bond structure Because tl ese faces behave like main faces it will be better to describe them as main/satellite faces This hybrid characterization of some of the faces of a modulated crystal is also justified from the purely geometrical point of view of the crystal form in superspace, for those 2D intersections between satellite and main 3D faces of the supercrystal that lie in the physical space (Janner, 1983)

In the case of an incommensurate modulation an $\{hklm\}$ slice contains an infinite number of now inequivalent lattice planes The reticular density of lattice points of each of these planes is, however, zero This shows that for a modulated incommensurate 3D crystal one can only speak in a formal sense of $d\{hklm\}$ as the distance between equivalent lattice planes Hence, we will call $d\{hklm\}$ the thickness of a crystal slice, *i e* the distance between planes of constant phase

The need for the distinction between main and satellite faces will be illustrated by the description of the morphology of TMA-ZC This will give us also some clues to the more detailed structural aspects of satellite faces

4. The phase-dependent morphology of $[(CH_3)_4N]_2ZnCl_4$

4 1 *Sphere experiments on crystal form and crystal symmetry*

Single crystals of TMA-ZC were grown at 303 K from acidified aqueous solutions of $[(CH_3)_4N]Cl$ and $ZnCl_2$ in a 2 1 molar ratio Clear transparent crystals were obtained that did not show any aging effects After grinding and polishing them into spheres, the crystals were grown for about one day in slightly supersaturated solutions at temperatures between 298 and 274 K

Their morphology, as measured by goniometry (at room temperature), can be indexed very easily using $\{hklm\}$ indices, taking the room-temperature lattice parameters $a = 15\ 541$, $b = 8\ 998$ and $c = 12\ 276$ Å (Wiesner, Srivastava, Kennard, DiVaira & Lingafelter, 1967) as a basis, while **q** changes from phase to phase Thus, the law of rational indices applied to *e g* $\{h0lm\}$ faces restricts the angle φ between [001] and $[h0l]$ to possible ratios

$$\tan \varphi = ha^*/(l + m\gamma)c^* \qquad (18)$$

In Table 4 the presence of main $\{hkl0\}$ faces is indicated for the various phases The classification of {0020} as a main face might seem a bit ambiguous, as it can be seen as a {0001} satellite face as well Geometrically it is an example of those main/satellite faces discussed above From the point of view of bond structure, it is seen that all slices are equivalent, if one views the modulation wave as a homogeneous plane wave polarized along **b** On the other hand, the presence of this orientation in the para phase shows its main-face character

Clearly, the appearance of the main faces is not affected by the phase transitions Throughout the whole temperature range considered here, the configurational point-group symmetry of these faces remains *mmm* Deviations from orthorhombicity could not be observed The $\{hklm\}$ indexing shows its convenience by the fact that it can be used not only in the incommensurate phase, where it is the only possible notation in terms of integers, but describes the morphology in the other modulated phases as well Moreover, one and the same $\{hkl0\}$ symbol can be used to describe the main faces observed so far in any of the modulated phases, using only the integers 0, 1 and 2

Table 5 *The satellite morphology of* $[(CH_3)_4N]_2ZnCl_4$

The comprehensive notation of column I is valid for all phases again The presence of a particular satellite is indicated by giving its three or four index symbol in the column of the phase in question

	Satellite faces of TMA ZC			
Phases	IV	III	II	I
$\{hklm\}$	$q = 1/3c^*$	$q = 2/5c^*$	$q \approx 0\ 42c^*$	para
$\{101\bar{2}\}$	$\{101\}$	$\{101\}$	$\{101\bar{2}\}$	—
$\{1002\}$	$\{102\}$	—	—	—
$\{1101\}$	$\{111\}$	$\{112\}$	$\{1101\}$	—
$\{1111\}$	$\{112\}$	$\{113\}$	$\{1111\}$	—
$\{0101\}$	$\{011\}$	$\{012\}$	$\{0101\}$	—
$\{0102\}$	$\{012\}$	—	—	—

A similar simplicity is seen in the description of the satellite faces given in Table 5 Again, the configurational symmetry observed was *mmm* (Fig 3), which indicates that the external (or three-dimensional) part of the four-dimensional point group is *mmm*, despite the fact that the point group of phase IV is $2/m$. Now, for the same reasons as in the diffraction pattern satellite faces $\{hklm\}$ change in orientation with respect to the main faces at each change of **q** In Fig 4 the morphologically derived changes in δ [where $\mathbf{q} = (1/3 + \delta)\mathbf{c}^*$] have been plotted as a function of temperature Each point represents the average δ value for a specific crystal as computed from the positions of all satellite faces found on that crystal Owing to surface roughness the spread in δ is crystal dependent and varies between ±0 005 and ±0 01 Qualitatively, the figure compares well with that based on diffraction data as given by Almairac, Ribet, Ribet & Bziouet (1980) and

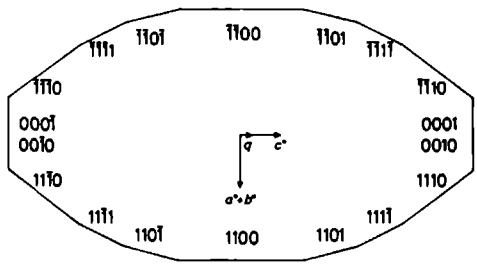

Fig 3 Faces normal to wave vectors $\mathbf{k} = h\mathbf{a}^* + k\mathbf{b}^* + l\mathbf{c}^* + m\mathbf{q}$ present in the $[1\bar{1}0]$ zone when $\mathbf{q} = 1/3\mathbf{c}^*$ A change in the modulation vector **q** results in a change of the orientation of the satellite faces only The morphological importance of satellites is exaggerated in this figure

Marion, Almairac, Lefebvre & Ribet (1981) Also in their measurements the incommensurate-commensurate phase transition appears to be rather smooth. The transition temperature deviates somewhat though, but this sample dependence is not abnormal.

Generally, apart from the value of the index m, satellite faces can be distinguished from main faces by the fact that the intensity of reflected light observed at the goniometer is rather weak. Only on crystals grown in phase IV were satellite faces observed as macroscopically visible facets, whereas, especially in the incommensurate phase, satellite faces are very difficult to observe. This indicates a relationship between MI and the modulation amplitude: generally it is observed that the amplitude of the modulation wave increases at lower temperatures (Hogervorst, 1983). In Table 6 the relative MI (crudely indicated by + and + +) of main and satellite faces of the [010] zone in phase III is compared with their $d\{hklm\}$. Evidently, the MI of satellite faces is less than what one would expect on the basis of their $d\{hklm\}$, which again stresses the importance of distinguishing between main and satellite faces.

In the commensurate case the way in which main and satellite faces are indexed is of course not unique. In each case our first purpose has been to keep the h, k, l indices as low as possible. Even then, in phase IV the {1002} can be indexed as $\{101\bar{1}\}$ as well (the same for $\{101\bar{2}\}$ and {1001}). This ambiguity is not present in the description of phase III. Hence, in a unified description of the satellite morphology, we prefer {1002} and $\{101\bar{2}\}$. Above all they beautifully demonstrate the $\{h0lm\}$ condition typical for the proposed superspace group. Also, all other observed main and satellite faces are compatible with $Pcmn(00\gamma)(1s\bar{1})$ as symmetry group.

From this description of the morphology of TMA-ZC we learn that it depends on the modulation vector. The positions of satellite faces are coupled to the modulation vector and extinction conditions seem to govern their appearance. The configurational point-group symmetry mmm of both main and satellite faces of TMA-ZC appears to be determined by the 3D component of the superspace point group.

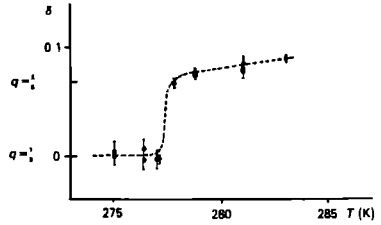

Fig 4 Morphologically monitored evolution of the incommensurability δ, where $\mathbf{q} = (1/3 + \delta)$, as a function of temperature. Instrumental error in δ is given by the spot size Error bars indicate the spread due to surface inhomogeneities

Table 6. *The relative MI of main and satellite faces in the* [010] *zone, as observed in phase* III

The faces are listed according to their $d\{hklm\}$ MI = + means that the facet is only visible as a reflection at the goniometer, whereas if MI = + + the facet is grown out as a macroscopically visible facet.

$\{hkl\}$	$d\{hkl\}$	MI	$\{hklm\}$
{100}	15 5	+ +	{1000}
{101}	14 3	+	$\{101\bar{2}\}$
{102}	11 9	+	{1002}
{103}	9 6	+ +	{1010}
{203}	6 6	+ +	{2010}
{106}	5 7	+	{1020}

4.2. *The microscopic structure of the satellite faces*

It appeared to be relevant to distinguish between satellite and main faces. The main faces can be treated as being independent of the modulation wave and behave according to the classical morphological laws. The satellite faces are strongly related to the modulation wave. Especially as their position seems to vary continuously with $\mathbf{q}$, their microscopic structure is far from evident. Also with respect to $d\{hklm\}$, main and satellite faces cannot be treated on the same level. On the other hand, the satellite face morphology is not completely independent of the habit of main faces. Satellite faces are only found in zones defined by a strong F face and the $\mathbf{q}$ direction of the modulation. The relation with the main faces is even such that, for each $\{hklm\}$, $\{hkl0\}$ is present as a main F face (disregarding for the moment possible slice halving of $\{hkl0\}$ due to the external part of the superspace group).

As the structural changes at the phase transitions are very small, the formation of new bonds is unlikely. However, there is a change in periodicity and the newly formed $\{hkl0\}$ faces consist of modulated bond structures $\{hkl\}$. As a structural model for the satellite faces one could then think of an $\{hklm\}$ face as being constructed from monolayer stepped $\{hkl0\}$ faces. Normally stepped interfaces are not stable. Only some coupling between (the phase of) the modulation wave and the step structure could result in an energetically stable orientation. Further stabilization would be achieved when the steps repel each other (Landau, 1965).

If the stability of step positions depends only on the relative phase of the modulation wave, macroscopic step structures will be most stable when the steps form equi-phase lines. Hence $\{hklm\}$ and $\{hkl0\}$ have to be situated in a zone whose axis is normal to $\mathbf{q}$.

Indeed, for TMA-ZC with $\mathbf{q} = \gamma\mathbf{c}^*$ and $\gamma = r/s$, satellite faces are found in the [110], [100] and [010] zones. In every zone each $\{hklm\}$ can be built up from

$|m|r$ steps per s $\{hkl\}$ bond structures The $m=2$ condition in zone [010] can now be understood from the geometry of the modulation wave with respect to the step structures in this zone The $\binom{m}{s}=(m,s)_y$ superspace-group symmetry element implies that the modulation wave remains invariant after reflection in a mirror normal to **b** and a shift by π of the modulation wave Hence, step structures will be most stable if they are invariant under the same operation and there will be at least two stable step positions per modulation period

Though the stepped surface hypothesis explains some of the morphological features of TMA-ZC, it is clear that it is still a rather phenomenological description of the satellite faces It would be interesting to see whether this description is compatible with the 4D electron density distributions of TMA-ZC

Recently, *in situ* microscopy on TMA-ZC and K_2ZnCl_4 (a β-K_2SO_4 modulated structure with $\mathbf{q}=1/3\mathbf{c}^*$) has been started, using oblique illumination as described earlier (Dam, Polman & van Enckevort, 1984) The first results showed no difference between the surface morphology of main and satellite faces In both cases circular steps around growth centres were observed To gain more insight into the binding properties of modulated crystals a more detailed surface characterization is needed A superspace embedding of the bond structure, analogous to that of the electron density, could help to recognize the relevant features, but such work has still to be done

The present derivation of the space-group symmetry of sections of the crystal embedded in superspace follows a suggestion by T Janssen, whose contribution is gratefully acknowledged Further, we are indebted to J W van Kessel for technical assistance Thanks are also due to the Stichting ZWO/SON and the Stichting FOM for partial support of the present investigation

References

ALMAIRAC, R, RIBET, M, RIBET, J L & BZIOUET, M (1980) *J Phys Lett* **41** L315 L318

DAM, B & JANNER, A (1983) *Z. Kristallogr* **165**, 247-254

DAM B, POLMAN E & VAN ENCKEVORT, W J P (1984) *Industrial Crystallization* 1984, edited by S J JANCIĆ & E J DE JONG, pp 97-102 Amsterdam Elsevier Science Publishers

DONNAY, J D H & DONNAY, G (1961) *C R. Acad Sci.* **252**, 908 909

EERDEN, J P VAN DER (1979) PhD thesis, Nijmegen

EERDEN, J P VAN DER, BENNEMA, P & CHEREPANOVA, T A (1978) *Prog Cryst Growth Charact* **1**, 219-254

FRIEDEL, G (1911) *Leçons de Cristallographie* Paris Hermann

HARTMAN, P (1968) *Acta Cryst* **A24**, 359-364

HERRING, C (1951) *Phys Rev* **82**, 87-93

HOGERVORST, A C R (1983) *Conference Proceedings Int Conf on Phase Transformations in Solids*

HOGERVORST, A C R (1985) Private communication To appear in PhD thesis, TH Delft The Netherlands

IIZUMI, M, AXE, J D & SHIRANE, G (1977) *Phys Rev B*, **15**, 4392-4411

International Tables for Crystallography (1983), Vol A Dordrecht Reidel

JANNER, A (1983) *Symmetries and Properties of Non rigid Molecules A Comprehensive Survey*, edited by J MARUANI & J SERRE *Studies in Physical and Theoretical Chemistry*, Vol 23, pp 461-486 Amsterdam Elsevier

JANNER, A & JANSSEN, T (1980) *Acta Cryst.* **A36**, 399-408, 408-415

JANNER, A, RASING, TH, BENNEMA, P & VAN DER LINDEN, W H (1980) *Phys Rev Lett* **45**, 1700-1702

JANSSEN, T (1985) To appear in *Ferroelectrics*

LANDAU, L D (1965) *Collected Papers of L D Landau*, edited by D TER HAAR, pp 540-545 Oxford Pergamon Press

MARION, G, ALMAIRAC, R, LEFEBVRE, J & RIBET, M (1981) *J Phys C*, **14**, 3177-3185

MURALT, P, AREND, H, ALTERMATT, D & CHAPUIS, G (1984) *Ferroelectrics*, **56**, 7-12

PLESKO, S, KIND, R & AREND, H (1980) *Phys Status Solidi A*, **61**, 87-94

RASING, TH (1982) PhD thesis, Nijmegen

RIJPKEMA, J J M, KNOPS, H J F, BENNEMA, P & VAN DER EERDEN, J P (1982) *J Cryst Growth*, **61**, 295-306

SAWADA, S, SHIROISHI, Y, YAMAMOTO, A, TAKASHIGE, M & MATSUO, M (1978) *J Phys Soc Jpn*, **44**, 687-688

TANISAKI, S & MASHIYAMA, H (1980) *J Phys Soc. Jpn Lett* **48**, 339-340

UNRUH, H G (1981) *Ferroelectrics*, **36**, 359-362

WIESNER, J R, SRIVASTAVA, R C, KENNARD, C H L, DIVAIRA, M & LINGAFELTER, E C (1967) *Acta Cryst* **23**, 565-574

WOLFF, P M DE (1977) *Acta Cryst* **A33**, 493-497

WOLFF, P M DE, JANSSEN, T & JANNER, A (1981) *Acta Cryst* **A37**, 625 636

In Situ Observation of a Roughening Transition of the $(10\bar{1}2)$ Satellite Crystal Surface of Modulated $((CH_3)_4N)_2ZnCl_4$

B Dam

Research Institute for Materials, Laboratory of Solid State Chemistry, Faculty of Science, Catholic University of Nijmegen, Toernooiveld, NL-6525 ED Nijmegen, The Netherlands

(Received 22 August 1985)

The first microscopic observation of a roughening transition *on* a crystal surface is reported. The surface involved is a so-called satellite face of a modulated $((CH_3)_4N)_2ZnCl_4$ crystal. The orientation of such a face is directly coupled to the length of the structural modulation wave vector **q**. At a change of **q** the stable satellite orientations change. Applying *in situ* optical microscopy we observed growth and etch features on the $(10\bar{1}2)$ satellite face at the first commensurate-commensurate phase transition the roughening features suggest a *sudden* decrease of the edge free energy to zero.

PACS numbers: 61.50.Em, 61.50.Cj

The notion that crystal form is determined by the crystal lattice and its symmetry is the historical basis of modern crystallography. Given the fundamental difference between surface and bulk properties the success of early crystallographers is quite remarkable.

Recent experiments show the influence of temperature on crystal form. Above a certain critical temperature a flat crystal face may disappear. The resulting rounding of crystals has been observed, e.g., on a hcp ^{4}He crystal in equilibrium with its superfluid,[1] and on an adamantane crystal approximately in equilibrium with its vapor.[2] Also the rounding of solution-grown organic crystals in nonequilibrium conditions has been reported.[3] The theory of the so-called roughening transition is extensively studied. With the use of Ising models, computer simulations of stepped surfaces[4] indicate that above the roughening temperature T_R the edge free energy γ becomes zero and the steps lose their identity. In the Wulff plot, the orientational plot of the surface free energy, a cusped minimum becomes rounded above T_R (see Rottman and Wortis[5] for a review). The relation between γ and T_R was made more explicit by van der Eerden and Knops.[6] Also, the character of the phase transition has been suggested to be of infinite order.[7] Recently, with use of the fact that the roughening temperature is close to the critical temperature of a two-dimensional Ising lattice, a method has been developed to estimate the roughening temperature of more complicated (non-Kossel-type) crystal surfaces.[8]

Here, I present the first direct microscopic observations of the changes occurring on a crystal surface during a roughening transition. However, in this case the vanishing of the edge free energy is not due to a change in temperature, but results from a change in crystal structure. More precisely, from a change in the wavelength of the displacive modulation in $((CH_3)_4N)_2ZnCl_4$ (here indicated as TMA-ZC). Consequently the transition is not of the Kosterlitz-Thouless (continuous order) type, but rather it is first order. Hence, from now on we shall generalize the notion of a roughening transition as any transition where the step free energy vanishes.

TMA-ZC, a K_2SO_4-type structure, shows a sequence of modulated phases.[9] All these phases can be characterized as a combination of a relatively unperturbed basic structure and a displacive modulation wave vector $\mathbf{q} = \gamma\mathbf{c}^*$, with γ taking several *commensurate* and *incommensurate* values (Table I).

The existence of extra, so-called satellite faces related to the length of the modulation wave and the supersymmetry of the crystal has been reported.[10,11] In the [010] zone of TMA ZC, only the very small (1002) and $(10\bar{1}2)$ satellite faces were identified.[11] Large satellite faces were found on the mineral crystal calaverite.[12]

Extending the classical geometrical morphological laws to modulated crystals, faces have to be labeled by four integers $(hklm)$. These integers indicate the face normals, which are parallel to the Fourier wave vectors $\mathbf{k} = h\mathbf{a}^* + k\mathbf{b}^* + l\mathbf{c}^* + m\mathbf{q}$ describing the crystal density distribution. In contrast to the main faces $(hkl0)$ whose orientation is not affected by the modulation wave, *satellite faces $(hklm)$ change in orientation with respect to $(hkl0)$ upon a change of* **q**. Indeed on TMA-ZC the change in length of the modulation wavelength as a function of temperature could be monitored by measuring the relative orientation of the satellite faces at different temperatures.[11] This approach to the mor-

TABLE I. The various phases of TMA-ZC between 0 and 30 °C. The wave vector **q** is taken along the pseudohexagonal axis, **c**, and the polarization is along the shortest axis, **b**.

IV	III	II	I
$q = \frac{1}{3}\mathbf{c}^*$	$q = \frac{2}{5}\mathbf{c}^*$	$q \simeq 0.42\mathbf{c}^*$	para
$T > 181$ K	$T > 276.5$ K	$T > 279$ K	$T > 293$ K
$P112_1/n$	$Pc2_1n$	?	$Pcmn$

phology of modulated crystals is inspired by the superspace approach introduced for the diffraction pattern of incommensurate crystals by de Wolff, Janner, and Janssen.[13] It can be shown that for TMA-ZC and related K_2SO_4-type compounds the whole sequence of modulated structures can be described by one superspace group.[11,14]

In the incommensurate case the concept of closely packed lattice planes (Bravais) is completely lost for satellite orientations; thus, the nature of a satellite face remained unclear up to now. Does a satellite surface behave like a normal, main surface? Generally, on normal, main faces growth steps develop around screw dislocations to form the so-called growth spirals, first predicted by Frank.[15] Upon dissolution, steep etch pits are formed around screw and edge dislocations. These features have been extensively studied experimentally by both *in situ* and *ex situ* optical microscopy.[16] From theory it is clear that neither steep etch pits nor growth spirals can occur on surfaces with a zero edge free energy γ. Hence, to study the nature of a satellite face, we started an *in situ* investigation of the surface morphology of the $(10\bar{1}2)$ satellite face of TMA-ZC in the T range between 0 and 10 °C and looked in particular for the existence of growth spirals.

Lately the possibilities to apply optical *in situ* microscopical techniques have increased enormously.[17] By recording the image on video tape with use of an analog contrast amplifier, it has been shown[18] that, with differential interference contrast microscopy, the kinetic behavior of growth steps as low as 100 Å can be observed. In the present study, oblique illumination microscopy[18] with conventional optics was used; it gives about the same vertical resolution as differential interference contrast microscopy. Even better results can be obtained by application of specially designed optics.[19]

After cutting a crystal, grown in the phase I at about 30 °C, along approximately the $(10\bar{1}2)$ orientation, the crystal is placed in a thermostated, stagnant-solution, growth cell[20] filled with a saturated TMA-ZC solution. Upon growth, the cut crystal surface develops into small isles of satellite faces partly bounded by strong main faces. The orientation of the grown satellite face can be checked quite accurately by optical goniometry *(ex situ)*.

The most important result of these observations is that indeed growth spirals and etch pits, circular in shape, can be observed in the incommensurate phase II and the commensurate phases III and IV, implying that the edge free energy of the $(10\bar{1}2)$ satellite face is larger than zero in each of the three modulated phases investigated here. In Fig. 1 a growth spiral is shown rotating on a $(10\bar{1}2)$ facet of a crystal growing in its incommensurate phase. The behavior of the growth spiral is quite normal. Upon increasing the supersaturation (by lowering the temperature in the growth cell) the rotational velocity of the spiral increases and the step distance decreases, eventually preventing observation of the spiral.

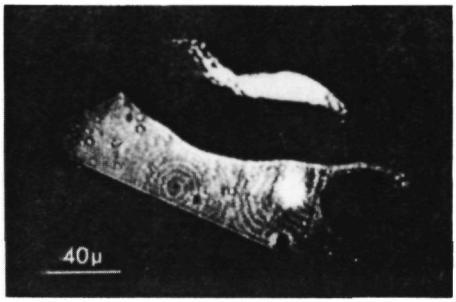

FIG. 1. *In situ* observation of a growth spiral on an *incommensurate* $(10\bar{1}2)$ face of $((CH_3)_4N)_2ZnCl_4$. $T = 8.1$ °C.

Apart from spirals and etch pits, the occurrence of so-called hollow cores[21] is also an indication that γ is nonzero. These holes in the crystal surface may develop around strong dislocations. Their radius increases with decreasing supersaturation while their equilibrium radius is inversely proportional to γ and approximately given by [21]

$$r_0 = (\mu b^2)/(8\pi^2\gamma), \tag{1}$$

with μ being the shear modulus and b the dislocation's Burgers vector. Hollow cores can be explained by a reduction of the effective supersaturation due to the stress in the dislocation center. Indeed, in the satellite crystal surface we observed holes which, once formed, expand upon lowering the supersaturation. Below the equilibrium temperature the hollow cores suddenly open up and form etch pits, a process already observed more quantitatively by van der Hoek, van Enckevort, and van der Linden.[22] Such hollow cores could not be observed on several TMA-ZC main faces in any of the three modulated phases, which suggests that though $\gamma(10\bar{1}2)$ is larger than zero it is much smaller than the edge free energy of a main crystal face.

These surface morphological features support the idea that the $(10\bar{1}2)$ satellite face is a thermodynamically stable equilibrium form in each modulated phase. Hence each change in $\mathbf{q}$ implies an instability of the old $(10\bar{1}2)$ orientation with respect to the new one. Still, neither within the incommensurate phase nor at the incommensurate-commensurate transition were any peculiar surface features detected. The satellite face rotates over $\sim 3°$ during this process, but optical goniometry showed that this tilting is a very slow process. Only after growing the crystal for about one day at constant temperature does the surface fully adopt its equilibrium orientation.

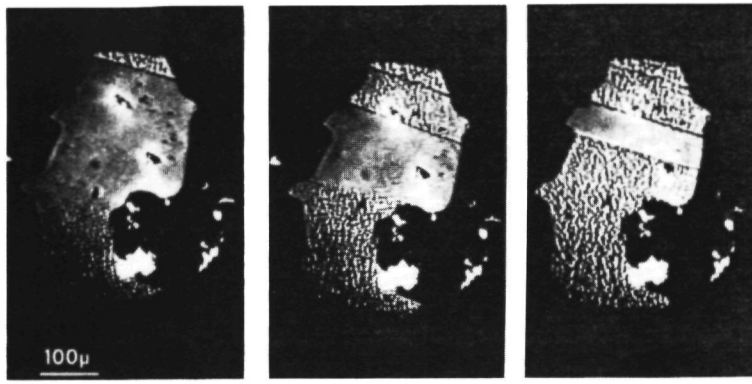

FIG. 2. *In situ* observation of the consecutive stages of the roughening of a $(10\bar{1}2)$ face of TMA-ZC at a change of the modulation wave vector $\mathbf{q}$ from $\frac{2}{5}\mathbf{c}^*$ to $\frac{1}{3}\mathbf{c}^*$. Roughening proceeds from both the upper and the lower edge of the satellite face, the boundary separating the rough and flat surface parts being along [010].

At the commensurate-commensurate transition $\mathbf{q}$ jumps from $\mathbf{q}=\frac{2}{5}\mathbf{c}^*$ to $\mathbf{q}=\frac{1}{3}\mathbf{c}^*$. Correspondingly the $(10\bar{1}2)$ satellite face rotates with respect to the main (0010) face over 9.5° in orientation. This is indeed found to be a discontinuous process. At 3.9 °C the satellite surface is seen to roughen. In Fig. 2 a sequence of pictures taken from the video screen illustrates this process. The central, flat $(10\bar{1}2)$ surface is found to disintegrate from two sides. Though we are not exactly at equilibrium (upon lowering the temperature the supersaturation of the solution increases), the coexistence of flat and disintegrated surface areas suggests that the roughening process is a first-order transition. On some facets, rotating growth spirals were observed while at the sides of the facet the roughening had set in already. At the rough surface no layer growth can be observed. The boundary line separating the two phases in Fig. 2 preferentially lies along [010]. Curiously enough the lower phase boundary in Fig. 2 proceeds continuously, while the upper boundary seems to be temporarily pinned sometimes and moves stepwise. Only on very smooth surfaces can such two-phase regions be observed. Otherwise the surface transition proceeds from distorted areas and quickly covers the whole satellite surface. Hence the coexistence of smooth and disintegrated rough surfaces is not likely to be due to a temperature gradient or to the proceeding bulk transition. This suggests that the surface itself undergoes a first-order transition.

The formation of a new $(10\bar{1}2)$ facet orientation conforming to the new wave vector $\mathbf{q}=\frac{1}{3}\mathbf{c}^*$ again takes a long time (about one day). However, if one increases the temperature shortly after the phase transition to the old phase again, the disintegrated rough surface (upon which no growth features can be discerned) quickly recovers. Small isles are formed which gradually coalesce into a single flat satellite surface. No hysteresis could be observed in this process.

As stated before, the observed roughening is not a roughening transition in the sense of the Ising models described at the beginning of this Letter. In the first place we are dealing here with only a near-equilibrium situation. Secondly, roughening due to a structural change generally corresponds to a change in the Wulff plot such that a sharply cusped minimum is transformed into a curve without a minimum for the surface free energy in that orientation. Such a transition in the surface free energy is in accordance with the first-order character of the transition observed; i.e., the coexistence of flat and roughened surface areas.

In conclusion, the thermodynamic stability (i.e., $\gamma > 0$) of the $(10\bar{1}2)$ satellite face is established in the *incommensurate* and in the first two *commensurate* phases of TMA-ZC. The delicate orientational dependence of satellite faces on the length of $\mathbf{q}$ again shows the remarkable connection between crystal structure and surface stability. Note that the amplitude of the displacements in the modulation wave is only of the order of tenths of an angstrom. This poses a challenge to understand the bonding nature of the satellite faces.

I would like to thank Professor A. Janner, Professor P. Bennema, Dr. J. P. van der Eerden, and Dr. M. Elwenspoek for their stimulating interest and critical reading of the manuscript. This work is supported by the Netherlands Foundation for Pure Research (ZWO/SON).

[1]J E Avron, L S Balfour, C G Kuper, J Landau, S G Lipson, and L S Schulman, Phys Rev Lett **45**, 814 (1980)

[2]A Pavlovska, J Cryst Growth **46**, 551 (1979)

[3]H J Human, J P van der Eerden, L A M J Jetten, and J G M Odekerken, J Cryst Growth **51**, 598 (1981), L A M J Jetten, H J Human, P Bennema, and J P van der Ferden, J Cryst Growth **68**, 503 (1985)

[4]H J Leamy and G H Gilmer, J Cryst Growth, **24/25**, 499 (1974)

[5]C Rottman and M Wortis, Phys Rep **103**, 59 (1984)

[6]J P van der Lerden and H J F Knops, Phys Lett **66A**, 334 (1978)

[7]H van Bijeren, Phys Rev Lett **38**, 993 (1977)

[8]J J M Rijpkema, H J F Knops, P Bennema, and J P van der Eerden, J Cryst Growth **61**, 295 (1982)

[9]S Tanisaki and H Mashiyama, J Phys Soc Jpn **48**, 339 (1980), K Gesi, J Phys Soc Jpn **51**, 2532 (1982)

[10]B Dam, A Janner, P Bennema, W H v d Linden, and Th Rasing, Phys Rev Lett **50**, 849 (1982), B Dam and A Janner, Z Kristallogr **165**, 247 (1983)

[11]B Dam and A Janner, to be published

[12]B Dam, A Janner, and J D H Donnay, Phys Rev Lett **55**, 2301 (1985)

[13]P M de Wolff, Acta Crystallogr, Sect A **33**, 493 (1977), A Janner and T Janssen, Phys Rev B **15**, 643 (1977), P M de Wolff, T Janssen, and A Janner, Acta Crystallogr, Sect A **37**, 625 (1981)

[14]T Janssen, to be published

[15]F C Frank, Discuss Faraday Soc **5**, 48 (1949)

[16]W J P van Enckevort, Prog Cryst Growth Charact **9**, 1 (1984)

[17]K Tsukamoto, J Cryst Growth **61**, 199 (1983)

[18]B Dam and W J P van Enckevort, J Cryst Growth **69**, 306 (1984)

[19]K Tsukamoto and I Sunaguwa, J Cryst Growth **71**, 183 (1985)

[20]B Dam, E Polman, and W J P van Enckevort, in *Industrial Crystallization 84*, edited by S J Jancic and E J de Jong (Elsevier, Amsterdam, 1984), p 97

[21]N Cabrera and M M Levine, Philos Mag **1**, 450 (1956), B van der Hoek, J P van der Eerden, and P Bennema, J Cryst Growth **56**, 621 (1982)

[22]B van der Hoek, W J P van Enckevort, and W H van der Linden, J Cryst Growth **61**, 181 (1983)

Crystal Form and Surface Morphology of Modulated β-K_2SO_4-type Structures

B. Dam and P. Bennema

RIM, Laboratory of Solid State Chemistry,
Faculty of Science, Catholic University of Nijmegen,
Toernooiveld, NL-6525 ED Nijmegen, The Netherlands.

Abstract

The morphological consequences of a displacive modulation of the $((CH_3)_4N)_2ZnCl_4$ crystal structure are investigated. The morphology can be divided in a main part, relatively unperturbed by the properties of the modulation wave, and the so-called satellite morphology. On the main faces the surface morphology appeared to remain unaffected by the successive changes of the modulation wave vector in dependence of temperature. Optical goniometry suggests a continuous orientation change of the satellite faces with respect to the main morphology upon a change of the modulation wave vector $\vec{q}$. The corresponding surface morphological changes have been studied by in-situ optical microscopy. The satellite $(10\bar{1}2)$-surface is observed to behave as a flat F-face. We suggest the stabilization of certain step-trains by the modulation wave to be responsible for this F-face behaviour.

I. Introduction

In the study of crystal form the attention has gradually shifted from the crystal bulk structure to an analyis of the crystal surface structure. On one hand surface reconstruction is extensively studied [1], whereas on the other hand a lot of effort is spent on the roughening of the solid-liquid interface [2]. Still, the 3D-crystal structure is of utmost importance for the crystal form. The crystal form allows in principle for the determination of unit-cell constants and, in fortitious cases, even of the crystal space group. In the history of classical morphology the role of superstructures on the crystal form has been almost totally neglected. Partly this may be due to the fact that satellite reflections were interpreted in terms

of a superstructure at a time when classical morphological crystallography was already getting out of fashion [3].

In 1980, a 4-index approach to the description of the morphology of the so-called modulated structures was introduced [4]. This paper was followed by two others, showing the innate connection between the length and symmetry of periodic structural displacement waves and crystal form [5,6]. In the one-dimensional modulated case the modulation wave vector $\vec{q}=\alpha\vec{a}^*+\beta\vec{b}^*+\gamma\vec{c}^*$ can be added as a fourth basic vector to the three recipocal basic vectors of the undistorted unit-cell: $\vec{a}^*,\vec{b}^*,\vec{c}^*$. Then the crystal faces can be indicated by the integers (hklm), the indices of the new face normals $\vec{k}=h\vec{a}^*+k\vec{b}^*+l\vec{c}^*+m\vec{q}$.

The four index method to describe the morphology of modulated crystals corresponds to the four indices describing the diffraction pattern of incommensurate crystals, which lead to the superspace approach introduced for these substances by De Wolff, Janner and Janssen [7-9]. The wave vectors $\vec{k}$ describing the Fourier density waves of a one-dimensional modulated crystal can be expressed as integral linear combinations of (3+1) basic vectors. The same basic vectors of course are used in our morphological description and the indices hklm indicate the wave vectors of the Fourier matter density wave fronts parallel to the crystal face surface. Irrespective of the fact whether the length of $\vec{q}$ fits with the basic lattice or not (the commensurate and the incommensurate case respectively), crystal faces of modulated structures can thus be indicated by four low integers.

The main faces (hkl0) whose orientation is not affected by the appearance of a structural modulation, can be distinguished from the satellite faces (hklm). The latter are only present in modulated crystal phases and change in orientation with respect to (hkl0) upon any change of $\vec{q}$. If $\vec{q}$ changes continuously with temperature (as is often the case in incommensurate phases) a continuous orientational change of the (hklm) faces is to be expected.

Such a continuous behaviour would be clearly in conflict with present theories on the stability of crystal faces such as the PBC [10] and connected net analyses [11], currently used to describe the stability of normal, main faces. Even the Bravais concept of the morphological importance (MI) of lattice planes with a high reticular density is completely lost. The question then arises whether satellite faces must be considered to be fundamentally different from main faces. Do satellite faces differ from F-faces which are defined as faces with a roughening temperature larger than zero K, i.e. with an non-zero edge free energy [12]?

These questions on the nature of satellite faces have been studied by in-situ microscopy. In a preliminary communication [13] we already reported the occurrence of growth spirals, etch pits and so-called hollow cores on the $(10\bar{1}\bar{2})$ satellite face of $((CH_3)_4N)_2ZnCl_4$, here denoted as TMA-ZC, in its commensurate and incommensurate phases. Thus it was suggested that in each phase, commensurate or incommensurate, the edge free energy on this satellite face is larger than zero. Secondly, at the commensurate-commensurate phase transition characterized by an abrupt change of $\vec{q}$ from $2/5\vec{c}^*$ to $1/3\vec{c}^*$, the roughening of the corresponding $(10\bar{1}\bar{2})$ satellite orientation was observed. Though the bonding nature of the satellite faces is still unclear these observations support the idea that they behave indeed as stable F-face orientations.

In this article we intend to give a general overview on the morphological consequences of structural modulations for modulated K_2SO_4-type structures, concentrating mainly on TMA-ZC. First we will show that the position of a satellite face on $((CH_3)_4N)_2ZnCl_4$ can be monitored as a function of temperature. The results suggest indeed a continuous orientational change. Secondly, surface morphological features on both main faces and the $(10\bar{1}\bar{2})$-satellite face will be analysed. A qualitative model for the stability of the satellite faces will be given.

The derivation of laws governing the appearance of satellite faces might be important to derive a kind of perturbative approach to the morphology of complicated crystal structures. The latter will be the topic of a forthcoming communication [14].

II. Structure and Crystal Form

II-1 Modulated β-K_2SO_4-type structures

Previously several satellite faces were identified on Rb_2ZnBr_4 [4], called RZB here, and TMA-ZC [6] single crystalline spheres, which had been grown at the temperatures of their modulated phases.

These modulated structures essentially have the same basic β-K_2SO_4-type structure in common. Superposed on the undistorted structure (spacegroup Pcmn) is a displacive modulation with a wave vector $\vec{q}=\gamma\vec{c}^*$. This wave vector attains several commensurate and incommensurate values.

In RZB $\vec{q}$ is incommensurate (γ 0.29) for T<355K before it locks in to $\gamma=1/3$ at T=193K, the ferroelectric commensurate phase [15].

In TMA-ZC the sequence is more complicated. Up to six modulated phases have been identified now. Most important here are the first three modulated phases immediately below the para phase, see table I.

The various phases of $((CH_3)_4N)_2ZnCl_4$			
IV	III	II	I
q=1/3c*	q=2/5c*	q=0.42c*	para
T>181K	T>276.5K	T>279K	T>293K
$P112_1/n$	$Pc2_1n$	?	Pcmn

Table I: The various phases of TMA-ZC between 0-30°C [16,17]. The wave vector $\vec{q}$ is taken along the pseudo-hexagonal c-axis, the polarization along the shortest axis $\vec{b}$.

It has been shown [6] that the morphology in all these four phases can be described by one superspace group $Pcmn(1s\bar{1})$ (see De Wolff [18] for 4D groups and their extinction conditions). This group consistently describes both the commensurate phases and the incommensurate phase in one supergroup-group framework. Even phase IV, being monoclinic, still has a pseudo-orthorhombic lattice. The deviation of γ from 90° is very small (γ=90.1 at T=263K [16]) and can be seen as a symmetry breaking: the superspace group requiring an orthorhombic lattice which is not imposed by any of the elements of the 3D-space group. In particular the superspace group mentioned above predicts an extinction condition (h0lm; m=2n) which is not required by any of the 3D-groups describing the commensurate superstructures. This extinction condition was actually found in the TMA-ZC morphology [6].

It was shown also that the morphology of TMA-ZC can be separated in a main and a satellite part. The main part was found to be hardly affected by the modulation wave in any of the three observed modulated phases (II-IV). In contrast, the orientation and the morphological importance (MI) of the six identified satellite faces were strongly $\vec{q}$-dependent. In general the MI of the satellite faces is smaller than the MI of main faces. Usually only with an optical goniometer the satellite orientations manifest themselves as weak but distinct reflections.

The incommensurate diffraction pattern of TMA-ZC is characterized by a continuous shift in position of the satellite diffraction spots with respect to the main spots as a function of temperature. This reflects a continuous change in the length of the modulation wave λ,

the distance between main and satellite spots being equivalent to $\vec{q}=\vec{c}^*/\lambda$.

In the following sections we concentrate on the orientational behaviour of the strongest satellite face $(101\bar{2})$. The temperature dependance of the length of the modulation wave length is found to result in an orientational shift of the satellite face. In chapter III the corresponding changes of the surface morpology of both the $(101\bar{2})$ and some main (hkl0) faces will be analysed.

II-2. Morphological determination of $\vec{q}$

II-2-1. Experimental procedure

The orientation of the $(101\bar{2})$ satellite face as a function of temperature has been measured as follows. A large single crystal of about $2x1x1cm^3$ was grown in the para-phase at 30°C from a supersaturated, slightly acidified solution. After cutting a crystal slice approximately along $(101\bar{2})$ and polishing it with a soft slightly wetted tissue, this slice is grown for about one day in a thermostated, slightly supersaturated solution at temperatures ranging from 25 to 1°C. Upon growth the initially polished crystal surface develops into small isles of satellite faces bounded partly by strong main faces. The orientation of the satellite face can then be measured quite accurately with respect to these main faces by optical goniometry. Only when the slice is grown at low supersaturation a sharp reflection is obtained.

This method is more accurate than growing crystalline spheres, which on the other hand has the advantage that in principle all crystal orientations get an equal chance to develop. Using a crystal slice one, so to speak, encourages a certain direction to develop and the goniometer reflection of an orientation parallel to the slice improves accordingly. In principle orientations can be obtained within 10′, in practice, given the quality of the satellite surface, one obtaines angles at least within ±20′; also the reproducibility lies whithin these limits.

II-2-2 Results

As in our case $\vec{q}=\gamma\vec{c}^*$, the relation between ϕ (the angle between [001] and [holm]) and $\vec{q}$ is simply given by:

$$\tan\phi = ha^*/(l+m\gamma)c^* \qquad (1)$$

Below 15°C the first weak $(101\bar{2})$ satellite reflection was measured.

The intensity of the reflection increases gradually upon lowering the temperature. In fig.1 the morphologically obtained values for γ are plotted. The plot is quite comparable with X-ray and neutron studies by Almairac et al.[17] and Marion et al.[19] respectively. Two plateaus of constant $\vec{q}$ can be discerned at $\vec{q}=1/3$ and $\vec{q}=2/5$. Our transition temperatures and values for γ deviate somewhat from theirs but this is not uncommon for this class of compounds and is generally ascribed to the effects of defects and impurities [20]. The transition temperatures which are found to lie around 6 and 4 °C respectively, can not be determined with higher accuracy as the reflection is not so sharp at the transition.

The error bars indicated correspond to the maximum angular spread of ±20′. It is clear that the orientation of the incommensurate satellite orientation differs significantly from the one corresponding to $\vec{q}=2/5$. In addition significant orientational shifts can be observed within the incommensurate $\gamma=2/5$ phase, suggesting indeed a continuous behaviour of the satellite orientation.

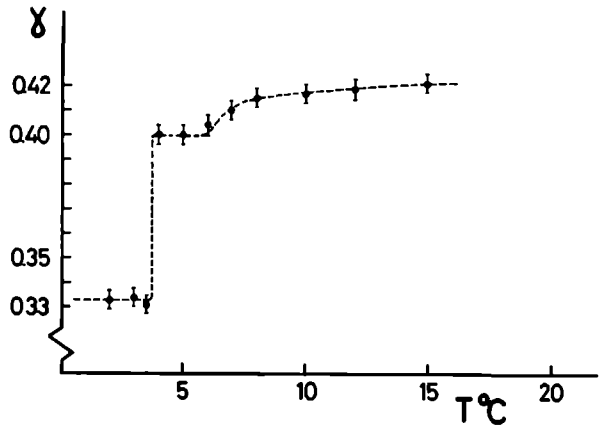

Fig.1 Morfological determination of the temperature dependence of the TMA-ZC wave vector $\vec{q}=\gamma\vec{c}^*$, as measured by optical goniometry.

The surface orientation was found to resist fast temperature changes. The equilibrium orientation is obtained only after a growth time of about 12-24 hours.

This extraordinary behaviour of the satellite face once more stresses that in addition to the lattice periodicity also the periodicity of a displacive modulation plays an important role in crystal morphology. Note that the amplitude of such a modulation wave typically lies in the order of 0.1-0.5 Å [21].

To gain a deeper insight in what structurally happens at the crystal surface during these phase transitions, we will now turn to the surface morphology of modulated crystals.

III. Surface morphology

III-1 Experimental procedure

The in-situ experiments were performed with an Olympus Vanox optical reflection microscope using oblique illumination and conventional optics. The apparatus has been described before [22] and follows from the methods introduced by Tsukamoto [23,24] and Van Enckevort [25].

Again, the crystal plate is sawn from a large single crystal grown at 30°C. The slice, roughly oriented along $(10\bar{1}2)$, is placed in a thermostated stagnant solution growth cell [26]. Close to the crystal surface the temperature of the solution is measured with a plastic-coated thermo-couple. The microscope image is recorded on video tape using an analogue contrast amplifier. With this system step heights of the order of 100Å can be observed [27].

III-2 The surface morphology of the main $((CH_3)_4N)_2ZnCl_4$ faces

As remarked above in the section on crystal form, the TMA-ZC main faces (hk10) remain relatively unperturbed at the advent of structural modulations. By definition the distance between equivalent lattice planes, $d_{(hk10)}=\vec{k}^{-1}$, is not affected by a change of $\vec{q}$. Structurally, the only change upon superstructure formation is the increase of the surface area of the 2D unit mesh of these main faces. In the incommensurate case of course it is impossible to speak of a unit mesh: it is infinite.

Still it was disappointing to find in our microscopical investigation that even the crystal surface does not reveal any effects that can be related to the modulation wave. Circular growth spirals and etch pits were found but nothing happened to them at the phase transitions; no change in step height, step distance or step kinetics was observed. Not even on (0010). This face has a dual character as it is normal to the modulation wave vector and can also be seen as a satellite face (0001).

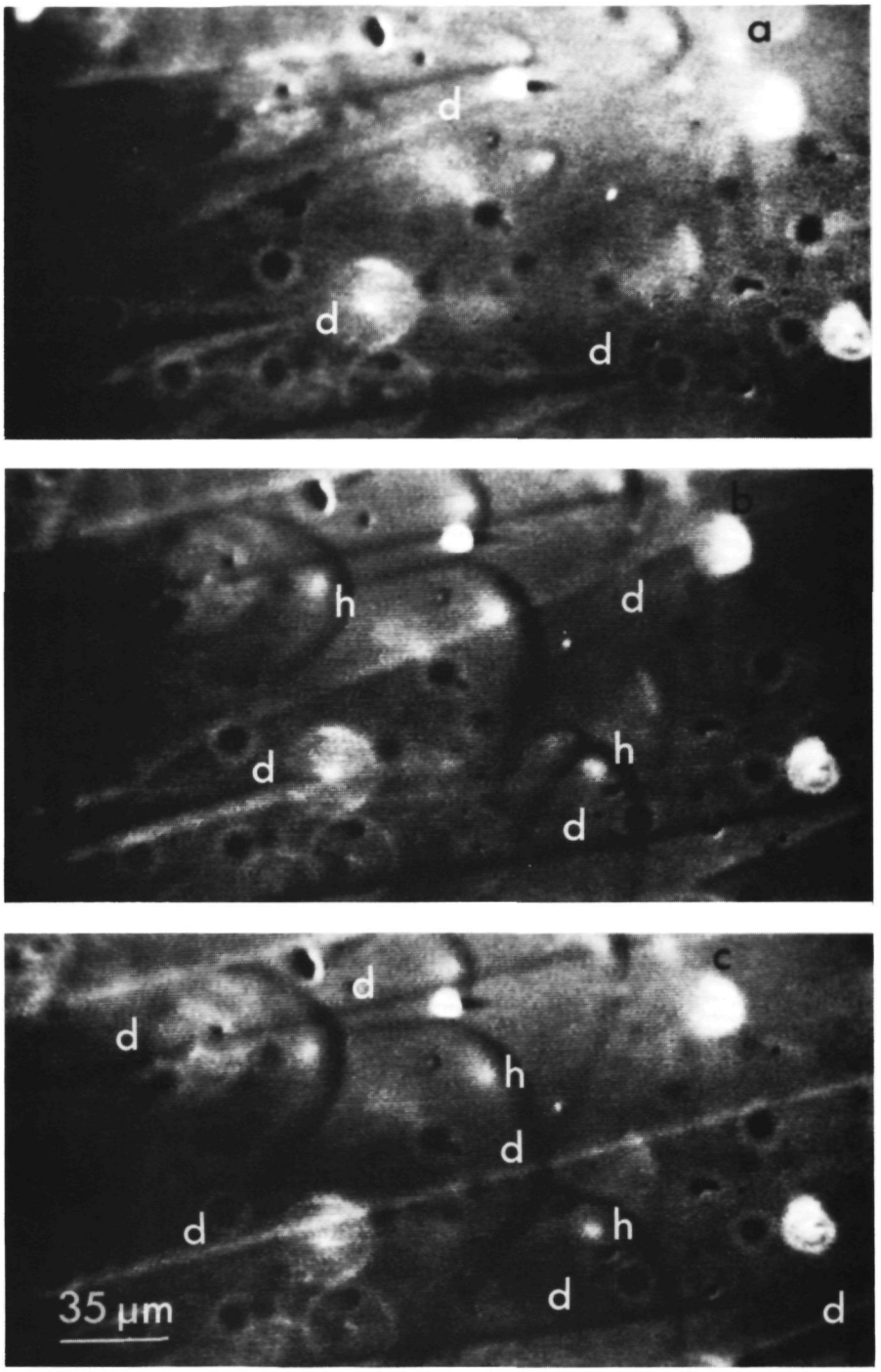
a
d
d
d
b
h
d
d
h
d
c
d
d
h
d
d
h
d
d
35 µm

Fig.2. Surface effects of monoclinic domain formation observed on TMA-ZC (0100) between 3.5 and 3 °C. a)Domain walls 'd' proceeding from left to right b)Roof-type surface structure develops c)stable configuration after re-arrangement. Growth hillocks are indicated as 'h'.

The only interesting effect observed is not due to the modulation wave but rather to the symmetry breaking in phase IV. On all but the faces lying in the [010]-zone we observed what we deduce to be the effect of the monoclinic domain formation. At T=3.4°C suddenly lines are formed which divide the surface into parallel strips of 20-50μm. As the crystal transforms to the monoclinic phase at this temperature, we suspect these strips to be the macroscopic result of the changes of the unit-cell parameters at this transition. Upon the monoclinic transformation at least two types of domains will be formed with a monoclinic angle $\gamma=90\pm0.1°$. Presuming a reorientation of the b-axis, all surfaces not lying in the [010]-zone, will break up in a kind of roof-type structure. Hence the observed lines must be twin boundaries deviding different surface inclinations corresponding to two types of domains. In fig.2 the successive stages of this process are shown. Twin boundaries oriented parallel $\vec{c}$ advance from left to right and after rearrangement divide the surface in strips of inclined surfaces. A small hysteresis was observed as the lines only disappeared when increasing the temperature to T=3.8°C. At the transition the twin-planes become very mobile and the surface fastly transformes back to its initial flatness.

Step advancement was not found to be hindered by this break up of the crystal surface.

Monoclinic domain formation in this phase was obseved earlier by Mashiyama et al. [28] using polarization microscopy. They found domain walls both parallel to a-c and to b-c. This seems to be at variance with our observation. It might be possible that only one of the two domains relaxes at the surface.

A surface feature that we could not quite interpret is the occurrence of large holes of about 5-10μm in diameter. Their radius is not very sensitive to the supersaturation and, in contrast to our observations on the main (2010)-surface of Rb_2ZnCl_4, they did not emit spiral steps.

III-3 The surface morphology of the (2010) main face of Rb_2ZnCl_4

Also the main faces of Rb_2ZnCl_4 (RZC) were investigated in our in-situ study. This compound is iso-structural with RZB. Incommensurability sets in below T=302K while the ferroelectric 1/3-phase is reached at T=192K [29]. Though RZC appeared to be less suitable for in-situ studies than TMA-ZC, one feature on (2010) was too impressive to remain unmentioned.

On the (2010) surface very large holes were observed with a typical diameter of again 5-10μm. Contrary to the ones observed on TMA-ZC, some of these holes were found to emit strongly bunched growth spirals, see fig.3. Moreover the radius of the hollow core could be decreased (or increased) somewhat by increasing (or decreasing) the supersaturation. Obviously one would interpret such a phenomenon as a hollow core and its growth spiral, which may develop around dislocations as described by Cabrera and Levine [30].

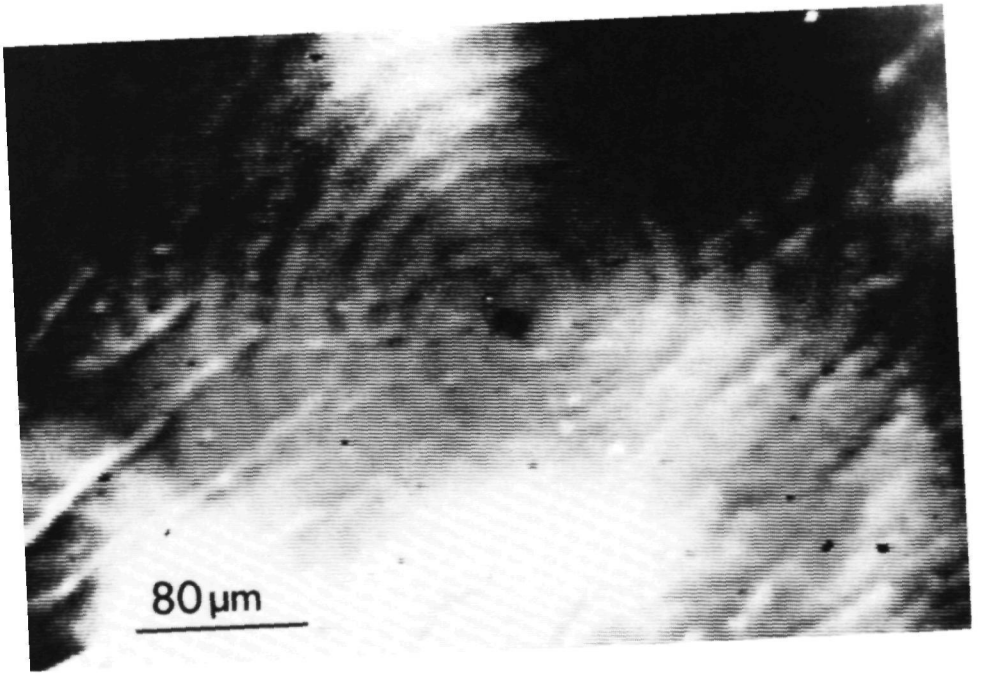

Fig.3
Meta-stable hollow core emitting bunched growth spiral on (2010) Rb_2ZnCl_4.

Such hollow cores are not commonly observed however on inorganic salts as their typical equilibrium radius should be at least one or two orders of magnitude smaller. For a pure screw dislocation Cabrera and Levine [30] give as the equilibrium radius:

$$r_0 = \frac{\mu b^2}{8\pi^2 \gamma} \qquad (2)$$

with μ being the shear modulus and b the dislocation Burgers vector. The surface free energy of the hollow core γ in this equation is supposed to be equal to the edge free energy of a nucleus on the surface. From e.g. the data summarized by Van der Hoek [31] for these parameters one easily calculates that on alum hollow cores will have a radius of ~100-1000Å, i.e. below the detection limit of optical microscopy.

Once, growing for sometime while slowly increasing the supersaturation, suddenly the hollow core was found to collaps instead of the slow closing down one would expect. The core was filled, while the spiral kept rotating as if nothing had happened. Dislocation splitting could be a possible cause for this effect. Only edge type dislocations should have bent away then, otherwise a change in the spiral behaviour would be expected. It is more probable that this hollow core was a meta-stable one probably formed upon the closing of an inclusion. In an X-ray diffraction-stress birefringence study on alum Van Enckevort [32] beautifully demonstrated the relation between hollow tubes followed by series of inclusions and the dislocation line connecting them. The formation of the tube and the inclusions are thought to be due to diffusion problems arising when step bunches are retarded around a dislocation outcrop. The fact that the core radius sometimes kept the same value while the supersaturation was varied, justifies the view that these cores cannot have their equilibrium radii.

On the other hand nothing is known yet on the strain fields of dislocations in incommensurate crystals and different strain properties are to be expected. Only one Lang-topograhic investigation has been published on the defect structure of TMA-ZC [33]. However, nothing was reported on the changes in the Burgers vector of the dislocations upon the onset of the modulation.

Looking only at the screw component of a dislocation one easily recognizes that generally to those with $\vec{b}=\vec{k}(hk10)^{-1}$ an extra stress term should be added. The length of such a Burgers vector does not depend on $\vec{q}$. However, as soon as $\vec{b}$ is not parallel to $\vec{q}$ a phase-shift of the modulation wave has to be accounted for. While connecting neighbouring lattice planes a phase jump of the modulation wave occurs normal to $\vec{b}$. Burgers vectors along a $\vec{k}(hklm)$ suffer both from an

increase in layer thickness (and hence of Burgers vector length) and from a phase shift.

Concluding we note that neither on TMA-ZC nor on RZC main faces we found any evidence for large, stable hollow cores.

IV Surface morphology of the TMA-ZC $(10\bar{1}2)$-satellite face

IV-1 Growth spirals and etch pits

It was already reported in a preceding letter [13] that in all three phases growth spirals and etch pits can be observed on the $(10\bar{1}2)$ satellite face. Here, we intend to treat the surface morphology of this satellite face in more detail.

The growth spirals become especially visible at low supersaturation, appearing in a strongly bunched, slowly rotating fashion. This bunching at low supersaturation might be an impurity effect as at higher supersaturation the bunches loose coherency while their rotation increases enormously. The etch pits obtained at dissolution persist on further etching and are concluded to be dislocation etch pits. Usually we did not find any correspondence between etch pits and growth hillocks. Probably this is due to the fact that etch pits are roughly proportional in strength to the Burgers vector of the dislocation, whereas growth centres are mostly strongest around Burgers vectors of unit length. Moreover always more etch pits than growth hillocks will be formed as the latter are only formed around dislocations with a screw component of the Burgers vector normal to the crystal surface.

IV-2 Stable hollow cores

Apart from the observation of layer growth and etch pits, which both indicate the F-face character of the satellite surface, it is worthwile to mention the frequent occurrence of large stable hollow cores. A correspondence exists between these holes observed during growth and the pits formed around them upon etching. In fig.4 these holes can be seen as white dots. Upon lowering the supersaturation the number of dots gradually increases along with a global increase of their radius. At equilibrium the maximum radius is reached and upon etching the hollow cores immediately open up to form the etch pits. These hollow cores were found in all three modulated phases. The equilibrium radius being always of the order of 5μm.

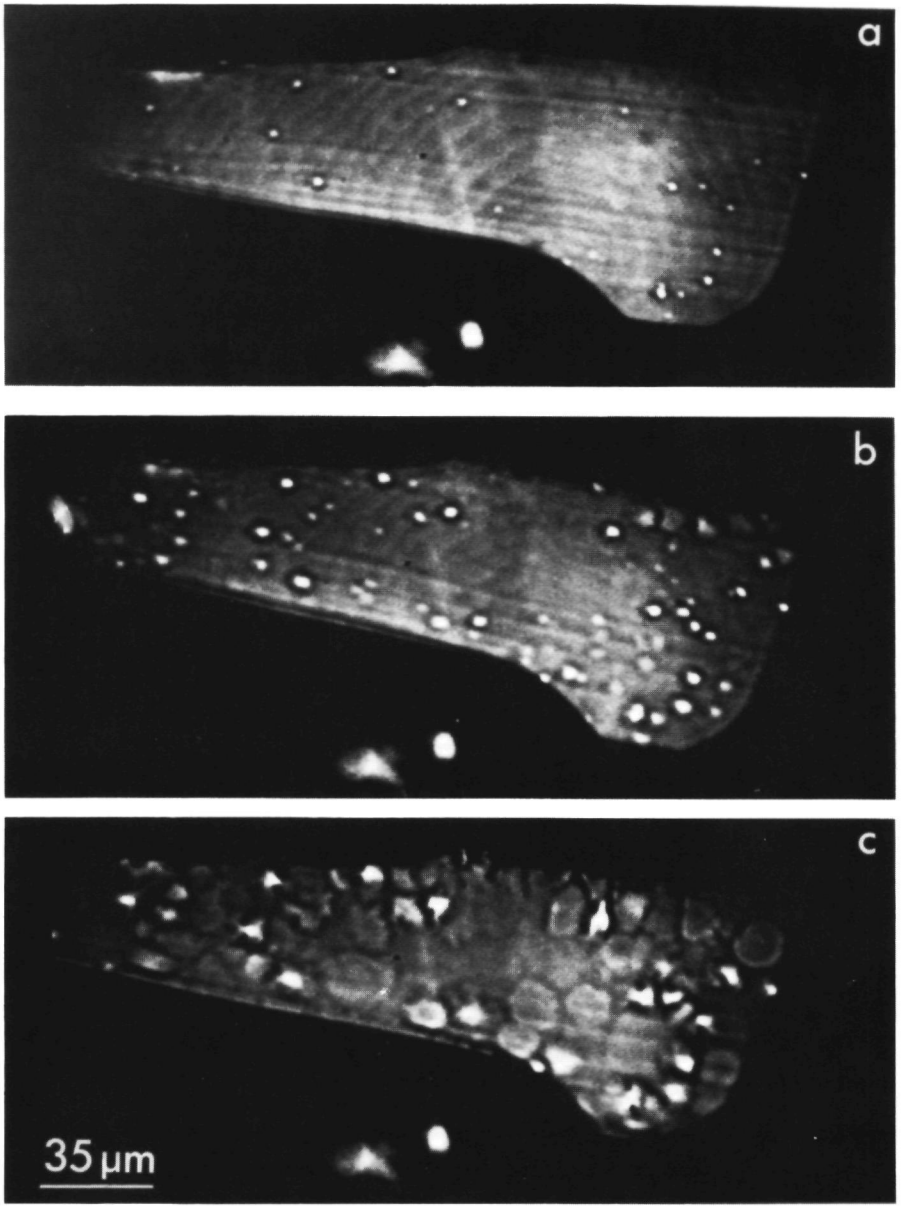

Fig.4 Sequence showing stable hollow core formation on $(10\bar{1}2)$ facet of TMA-ZC. a) growth spiral and some hollow cores b) approaching equilibrium: more hollow cores and an increase in radius c) etchpit formation during dissolution.

Contrary to the holes observed on the main faces, in this case no irreversible effects appeared and we believe the holes to be real stable hollow cores. Nevertheless, non of these hollow cores was found to emit growth steps.

According to recently developed theories on the occurrence of stable hollow cores by the stress field of dislocations [34,35], the radius of a hollow core r_{hc} is generally given by:

$$r_{hc}=r_0\ f(\frac{\Delta\mu}{kT}) \tag{3}$$

The function $f(\frac{\Delta\mu}{kT})$ is monotonically decreasing function of the driving force of crystallization, where $\Delta\mu$ is the difference of the chemical potential of the solute and the solid particles. Qualitatively we see that our hollow cores behave as they should according to equation (3). Assuming for the moment that eqn.(3) is valid for this situation and keeping in mind that the stable hollow cores are only found on the satellite surface and not on any of the main surfaces, we will discuss two causes for the anomalous hollow core radius:

1) An anomalous behaviour of the stress field of the dislocations emerging at this surface.

2) An extremely low edge free energy of the satellite surface.

As we have seen in section III-3 the behaviour of dislocations in modulated structures is rather complicated. Dislocations with an extremely large stress field can not be excluded. As the cores are never found to emit spirals one is tempted to link the cores to anomalous edge dislocations. On the other hand it is known from theory [35] that spiral centres with a high Burgers vectors have a lower angular velocity and produce a lower flux of steps than spirals originating from smaller Burgers vectors. Thus, such a weak step source might be easily overwhelmed by other, stronger step sources. Regarding point 2, the edge free energy of a satellite face certainly must be low. This is indicated by the fact that the morphological importance of these faces is very low on TMA-ZC. Moreover the disappearance of satellite faces at higher supersaturation is possibly due to kinetical roughening, which is only possible when the equilibrium edge free energy is low. Concluding, we can not distinguish between the two effects. The study of the properties of dislocations in TMA-ZC and the study of the kinetical roughening on $(10\bar{1}2)$ would be a very promising tool to gain a deeper understanding of the structural nature of the satellite surfaces.

IV-2 The phase transitions

IV-2-1. The III-IV transition

In the preceding letter [13] we concentrated on the surface effects at the III-IV transition. A roughening transition was observed. Contrary to the normal sense in which this term is used, the roughening reported there was not due to a temperature effect but resulted from a change in structure. The structural change makes the old satellite orientation instable in the new phase. From the coexistence of rough and flat surface parts, we concluded the transition to be of first order character. As the features of the transition were seen to depend strongly on the surface involved, we suggested a surface phase transition triggered by the changes in the bulk structure.

At the II-III transition the orientational changes are not so dramatic and more subtle effects are to be expected. Here we will show that the surface morphology of the $(10\bar{1}2)$ face might give a clue to the continuous adjustment to the modulation wave length.

IV-2-2. The II-III transition

At the incommensurate-commensurate II-III transition no dramatic surface changes were found. In fact we could not distinguish between changes within the incommensurate phase and the phase transition itself. Very often however straight lines parallel to [010], i.e. normal to $\vec{q}$, were observed especially in the incommensurate phase. Such lines can be seen vaguely on fig.4 and more ponounced on fig.5. These lines were formed in particular at a change of temperature. They gradually develop, but are hardly ever seen to move. The spiral steps pass them as if they are thick immobile bunches. The nature of these bunches was not immediately clear, they were found both in the incommensurate as well as in the commensurate 2/5 phase. Their thickness seemed to depend only on the temperature changes applied. To check the influence of any bulk effects we dissolved the bunched surface a bit. On the etched surface no lines were observed. Only after regrowing the surface, the lines reappeared though at different positions. The only way to get rid of the lines was to keep the temperature stable or to grow and observe the crystal slice only in the commensurate 2/5-phase. In the latter case only a few lines are formed which are not affected by temperature changes as long as one stays within the commensurate phase.

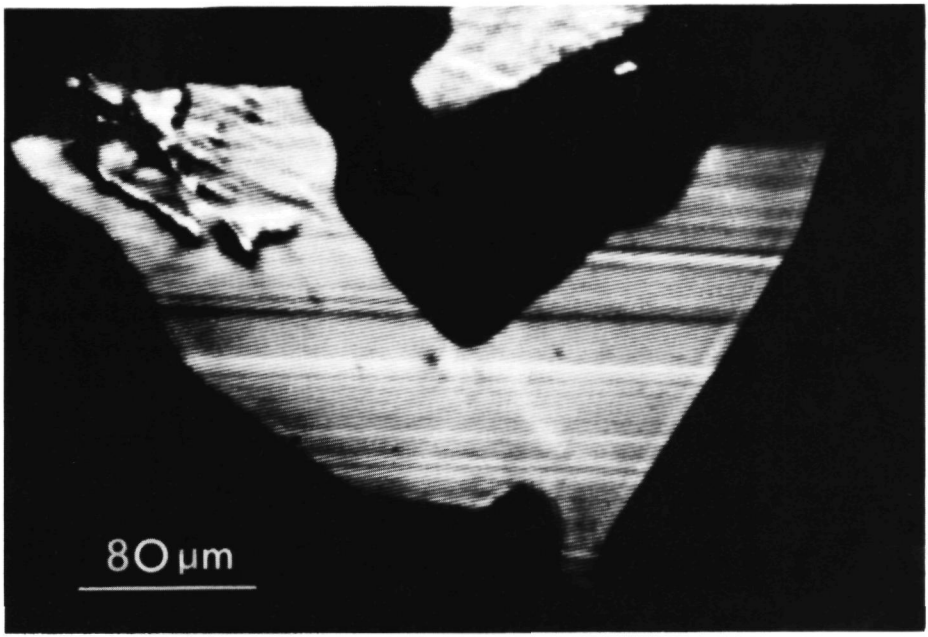

Fig.5. Immobile bunches ('discommensurations') on $(10\bar{1}2)$ TMA-ZC.

Combining our observations on the behaviour of these lines with the orientational changes plotted in fig.1, we conclude that the bunches may accomodate steps which have become superfluous at an orientational change of the satellite surface. Such a behaviour would be in accodance with a 'stabilized step' model describing the stability of satellite faces.

The stability of interacting stepped configurations has received an increased attention lately, after being introduced already in 1965 by Landau [36]. Normally stepped orientations are not thermodynamically stable and have a roughening temperature T_c=0K. Various authors [37,38] now have shown that already weak step-step interactions lead to substantial increase of the roughening temperatures T_c for whole families of stepped configurations.

Possibly, some of these orientations can profit from an interference with the periodicity of the modulation wave length, assuming that the step free energy will become function of the step postition on the surface plane. E.g. for $\vec{q}=\gamma\vec{c}^*$ a stepped (100) surface will be extra stabilized for orientations formed by a regular array of steps along $\vec{c}$ with a spacing of $1/\vec{q}$.

Imagine now what will happen at a change of $\vec{q}$. Steps will have to rearrange untill they have found their new equilibrium positions with respect to the modulation wave. However, at first the average orientation of the facet is conserved and there will be an excess of steps. The excess of step energy can be reduced in two ways: either the steps reach the facet edge and form an F-face, or they merge into large macro-steps on the satellite surface. These macro-steps will have the orientation of a neighouring F-face. Their relative immobility can be understood if one realizes that such a main F-face orientation is of course less rough than the satellite orientation and might even need some nucleation mechanism to proceed over the satellite crystal surface. It remains difficult to imagine how spiral steps are able to pass the macro-steps without being visibly affected and how these spiral steps differ from the ones constituting the macro-steps. Experimentally we are limited here by the fact that mono-layer steps cannot be observed.

Calculating the number of excess steps in this model at a 30′ change of the $(10\bar{1}2)$ satellite face (assuming this to be a stepped (100) surface), one arrives roughly at an excess of 3 steps per 1000 ledge positions. Hence, 300Å bunches spaced at 10 μm distance are expected, which corresponds in order of magnitude to our observations.

An orientational change of a satellite surface appears to be characterized by three stages:

1) Mono-layer steps rearrange to find their new equilibrium distances

2) Excess steps move towards the facet edges or form bunches

3) The bunches gradually disappear during growth, by emitting steps.

During the third stage the quality of the satellite reflection at the goniometer will gradually improve when the spacing between the bunches increases and their height diminishes. As long as the bunch spacing is too small no orientational change will be observable. The mechanism of the third stage is not understood.

Note, that the bunches can be considered as a kind of discommensurations [39], accomodating a phase shift to keep the other satellite surface parts in accordance with the phase of the modulation wave.

V Conclusion

New measurements on the temperature dependence of the satellite face orientation, once more show that it closely follows any change of $\vec{q}$, whether discrete of continuous. This is the first indication up to now that subtle displacive modulations manifest themselves also at the crystal surface. The surface morphology of the satellite faces suggest that its stability origins from a kind of stabilized step configuration, which is coupled to the periodicity of the modulation wave. Large stable hollow cores observed on the $(10\bar{1}2)$ satellite indicate that the edge free energy of these faces is much lower than the edge free energy on the main faces of TMA-ZC. It must be noted though, that the stress field of dislocations is badly understood in this class of compounds.

Apart from a monoclinic domain formation, which is secondary to the change in modulation wave length the main faces remain unperturbed.

Crystal morphology appears to be very sensitive for periodicities in the crystal structure; the morphology is not limited to the three periodicities of the ordinary space lattice only. Especially the surface structure of satellite faces deserves therefore further investigation.

Acknowledgements

We are indebted to A. Janner and M. Elwenspoek for their critical reading of the manuscript.

References

1) J.D. Weeks and G.H. Gilmer in: Advances in Chemical Physics Vol.XL. Eds. I. Prigogine and S.A. Rice (1979) 157.

2) W. Monch, Surf. Sci. 86 (1979) 672.

3) U. Dehlinger, Z. Kristallogr. 65 (1927) 615.

4) A. Janner, Th. Rasing, P. Bennema and W.H. van der Linden, Phys. Rev. Lett. 45 (1980) 1700.

5) B. Dam and A. Janner, Z. Kristallogr. 165 (1983) 247.

6) B. Dam and A. Janner, Acta Cryst. B, in press.

7) P. M. de Wolff, Acta Cryst. A33 (1977) 493.

8) A. Janner and T. Janssen, Acta Cryst. A36 (1980) 399; A36 (1980) 408.

9) A. Janner in: Symmetries and properties of non-rigid molecules: A comprehensive survey. Eds. J. Marnani and J. Serre (Elsevier, Amsterdam, 1983) Studies in Physical and Theoretical Chemistry, Vol. 23, p461-486.

10) P. Hartman in: Crystal Growth: an Introduction. Ed. P. Hartman (North-Holland, Amsterdam, 1973)p.367.

11) J.J.M. Rijpkema, H.F.J. Knops, P. Bennema and J.P. van der Eerden, J. Crystal Growth 61 (1982) 295.

12) J.P. van der Eerden, P.Bennema and T.A. Cherepanova, Progr. Crystal Growth Characterization 1 (1978) 219.

13) B. Dam, Phys. Rev. Lett. 55 (1985) 2806.

14) J.P. van der Eerden and B. Dam, work in progress.

15) C. J. de Pater and C. van Dijk, Phys Rev. B18 (1978) 1281.

16) S. Tanisaki and H. Mashiyama, J. Phys. Soc. Japan Lett. 48 (1980) 339.

17) R. Almairac, M. Ribet, J.W. Ribet and M. Bziouet, J. Physique Lett. 41 (1980) 315.

18) P.M. de Wolff, T. Janssen and A. Janner, Acta Cryst. A37 (1981) 625.

19) G. Marion, R. Almairac, J. Lefebvre and M. Ribet, J. Phys. C: Solid State Phys., 14 (1981) 3177.

20) H. Mashiyama, S. Tanisaki, K. Hamano, J. Phys. Soc. Japan 51 (1982) 2538.

21) A.C.R. Hogervorst, Conference Proceedings Int. Conf. on Phase Transformations in Solids.

22) L.A.M.J. Jetten, B. van der Hoek and W.J.P. van Enckevort, J. Crystal Growth 62 (1983) 603.

23) K. Tsukamoto, J. Crystal Growth 61 (1983) 199.

24) K. Tsukamoto and I. Sunagawa 71 (1985) 183

25) W.J.P. van Enckevort, Progr. Crystal Growth and Characterization 9 (1984) 1.

26) B. Dam, E. Polman and W.J.P. van Enckevort in: Industrial Crystallization 84, Eds. S.J. Jancic and E.J. de Jong (North-Holland, Amsterdam, 1984) p97.

27) B. Dam and W.J.P. van Enckevort J. Crystal Growth 69 (1984) 306.

28) H. Mashiyama, K. Hasebe, S. Tanisaki, J. Phys. Soc. Japan B49 (1980) 92.

29) S. Sawada, Y. Shiroishi, A. Yamamoto, M. Takashige, M. Matsuo, J. Phys. Soc. Japan 43 (1977) 2099.

30) N. Cabera and M.M. Levine, Phil. Mag. 1 (1956) 450.

31) B. van der Hoek, W.J.P. van Enckevort and W.H. van der Linden, J. Crystal Growth 61 (1983) 181.

32) W.J.P. van Enckevort and J. Odekerken, thesis (Nijmegen, 1982).

33) M. Ribet, J. Physique Lett. 44 (1983) L963.

34) B van der Hoek, J.P. van der Eerden and P. Bennema, J. Crystal Growth 56 (1982) 621.

35) B. van der Hoek, J.P. van der Eerden, P. Bennema and I. Sunagawa, J. Crystal Growth 58 (1982) 365.

36) L.D. Landau in: Collected papers of L.D. Landau, Ed. D. Ter Haar (Pergamon Press, Oxford) 540 (1965).

37) C. Rottman and M. Wortis, Physics Repts. 103 (1984) 59.

38) H. J. Schulz, J. Physique 46 (1985) 257.

39) W.L. McMillan, Phys. Rev. B14 (1976) 1496.

5. Calaverite: An anomaly resolved

Incommensurate Morphology of Calaverite ($AuTe_2$) Crystals

B Dam and A Janner

Research Institute for Materials Laboratory of Solid State Chemistry and Institute for Theoretical Physics Faculty of Science Catholic University of Nijmegen NL 6525 ED Nijmegen The Netherlands

and

J D H Donnay

Department of Geological Sciences McGill University Montreal H3A 2A7 Quebec Canada

(Received 19 July 1985)

The existence of large sized satellite faces on crystals of the mineral calaverite ($Au_{1-x}Ag_xTe_2$) is reported These anomalous high index faces can be related directly to the wave vector q of the displacive incommensurate modulation recently found in the crystal structure If we extend the classical morphological law of rational indices to include q as a fourth basic vector the high index faces can be described by four low integers ($hklm$)

PACS numbers 61 50 Em 61 50 Cj

In the past two centuries the determination of lattice parameters and crystal symmetry from the morphology of crystals has been a powerful research program The subsequent development of x-ray crystallography made this branch of crystallography go out of fashion Still, the persistence of a few anomalies deserves attention One of them is found in calaverite, which together with sylvanite and krennerite belongs to a class of related gold silver tellurides, calaverite contains up to 15-at % Ag In 1931 Goldschmidt, Palache, and Peacock[1] (GPP) published an extensive morphological research on calaverite, a mineral which had already puzzled the mineralogists during the preceding century After compiling the morphological data of 105 of the finest-quality single crystals found in nature, they were not able to give an adequate classical description of the morphology Though the crystal morphology allows for a $2/m$ point-group symmetry, only 10 out of the 92 crystal forms (i e , sets of symmetry-equivalent crystal faces $\{hkl\}$) constituting the rich morphology could be indexed as $\{hkl\}$'s with h, k, and l low integers After discarding all trivial error sources, such as twinning, GPP had to admit that inevitably the law of rational indices is not a general law This statement deprives crystallography of its historical basis!

The reason for the failure was sought in a badly understood "singular" crystal structure Four years later, one of us[2] (J D H D) tried to recover the validity of the law of rational indices by attempting to solve the problem in terms of a new type of twinning This paper was dubbed a "preliminary communication" and now, fifty years later, we all want to look at the problem from the point of view of incommensurability

As early as 1979 Sueno Kimata and Ohmasa[3] proposed a modulated structure for calaverite Their x-ray studies were followed by a number of electron-microscope studies on the $(Au,Ag)Te_2$ compounds[4] With use of pure $AuTe_2$ for calaverite, the electron-microscope diffraction pattern shows a beautiful series of satellite spots, which reveal the modulated incommensurate structure Around the main diffraction spots, satellites up to the sixth order could be observed The main diffraction spots are consistent with the $C2/m$ space group as determined earlier by Tunell and Pauling[5] The displacement of Au atoms along [010] forms the main contribution to the modulation wave The orientation of the modulation wave vector could not be determined precisely The diffraction pattern shows that it deviates slightly from $[202]^*$ and has a wavelength of $4.5 d_{202}$ Sylvanite ($AuAgTe_4$), on the other hand, appears to be commensurately modulated with $\lambda = 4 d_{202}$ Note that in the paper of Van Tendeloo, Gregoriades, and Amelinckx[4] a left handed coordinate system has been used With respect to the coordinate system defined by Tunell and Pauling adopted here, the direction of q is near $[\bar{2}02]^*$

Already in 1936 Tunell and Ksanda,[6] in a study of the x-ray diffraction pattern of calaverite, found some extra (so-called adventive) spots that could not be ascribed to the structural lattice They suggested a relation with the high index faces but did not go into any detail Here we intend to show that with the new structural information a large part of the morphology of calaverite can be described in a consistent way that shows a close connection between the crystal form and the periodic displacive modulation

In previous publications it has been shown that the morphology of modulated crystals is determined not only by the lattice periodicity of the average structure, but also by the additional periodicity of displacive modulation waves[7,8] By extending classical morphological laws, we can index a crystal face by four integers ($hklm$) indicating the Fourier wave vector $\mathbf{K} = h\mathbf{a}^* + k\mathbf{b}^* + l\mathbf{c}^* + m\mathbf{q}$ normal to it For $m \neq 0$ these Fourier vectors, which can be associated with satellite diffraction spots, explicitly reveal the relation

between the modulation wave and the satellite faces These observations can be consistently described in the superspace approach which was introduced for the characterization of the diffraction pattern of incommensurate crystals by de Wolff, Janner, and Janssen [9] In particular, from the absence of second-order satellites in the net plane of $h0l$ reflections reported by Van Tendeloo, Gregoriades, and Amelinckx,[4] it is possible to identify the superspace group of calaverite as $C2/m(\alpha,0,\gamma)(\bar{1}\ s)$ With the assumption that the three-dimensional part of the four-dimensional point group determines configurational morphology, the set of symmetry related faces, i e , the crystal form, is indicated by the braces of the $\{hklm\}$ symbol (in this case indicating a $2/m$ point-group symmetry)

From the morphology of Rb_2ZnBr_4 crystals grown in the incommensurate phase,[10] the relative length of the modulation wave could be determined from the orientation of the satellite faces $(hklm)$ with respect to the main faces $(hkl0)$ Furthermore, it appeared that for $[(CH_3)_4N]_4ZnCl_4$ one single superspace group characterizes the symmetry consistent with what is known about structure and morphology of its various modulated phases [11] In all these experiments, however, the observed satellite faces had very small sizes (up to a single one), and the limited number of observations prevented the testing of morphological laws

Quite different is the situation with calaverite, for which not less than 1849 very accurate observations have been made[1] on more than a hundred crystals involving 92 different forms, 82 of which appear to be of satellite character

The morphology as described by GPP can be reindexed in the following way As a basic lattice we take a pseudo-orthorhombic instead of a monoclinic lattice ($\beta = 90°12'$) The base vectors $a = 7.19$ Å, $b = 4.40$ Å, and $c = 5.07$ Å[4] were combined with a wave vector $q = \alpha a^* + \gamma c^*$ (with q near $[\bar{2}02]^*/4\ 5$) to span the "integer space" generated by the a^*, b^*, c^*, q of our $(hklm)$ indexing Reinterpreting in this way the very important "singular" face C, we arrive at $\{11\bar{1}2\}$ instead of GPP's high index $\{5\,2\,9\,\bar{3}\}$ In turn, on the basis of the experimentally observed orientation of C, this indexing allows for the refined determination of the modulation wave vector

$$q = [-0.4095 \quad ,0\ 0.4492 \quad] \sim [-0.41, 0, 0.45]$$

Many satellite forms $\{hklm\}$ can now be constructed by adding multiples m of q to the normal vectors of the so-called main forms $\{hkl0\}$, i e , those observed forms which can be indexed classically with three integers $\{hkl\}$, even in an incommensurate phase Here as main forms we take GPP's low-index forms, the so-called S forms listed in their Tabelle I In Table I the thus obtained satellite forms $\{hklm\}$ which are actually observed, are indicated by their index m with respect to the corresponding main forms $\{hkl0\}$ (neglecting for the moment possible superspace-group extinction conditions) The alphabetical description and the morphological importance (in parenthesis) given in GPP of the high-index faces is indicated in the last column

In this way 31 of the 82 high-index forms can be reinterpreted as $\{hklm\}$'s Satellite forms up to the sixth order [see, e g , $\{\bar{1}12\bar{6}\}$ or the Σ face] are found, and one observes from Table I a general tendency of the main forms to have more satellites the more morphologically important that they are On the other

TABLE I Reinterpretation of a part of Goldschmidt, Palache, and Peacock's high-index faces on calaverite The GPP symbol of the so-called main forms are given in column 1 Related to these main forms, which are reinterpreted as $\{hkl0\}$ in column 2, are the so-called satellite forms $\{hklm\}$ whose order m is indicated in column 3 The corresponding GPP symbol of these series of satellite faces is given in column 4 (e g , $h = \{3101\}$ and $g = \{1111\}$) Morphological importance (MI) is indicated in parentheses in terms of the number of times such a set of faces was found by GPP in their sample of 105 crystals

Main forms $\{hkl0\}$ GPP(MI)	$hkl0$	Related satellite forms $\{hklm\}$ m	GPP's letter (MI)
β(2)	3100	1 4	h(1) F(1)
f(3)	1120	−1 −3 −4	t(23) α(1) χ(1)
p(139)	1110	1 −1 −2 −3	g(17) d(19) ϕ(16) γ(1)
m(122)	1100	4 3 2 1 −1 −2	κ(2) G(4) ν(18) 0(131) θ(13) σ(1)
s(18)	$11\bar{2}0$	2 3 4 5 6	M(24) γ(39) τ(44) θ(11) Σ(1)
w(72)	$1\bar{1}10$	−1 1 2 3 4 5	ξ(6) u(65) C(103) r(50) W(22) Ξ(2)
b(5)	0100	2	Y(5)
a(14)	1000	1	ω (7)
c(5)	0010	−1 −2	A(60) E(57)
V(6)	$\bar{1}0\bar{1}0$	3	z (10)

hand, rare main forms such as {0010} can be surrounded by the frequently observed satellite faces $(001\bar{1}) = A$ and $(001\bar{2}) = E$

From Table I we can conclude that the stability of $\{hkl0\}$ is an important factor for the satellite morphology A restriction on m is that it be not too large an integer Finally, it can be seen that, around a single $\{hkl0\}$, the decreases of the morphologic importance (MI) with m is not linear, this observation suggests that $d_{\{hklm\}}$ too is a relevant morphological factor, despite the fact that the distance now is not one between net planes in a lattice, but one between fronts of Fourier matter waves

In Table II some few examples are given of comparison between the observed orientational angles (GPP) and those calculated on the basis of our h,k,l,m indexing for the parameter values given above The agreement is astonishing if one remembers that the crystals measured are native minerals This shows the power of classical crystallography, whose modern extension reveals how profound an effect subtle periodic lattice distortions of the microscopic structure can have on the macroscopic crystal morphology

The morphological importance of satellite faces is directly recognized on a drawing reproduced from GPP (Tafel X), which shows a twin comparison of a left-handed and a right-handed crystal Both main faces $(hkl0)$ and satellite faces $(hklm)$ can be found, when

TABLE II Examples of indexing calaverite crystal faces The letter symbol and the spherical angles ϕ_{obs} and ρ_{obs} are those reported by GPP in 1931 The calculated values are based on the $hklm$ indices in the last column and a modulation vector $\mathbf{q} = [-0\,41\,0\,0\,45]^*$

GPP symbol	ϕ_{obs}	ρ_{obs}	ϕ_{cal}	ρ_{cal}	$hklm$
C	−38°30	08°03	−38°13	07°58	$11\bar{1}2$
B	−57°05	90°00	−57°16	90°00	$000\bar{1}$
A	62°12	90°00	62°16	90°00	$001\bar{1}$
M	−83°36	44°00	−83°25	43°51	$11\bar{2}2$
u	−52°58	30°58	−52°53	30°54	$11\bar{1}2$

comparing GPP's lettering in Fig 1(a) with those in Fig 1(b) The enormous prismatic faces Λ, Π, and E show the morphological importance of satellite faces as habit-controlling factors Satellite faces Λ and Π can be described as $\Lambda = (20\bar{1}2)$ and $\Pi = (20\bar{1}4)$, the difference being that now $(20\bar{1}0)$ is not an observed main face In a subsequent paper it will be shown that the complete crystal morphology can be described in terms of combinations of four low indices $\{hklm\}$

In conclusion, it can be said that the classical law of rational indices still holds for incommensurate crystals, provided the correct number of indices is used (four in the case of calaverite) This reveals the sensitivity of

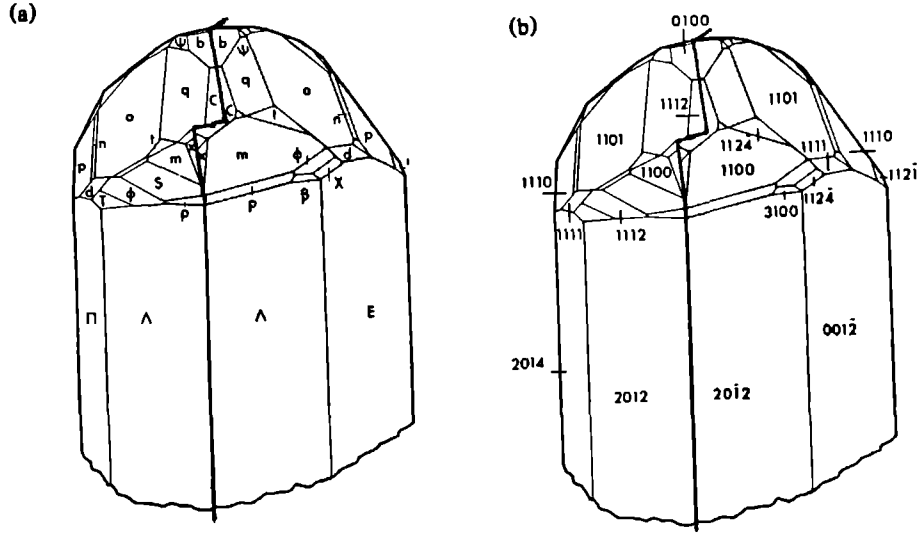

FIG 1 Copy of a drawing (Tafel X) by Goldschmidt, Palache, and Peacock of a calaverite twin showing large high index faces (a) Form letters according to GPP Some of the letters have been omitted for the sake of clarity (b) Reinterpretation in terms of four-index symbols using the modulation wave as a fourth basic periodicity

crystal morphology to the periodicity of atomic interactions After a closer analysis of the laws governing the appearance of satellite faces, we hope to get some idea about the nature of their microscopic structure Note however, that for an incommensurate satellite face the Bravais concept of a high reticular density of the parallel net plane is completely lost Thus the investigation of the surface of satellite faces opens a new field of experimental research.[12]

One of us (B D) acknowledges the critical comments and kind hospitality of Dr P G Embrey (British Museum) Part of this work is supported by The Netherlands Foundation for Pure Research (ZWO/SON).

[1]V Goldschmidt, Ch Palache, and M Peacock, Neues Jahrb Mineral Geol Palaeont , Ref , Beil Bd 63, 1 (1931)

[2]J D H Donnay, Ann Soc Geol Belg 18, B222 (1935)

[3]S Sueno, M Kimata, and M Ohmasa, in *Modulated Structures—1979* AIP Conference Proceedings No 53, edited by J M Cowley, J B Cohen M B Salamon, and B J Wuensch (American Institute of Physics, New York, 1979), p 333

[4]G Van Tendeloo P Gregoriades and S Amelinckx J Solid State Chem 50, 321 (1983), and 50, 335 (1983), and 53, 281 (1984)

[5]G Tunell and L Pauling, Acta Crystallogr 5, 375 (1952)

[6]G Tunell and C J Ksanda, J Wash Acad Sci 26, 507 (1936), and 26, 509 (1936)

[7]A Janner, Th Rasing, P Bennema, and W H van der Linden, Phys Rev Lett 45, 1700 (1980)

[8]B Dam, A Janner, P Bennema, W H van der Linden, and Th Raising, Phys Rev Lett 50, 849 (1982)

[9]P M De Wolff, Acta Crystallogr , Sect A 33, 493 (1977), A Janner and T Janssen, Phys Rev B 15, 643 (1977), P M de Wolff, T Janssen, and A Janner, Acta Crystallogr , Sect A 37, 625 (1981)

[10]B Dam and A Janner, Z Kristallogr 165, 247 (1983)

[11]B Dam and A Janner, Acta Crystallogr , Sect A (to be published)

[12]B Dam, Phys Rev Lett (to be published)

INCOMMENSURATE MORPHOLOGY OF CALAVERITE ($AuTe_2$) CRYSTALS, PART II

I Introduction

In the preceding letter [1] we offered a partial re-interpretation of the crystal morphology of calaverite, taking advantage of recent electron diffraction results of Van Tendeloo et al. [2]. Here, we will give a full re-interpretation of the morphology of this famous, anomalously behaving mineral. After an account of the morphological literature, as well as of the diffraction studies on calaverite, a four integer (hklm) identification is presented. Again the morphological data collected by Goldschmidt, Palache and Peacock [3], from now on indicated as GPP, serve as a basis for our approach.

The (hklm) notation, which uses only one set of basis vectors, proves to be consistent with GPP's interpretation, which uses at least four interprenetrating lattices.

The re-interpretation in terms of (hklm) is based on the recognition of a displacive modulation wave superimposed on a basic structure with a pseudo-orthorhombic lattice. But the basic structure itself can also be considered as modulated. In that case a modulation of composition describes the periodic ordening of gold and tellure layers in a primitve cubic lattice. This allows for a further simplification of the structure and morphology of calaverite.

II Historical review

II-1 Morphological investigations on calaverite

The first detailed morphological account of calaverite is given by Penfield in 1895 [4], after the mineral was first identified in 1868 by Genth [5]. The latter described the $(Au,Ag)Te_2$ compound as a soft, brittle substance without a well defined cleavage plane. Penfield describes the crystal morphology as essentially triclinic. His paper is rapidly followed by two extensive and detailed studies by Smith [6] and by Penfield and Ford (PF) [7]. These papers describe an amazing rich variety of forms of which only a few can be indexed with three small integers. From the low index forms both papers identify a monoclinic lattice with a 2/m point group symmetry. The cell constants of this pseudo-orthorhombic lattice (β=90.13 [7]) were found to bear a

remarkable similarity with the lattice of sylvanite, another $(Au,Ag)Te_2$-compound with an Ag/Au ratio of approximately 1. The configurational symmetry of the total morphology conformed to a 2/m point group. Penfield and Ford therefore chose the monoclinic lattice to describe the total crystal morphology though they have to admit: 'Die Krystalle scheinen geradezu einen Widerspruch gegen einige Gesetze der Krystallographie darzubieten'.

An alternative for the high indices necessary in the PF description to index all crystal forms, is given by Smith [6]. He examined a large number of crystals, which all show a pronounced prismatic habitus with many small crystal faces on top. The 135 crystal forms he distinguished forced him to assume at least three independent lattices (one monoclinic, two triclinic). To account for the monoclinic 2/m configurational symmetry of the crystal form, Smith assumes that the triclinic lattices are twinned bringing the total number of lattices to five: 'Thatsächlich scheinen fünf verschiedene Gitter da zu sein, welche incongruent, aber nich von einander unabhängig sind' [6]. Two other important statements from Smith are cited by PF: 'Unless, however, the crystals are regarded as triclinic twins it is impossible to obtain simple indices' and, as he did not find any re-entrant angles, 'there must be an extra-ordinarily intimate penetration'. In addition to this special kind of twinning Smith identified two new twin laws in addition to the one already reported by PF.

The dilemma of either giving up important crystallographic laws or assuming an otherwise indistinguishable twinning, occupied many crystallographers in the following 30 years. These efforts remained unpublished as they failed to reconcile the experimental evidence with the accepted laws of crystallography. Finally, all these efforts resulted in a joint paper by GPP, based on the morphological data of 105 crystals of finest quality. Confirming in essence the results of Smith and PF, GPP have to admit that it is not possible to choose an axis system such that the majority of forms can be described by simple rational indices. They resort to a description which applies not less than four distinct lattices, one monoclinic and three triclinic. And even this does not describe all forms satisfactorily. In the end the Law of Rational Indices is given up with the statement that: 'das Gesetz der Rationalen Indices () nicht ein algemeines Gesetz ist'. Only with an ad hoc extension of the law of complication GPP satisfy themselves with their four lattice description. They do not deal with the physical meaning of this extension, which seems to say nothing more than that the construction of four interprenetrating lattices is now allowed. The morphological literature on calaverite is temporarily concluded by a preliminary communication of Donnay [8] in

1935. He proposes a new kind of twinning, due to a deformation of the crystal structure. At the same time X-ray crystallography gradually takes over.

II-2 X-ray and electron diffraction studies on calaverite

The first Weissenberg photographs made by Tunell and Ksanda (TK) [9] confirm the monoclinic (sylvanite-like) lattice, as the structural one. Excluding any orthorhombic groups the C2/m space group is proposed. In a subsequent paper [10] the correspondence between the structural and the morphological unit cell is established. Also extra, so-called adventive diffraction spots are observed, which could not be ascribed to planes of the structural lattice, unless the monoclinic unit cell is enormously expanded. An attempt to correlate these adventive spots with the high index faces is only partly successful. The structure determination by Tunell and Pauling (1952) [11] confirms the formerly obtained space group, acknowledging that it disregards the extra diffraction spots. Recent work in 1984 by Pertlik [12] contradicts these results. He proposes a Pc or even a P1 space group; he does not mention the extra spots though. The Pc structure determination reflects, as he states, an average structure, which otherwise should be indicated by a P1 space group.

The modulated nature of calaverite is first acknowledged by Sueno et al. [13] in 1979. The adventive spots are characterized as satellite spots with a wave vector normal to the $(30\bar{4})$ lattice plane. Still, the structure is again interpreted in terms of a P1 space group and an enlarged supercell.

Shortly afterwards Van Tendeloo, Gregoriades and Amelinckx [2] present their impressive electron microscope high resolution images and the corresponding electron diffraction results. They confirm the Tunell and Pauling lattice as the basic one, on which a displacive incommensurate modulation of mainly the gold atoms along the b-axis is superposed. The basic unit cell of calaverite equals the one of sylvanite. The modulation being commensurate in the latter case: $\vec{q}$=[0.5 0 0.5]*, whereas in calaverite slight deviations in length and orientation yield: $\vec{q}$=[202]*/4.5.

The diffraction studies reviewed so far are rather confusing as far as the sign of the $\vec{a}$*-component in the q-vector is concerned. In our letter [1] we proposed on morphological arguments $\vec{q}$=[-0.41 0 0.45]*. Recent X-ray diffraction work by De Boer confirmed the sign of this direction [14].

III The morphology of calaverite

III-1 A re-interpretation

A large portion of the calaverite morphology was re-interpreted quite easily: Satellite face normals $\vec{k}(hklm)$ were obtained by adding $m\vec{q}$ to the $\vec{k}(hkl)$ normals of the main faces belonging to the monoclinic basic structure [1]. The face normals were described in terms of four integers $\vec{k}\ (hklm)=h\vec{a}^*+k\vec{b}^*+l\vec{c}^*+m\vec{q}$. On the basis of the accurate data supplied by GPP for C=no.3 we calculated for the modulation vector: $\vec{q}=[-0.4095..\ 0\ 0.4492..]^*$. From now on we again use the approximative value $\vec{q}=[-0.41\ 0\ 0.45]^*$ and a pseudo-orthorhombic instead of a monoclinic lattice to reinterpretate the remaining high index faces. This problem is not so straightforward and it is attacked here in two ways. First all ρ(obs) and ϕ(obs) spherical coordinates are transformed to (h1l) fractional indices. Then one adds $m\vec{q}$ to each of these fractional coordinates, until one is close enough to an integer coordinate of the basic reciprocal lattice. Though this (h110) coordinate, to be called 'origin' from now on, does not represent a face normal, still the satellite face can be indicated now as (h1lm). In order to keep m as low as possible (i.e. m<15) one is sometimes forced to assume that k≠1. The (hk10) origins are then of course found be adding $(m\vec{q})/k$ to the fractional coordinate of each satellite face.

The other approach is to make a list of all spatial coordinates of faces with h,k,l,m,<5. All but a few sattelite faces can then be identificated by comparing with the GPP list of spherical coordinates. Some ambiguities can be resolved by assuming that the satellites in a certain zone $\vec{k}(hklm)x\vec{q}$ will usually belong to one and the same (hk10) origin. The methods both yield surprisingly unique results because (hk10) origins have to be situated in the zone spanned by $\vec{k}(hklm)x\vec{q}$ and have to lie at a distance $m\vec{q}$ separated from $\vec{k}(hklm)$. Combining the two methods a re-interpretation covering all high index faces is presented in table I.

III-2 Discussion of Table I

All 92 forms are re-interpreted with respect to a single set of four base vectors, using only relatively small integers. Of course we admit that in a few cases the difference between the observed and calculated angles is a bit large, e.g. no.15,54,72,74,75. Also the high indices for m necessary in a few cases is a bit suspicious. Note, by the way, that these high values for m require a very accurate determination of $\vec{q}$, so that the angular deviations are not to surprisingly in these cases.

Table I

GPP Miller basis ABC			C_1-forms				hklm assignment	
no.	GPP	Miller	φ(obs)	ρ(obs)	Δφ	Δρ	hklm	MI
1	C	001	-38°30′	8°03′	17′	-05′	$11\bar{1}2$	103
2	B	010	-57 05	90 00	-11	00	$000\bar{1}$	48
3	A	100	62 12	90 00	04	00	$001\bar{1}$	60
4	E	110	9 50	90 00	-02	00	$001\bar{2}$	57
5	c	$1\bar{1}0$	89 54	90 00	06	00	0010	84
6	V	610	54 36	90 00	12	00	1010	4
7	l	103	20 34	11 46	-07	-05	$33\bar{2}5$	1
8	q	102	32 37	15 42	11	-03	$22\bar{1}3$	92
9	o	101	47 07	28 05	07	-05	1101	131
10	n	302	52 01	38 49	16	-20	2211	8
11	p	201	54 43	46 50	05	-07	1110	139
12	i	301	57 12	58 07	07	-10	$112\bar{1}$	23
13	L	$\bar{1}03$	-83 32	13 48	18	05	$33\bar{4}7$	2
14	Q	$\bar{1}02$	-92 53	18 10	12	-08	$22\bar{3}5$	7
15	y	$\bar{1}01$	-101 12	30 24	-2°48	-14	$11\bar{2}3$	39
16	P	$\bar{2}01$	-110 39	48 18	03	-15	$11\bar{3}4$	19
17	I	$\bar{3}01$	-113 01	58 49	06	-03	$11\bar{4}5$	2
18	u	011	-52 58	30 58	05	-04	$11\bar{1}1$	65
19	w	021	-54 58	46 49	10	-06	$11\bar{1}0$	72
20	ξ	031	-55 43	56 47	10	-02	$11\bar{1}\bar{1}$	6
21	r	$0\bar{1}1$	114 41	18 26	10	04	$11\bar{1}3$	50
22	W	$0\bar{2}1$	119 20	38 29	05	04	$11\bar{1}4$	22
23	Ξ	$0\bar{3}1$	120 21	51 21	17	13	$11\bar{1}5$	2
24	τ	122	-26 54	28 29	47	-02	$22\bar{1}1$	1
25	ι	$\bar{1}22$	-72 02	37 07	15	-07	$22\bar{3}3$	1
26	m	111	-0 04	31 30	04	-03	1100	122
27	θ	121	-24 33	43 32	12	-06	$110\bar{1}$	13
28	σ	131	-35 16	53 41	14	-01	$110\bar{2}$	1
29	v	$1\bar{1}1$	81 51	38 21	07	-06	1102	18
30	G	$1\bar{2}1$	96 46	49 36	05	07	1103	4
31	κ	$1\bar{3}1$	103 38	58 05	26	04	1104	2
32	M	$\bar{1}11$	-83 36	44 00	11	-09	$11\bar{2}2$	24
33	s	$\bar{1}31$	-70 22	61 26	-12	02	$11\bar{2}0$	3
34	t	$\bar{1}\bar{1}1$	-155 57	23 14	-08	-03	$11\bar{2}4$	44
35	Θ	$\bar{1}\bar{2}1$	160 57	34 08	23	00	$11\bar{2}5$	11
36	Σ	$\bar{1}\bar{3}1$	145 34	46 55	13	17	$11\bar{2}6$	1

no.	GPP	Miller	φ(obs)	ρ(obs)	Δφ	Δρ	hklm	MI
37	d	211	28°54′	44°38′	03′	-03′	$111\bar{1}$	19
38	ϕ	221	4 22	48 15	05	-05	$111\bar{2}$	16
39	γ	231	-12 56	54 24	24	01	$111\bar{3}$	1
40	g	$2\bar{1}1$	73 55	52 43	04	-06	1111	17
41	D	$\bar{2}\bar{1}1$	-134 51	42 36	14	-10	$11\bar{3}5$	4
42	ϕ	$\bar{2}\bar{2}1$	-163 28	43 00	-17	-04	$11\bar{3}6$	17
43	Γ	$\bar{2}\bar{3}1$	173 41	48 47	-11	15	$11\bar{3}7$	1
44	α	321	22 23	56 00	04	-07	$112\bar{3}$	1
45	χ	331	6 03	58 24	04	-01	$112\bar{4}$	1
46	f	$3\bar{1}1$	70 29	61 35	05	-07	1120	38

GPP	Miller basis ABx		C_2-forms				hklm assignment	
47	x	001	-38 05	23 00	-08	-12	$31\bar{3}6$	42
48	e	101	19 42	32 04	45	15	$31\bar{2}5$	10
49	ω	201	39 48	47 25	01	-07	$31\bar{1}4$	12
50	X	$\bar{1}01$	-84 10	36 48	20	-14	$31\bar{4}7$	3
51	Ω	$\bar{2}01$	-98 07	50 52	06	-03	$31\bar{5}8$	3
52	Ψ	011	-48 37	41 23	24	-17	$31\bar{3}5$	9
53	K	021	-51 25	53 25	03	-18	$31\bar{3}4$	1
54	ψ	$0\bar{1}1$	57 08	8 12	1 26	28	$31\bar{3}7$	9
55	k	$0\bar{2}1$	108 11	28 30	01	13	$31\bar{3}8$	17
56	Λ	111	-11 35	40 38	-11	-16	$31\bar{2}4$	9
57	Z	121	-27 39	50 48	09	-07	$31\bar{2}3$	2
58	Π	$1\bar{1}1$	60 58	34 37	29	02	$31\bar{2}6$	10
59	O	$1\bar{2}1$	85 20	44 55	06	07	$31\bar{2}7$	4
60	λ	$\bar{1}\bar{1}1$	-115 09	21 48	-1 07	-39	$31\bar{4}8$	5
61	z	$\bar{1}\bar{2}1$	174 03	22 43	04	17	$31\bar{4}9$	18
62	Δ	211	15 12	48 21	27	00	$31\bar{1}3$	2
63	ρ	221	-3 52	53 21	08	-09	$31\bar{1}2$	16
64	j	$2\bar{1}1$	61 37	50 50	11	07	$31\bar{1}5$	7
65	U	$2\bar{2}1$	77 10	56 36	12	-05	$31\bar{1}6$	1
66	δ	$\bar{2}\bar{1}1$	-116 51	42 58	-16	-10	$31\bar{5}9$	2
67	H	$\bar{2}\bar{2}1$	-146 10	39 33	-1 01	-52	$31\bar{5}10$	1
68	h	321	14 05	58 44	-15	-14	3101	1
69	β	331	-0 18	61 22	18	03	3100	2
70	F	$3\bar{1}1$	61 40	60 08	17	24	3104	1

GPP Miller basis ABR			C_3-forms				hklm assignment	
no.	GPP	Miller	φ(obs)	ρ(obs)	Δφ	Δρ	hklm	MI
71	R	001	-39°03	35°33	50′	-31′	$51\bar{5}10$	6
72	S	101	1 30	39 00	1 35	-15	$51\bar{4}9$	1
73	π	201	25 17	49 49	1 02	-14	$51\bar{3}8$	1
74	η	$0\bar{1}1$	-11 23	17 27	3 09	-36	$51\bar{5}11$	2
75	u	$\bar{1}\bar{2}1$	-143 36	13 35	-3 35	-05	$51\bar{6}13$	13
76	T	211	5 00	53 48	42	-1 10	$51\bar{3}7$	1
77	ν	$2\bar{2}1$	66 29	54 34	35	07	$51\bar{3}10$	1
78	N	$\bar{2}\bar{1}1$	-100 37	46 06	-49	-35	$51\bar{7}13$	1
79	ε	$\bar{2}\bar{2}1$	-125 40	37 39	-1 02	-30	$51\bar{7}14$	1
GPP Miller basis ABb			C_0-forms				hklm assignment	
80	b	001	0 00	0 00	00	00	0100	34
81	J	102	62 12	15 15	04	-10	$021\bar{1}$	14
82	Y	$0\bar{2}1$	122 38	42 57	05	-05	0102	5
83	μ	112	9 58	14 17	-10	00	$021\bar{2}$	31
84	ζ	212	37 08	25 23	-18	-12	$022\bar{3}$	7
Miller basis* ABx:			CC_2-forms				hklm assignment	
85	a	111	0 00	90 00	00	00	1000	14
86	e:	421	32 10	90 00	38	00	$103\bar{4}$	2
87	ω:	101	47 03	90 00	11	00	1001	7
88	Π:	$1\bar{1}2$	72 40	90 00	17	00	$20\bar{1}4$	15
89	z:	$\bar{2}3\bar{1}$	167 11	90 00	16	00	$\bar{1}0\bar{1}3$	10
90	K:	011	-53 09	90 00	16	00	$10\bar{1}1$	5
91	x:	001	-38 34	90 00	36	00	$10\bar{1}2$	16
92	Λ:	112	-7 05	90 00	14	00	$20\bar{1}2$	79

Table I. Re-interpretation of the morphological data of Goldschmidt Palache and Peacock [1] on calaverite. The first three columns give the GPP symbols for each form, the Miller representation being based on four different lattices, the fifth degenerate Miller basis* is added by us. The observed spherical angles with respect to b=(0100) are given in column four and five. Our hklm assignment is based on the basic orthorhombic lattice with the modulation vector $\vec{q}$ = [-0.41 0 0.45]* added as a fourth basic vector. Adding Δφ and Δρ to the observed values one obtains the computed spherical angles according to our (hklm) assignment.

Still, the majority of forms is quite easily provided with remarkable low indices, especially when comparing with any other single lattice interpretation. For one case, ϕ=no.42=$(11\bar{3}6)$, we suppose ϕ(obs) to be erroneously given as 163°28′, while we find only a plausible form at ϕ=-163°28′. Assuming a mistake in sign the value for ϕ(obs) in table I is changed accordingly, this change being also justified in view of the position of ϕ on GPP's Tafel III.

Also in the case of y=no.15 we might be dealing with an erroneously given value for ϕ(obs). For the same face Smith [6] reports ϕ(obs)=104°04′ and ρ(obs)=30°21′, which is in much better agreement with our $(11\bar{2}3)$ assignment. Another interesting point in results presented by Smith is the fact that he reports the spread in the observed spherical angles to be much larger than usual. He typically finds a spread of ~1°.

The Miller indices in the third column are derived by GPP on the basis of their interpretation in terms of four lattices spanned by ABC, ABx, ABR and ABb respectively. The four bases are separately indicated in the table using GPP's notation for each set of forms. For the last eight forms no lattice is provided. For these eight forms the degenerate lattice ABx: can be derived from extrapolating b, C, x and R which all lie in the same zone [0.10 0 -0.18] (the zone is indicated in fractional coordinates of the basic lattice). The relation between the axes of the Miller bases is sketched in fig.1.

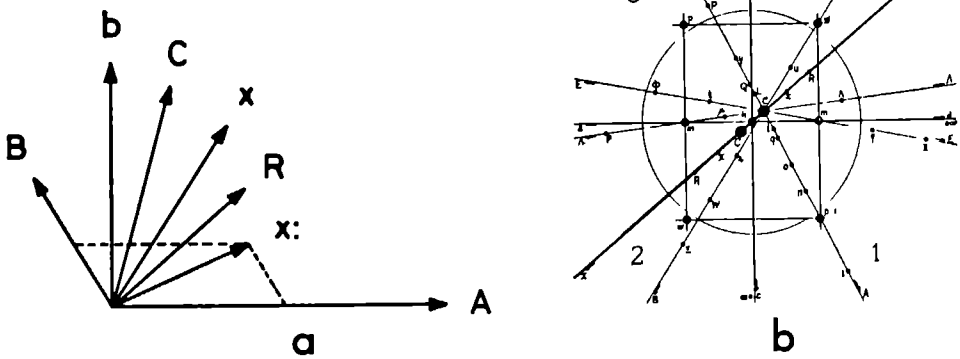

Fig.1.
a) The axes of the Miller bases of table I indicated in one drawing.
b) The same axes indicated in a gnomonic projection as reproduced from GPP.

Substituting for each of the lattice vectors A,B,C,x,R,b and x: the corresponding hklm indices, surprisingly one finds that our interpretation is fully compatible with the Miller indices given in Table I. The difference in the two approaches is that at the cost of an extra base vector we only need one set of 'lattice vectors'. At this stage the structural meaning of the five lattices with respect to our interpretation is not clear.

The hklm-indices we give in Table I do not take possible symmetry extinctions into account. In the crystal form of $((CH_3)_4N)_2ZnCl_4$ (TMA-ZC) we have observed morphological extinctions corresponding to the X-ray reflection conditions of the superspace group of this compound [15]. For calaverite we proposed [1] the C2/m(α 0 γ)(1s) superspace group, for which the conditions of reflection are [16]: h+k=2n and h0lm, m=2n. From GPP and PF we already know that all forms have a 2/m configurational symmetry, thus conforming to the external pointgroup of the proposed superspace group. The centering condition h+k=2n is fulfilled for most of the forms. In a few cases e.g. {0100}, {1010} or {0102} one would have to double all indices to conform to the centering condition, but this can not be deduced from these forms without a comparative study of the MI. Stronger is the case of $\{022\bar{3}\}$=no.84, where {0220} is the only possible origin of this satellite instead of {0110}. For the superspace glide condition h0lm, m=2n such morphological evidence is lacking. Only by doubling the indices of the CC_2-forms one obtains an even m. In principle one can also apply the Bravais-Friedel law, which states that the MI of a crystal face increases with increasing d(hkl); in the modulated case with increasing d(hklm). As noted in [1] this relation seems to hold in calaverite. On the other hand it is not quantitative enough to distinguish between space groups here. Taking our morphological results as a serious indication for the crystal spacegroup we would now prefer C2/m(α 0 γ)(1$\bar{1}$) which lacks the condition h0lm m=2n, rather than c2/m(α 0 γ)(1s) as the calaverite superspace group.

The satellite faces on calaverite are very large and numerous compared to the satellite faces found on TMA-ZC [15]. The incommensurate nature of the modulation wave, both in length and direction, prevents of course any possible overlap of the satellite faces of calaverite. Herewith, the high order of the satellite index m is not clarified. Also in the electron diffraction pattern high order satellite reflections occur. In the latter case the nature of the modulation wave, which is said to consist of a kind of micro-domains, is believed to result in the higher harmonics of the diffraction pattern. Apparantly these higher harmonics have some importance in crystal morphology too.

The problem of the high order satellite faces is of course coupled to that of their (hkl0) 'origins'; if d(hklm) is to be large, high index (hkl0) require high order satellites.

While dealing with the morphology of modulated TMA-ZC [15], we related the stability of satellite faces to the presence of (hkl0) F-faces, i.e. thermodynamically stable faces of the basic crystal structure. The calaverite morphology makes this assumption questionable. Are the non-existent (hkl0) origins F-faces which are just to weak to show up, or is there no such connection between (hkl0) and (hklm) faces. In table I 31 of the 82 satellite faces are related to an (hkl0) origin which is present as a crystal face. The summed MI of these 31 satellite faces covers over 50% of the summed MI of all (hklm) faces. This observation points to at least some relation between the stability of a certain series of satellite faces (hklm) and the stability of the corresponding (hkl0) origin.

To answer the question whether all derived (hkl0) origins are in fact F-faces, a detailed study of the morphology resulting from the calaverite basic crystal structure would be required. This is not a simple task, apart even from the question whether theory is advanced enough already to exclude the possible stability of certain crystal faces.

We will proceed therefore along another path. In the following section we will show that the basic pseudo-orthorhombic calaverite structure itself can be regarded as a substitutionally modulated cubic structure. In this approach a number of (hkl0) origins will appear to be related, which indicates that these origins may have a structural meaning.

IV The cubic approximation

Considering the calaverite basic structure one easily notes its pseudo-cubic character. In fig.2 a drawing of the crystal structure is reproduced from Van Tendeloo et al. [2]. Taking Au equal to Te the body diagonal of the primitive cubic cell is found along the calaverite c-axis. Along this cubic $[111]_{cub}$ direction the commensurate modulation vector $\vec{q}_{cub/comm}=1/3[111]^*_{cub}$ describes the ordening in two layers of Te and one layer of Au atoms. Thus the calaverite basic structure is approximately recovered, neglecting for the moment a small displacement of the Te-atoms.

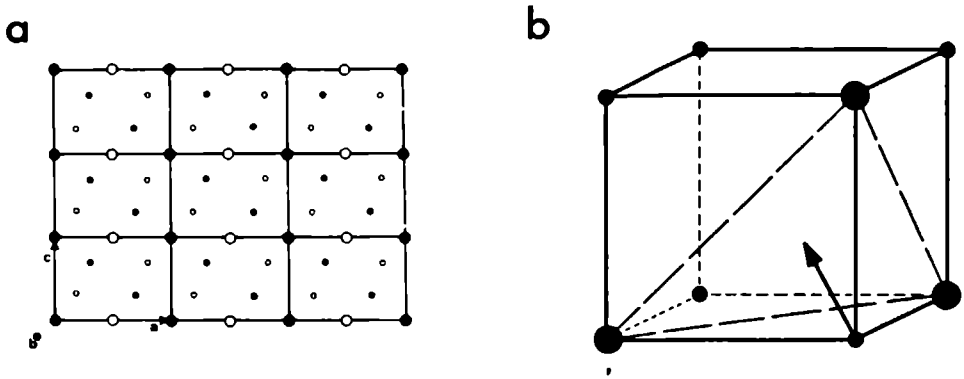

Fig.2. a) Basic structure of calaverite projected along [010]. Large circles represent Au-atoms. Open circles are at y=1/2 while filled circles are at y=0 (drawing reproduced from Van Tendeloo et al. [2]). b) The cubic basic unit-cell. Again are the gold atoms the large circles. Arrow points normal to the wave front of the occupational modulation wave [111]*.

The calaverite unit-cell is obtained from the cubic base vectors $(\vec{a},\vec{b},\vec{c})_{cub}$ according to the transformation:

$$\vec{a}=(\vec{a}+\vec{b}-2\vec{c})_{cub}$$

$$\vec{b}=(-\vec{a}+\vec{b})_{cub}$$

$$\vec{c}=(\vec{a}+\vec{b}+\vec{c})_{cub}$$

The calaverite unit-cell obtained in this way is C-centered orthorhombic. But, as we have seen in the superspace approach of the structure of TMA-ZC [15], such a lattice is very sensitive to distortions in the absence of symmetry elements demanding such an orthorhombic lattice. The monoclinic deviation (β=90°13′) is thus seen as a kind of symmetry breaking. Correspondingly, comparing the actual calaverite cell constants with those obtained from the cubic approximation one finds that the actual $\vec{b}/\vec{c}$ and the $\vec{b}/\vec{a}$ ratios are ~5% larger than the computed values $\sqrt{2/3}$ and $\sqrt{1/3}$ respectively.

At first sight the physical significance of this structural exercise might seem doubtful. It is not, when considering twinning. Usually twins appear if the lattice of a crystal has a pseudo-symmetry. The lost symmetry elements (with respect to the deduced higher symmetrical structure) are the ones which relate the individuals of the twin [17]. In GPP three twin planes are described:

(310), (101) and (111) and their symmetrical equivalents. Transforming these planes to the cubic system one obtains: $(01\bar{1})_{cub}$ and $(\bar{1}01)_{cub}$; $(110)_{cub}$; $(100)_{cub}$ and $(010)_{cub}$. These twin planes are all mirror planes of an m3m cubic lattice and, apart from the first set, they transform [111]* into its cubic equivalents. Along with the [111]* modulation the incommensurate modulation appears to have formed simultaneously. The two are obviously coupled as the incommensurate modulation vector also transforms according to the twin planes. In this way we view the calaverite structure as an distorted cubic, compositionally modulated structure, which is simultaneously subjected to an incommensurate displacive modulation of mainly the gold atoms. The fact that the deviation from the ideal orthorhombic, commensurately modulated structure is an extension along the b-axis while the polarization of the incommensurate modulation is along the same axis, points to some relation between the two.

Accepting the cubic modulation we can analyse the morphology of calaverite now with respect to the primitive cubic lattice and the 1/3[111]* modulation wave vector. Taking the first three indices of all (hklm) faces listed in table I these (hk10) origins (whether present as crystal faces or not) are re-indexed with respect to the cubic lattice and the extra modulation wave vector 1/3[111]* as the fifth basic vector; the incommensurate modulation vector is also transformed to the cubic system, yielding the fourth basic vector (table II). In the first four sections of table II a remarkable ordening of the (hk10) origins is observed. Generally, the distinction between the cubic (0100n), $(01\bar{1}0n)$, $(01\bar{2}0n)$ and $(\bar{1}100n)$ series parallels the GPP division in C_1, C_2, C_3 and C_0 forms. The correspondence is even stronger when transforming $(\bar{2}120n)$ and $(\bar{1}\bar{1}10n)$ to their (0k00n) alternative. Due to the commensurate nature of the compositional modulation this kind

Table II. Re-interpretation of the (hk10) origins of the pseudo-orthorhombic calaverite morphology, in terms of a primitive cubic lattice and the commensurate wave vector 1/3[111]*. The third column colums gives the MI of each (hk10) as far as observed, whereas the fourth column indicates the indices m of the observed satellites of this origin. All (hk10) have been given indices according to a C-centering of the pseudo-orthorhombic lattice. Only in the cases marked with a * indices have been multiplied in order to obtain suitable (h'k'l'0 n') indices. In the last section a few alternative (h'k'l'0 n') indices have been added.

Table II

cubic calaverite		pseudo-orthorhombic calaverite		
h′k′l′0 n′		hkl0	MI(hkl0)	m(obs)
01005̄		11$\bar{4}$0		5
01004̄		11$\bar{3}$0		5 6 7
01003̄		11$\bar{2}$0	3	3 4 5 6
01002̄		111̄0	72	-1 1 2 3 4 5
01001̄		1100	122	-2 -1 1 2 3 4
01000		1110	139	-3 -2 -1 1
01001		1120	38	-4 -3 -1
01$\bar{1}$00		3100	2	1 4
01$\bar{1}$01̄		31$\bar{1}$0		2 3 4 5 6
01$\bar{1}$02̄		31$\bar{2}$0		3 4 5 6 7
01$\bar{1}$03̄		31$\bar{3}$0		4 5 6 7 8
01$\bar{1}$04̄		31$\bar{4}$0		7 8 9
01$\bar{1}$05̄		31$\bar{5}$0		8 9 10
01$\bar{2}$02̄		51$\bar{3}$0		7 8 10
01$\bar{2}$03̄		51$\bar{4}$0		9
01$\bar{2}$04̄		51$\bar{5}$0		10 11
01$\bar{2}$05̄		51$\bar{6}$0		13
01$\bar{2}$06̄		51$\bar{7}$0		13 14
$\bar{1}$1000		0200	34	-4 4
$\bar{1}$1001		0210		-1 -2
$\bar{1}$1002		0220		-3
$\bar{2}$1$\bar{2}$01̄	03007̄	33$\bar{4}$0		7
$\bar{2}$1$\bar{2}$01	03005̄	33$\bar{2}$0		5
$\bar{1}$1$\bar{1}$00	02003̄	22$\bar{1}$0		1 3
$\bar{1}$1$\bar{1}$02̄	02005̄	22$\bar{3}$0		3 5
11100		0030*	84	-1 -2
00000		0000		1
00$\bar{1}$00		20$\bar{1}$0		2 3 4
00$\bar{1}$03		2020	4	3
00$\bar{1}$01̄		20$\bar{2}$0		1 2
11$\bar{2}$00		6000*	14	1

of ambiguity is unavoidable. With respect to the commensurate modulation, this makes main and satellite orientations indistinguishable for n'=3n (n=integer). Note, that looking at the MI of the (hkl0) origins one finds that in each of the sections of table II cubic main orientations relate to (hkl0) faces with a high MI.

Let us return to the intriguing set of faces generating the C_1,C_2 and C_3 forms: C, x and R. The systematic occurrence of the (11$\bar{1}$0), (31$\bar{1}$0) and (51$\bar{1}$0) series even in our cubic notation must have a structural cause. The hklm indices of C, x and R transform into the cubic system as follows:

$$C=(1,1,\bar{1},2)=(0,1,1,\bar{2},2)$$

$$x=(3,1,\bar{3},6)=(0,1,\bar{1},\bar{3},6)$$

$$R=(5,1,\bar{5},10)=(0,1,\bar{2},\bar{4},10)$$

For simplicity the indices have been separated by comma's here. The four indices relate to the pseudo-orthorhombic lattice, the five indices relate to the three cubic reciprocal base vectors, $\vec{q}_{cub/comm}$ and $\vec{q}_{cub/incomm}$. In the five integer notation the incommensurate displacive modulation vector is transformed to the cubic system giving: $\vec{q}_{cub/incomm}=[0,0,0,1,0]^*=[0.08\ 0.08\ 0.29]^*_{cub}$. The faces C, x and R are related by a constant increment vector $\vec{i}=[0,0,\bar{1},\bar{1},4]^*$. If one transforms this vector to fractional cubic coordinates, surprisingly one finds that it is directed along a cubic main axis: $\vec{i}=[0\ 0\ 0.17]^*_{cub}$. Thus this vector seems to account for the difference between the two modulation vectors which are just unable to cancel each other. On the other hand we may as well take the $(010)_{cub}$, $(01\bar{1})_{cub}$ and $(01\bar{2})_{cub}$ series as a whole and say that they are related by an increment vector $[001]^*_{cub}$.

V Conclusion

We are still far away from a thorough understanding of the morphology of calaverite. In the pseudo-orthorhombic lattice the full description of the 92 independent forms of calaverite shows the power of the application of the incommensurate modulation wave vector as a fourth base vector. The reason for the stability of the satellite faces and the role the so-called (hkl0) origins plays remains unclear, though some extended classical laws seem to hold. In the cubic approach even more order can be brought into the morphological description of calaverite. On the other hand the cubic approach still

poses us for a lot of questions. It is hoped that more structural information will bring us further, the truth on calaverite appearing to be manifold, as ever.

References

1) B. Dam, A. Janner, J.D.H. Donnay, Phys. Rev. Lett. 55 (1985) 2301.

2) G. van Tendeloo, P. Gregoriades and S. Amelinckx, J. Sol. State Chem. 50 (1983) 321; 50 (1983) 335; 53 (1984) 281.

3) V. Goldschmidt, Ch. Palach and M. Peacock, Neues Jahrb. Mineral. Geol. Paleont, Ref., Beil.-Bd., 63 (1931) 1.

4) S. L. Penfield, Amer. Journ. Sci. 50 (1895) 128.

5) F.A. Genth, Amer. Journ. Sci. 45 (1868) 304.

6) Herbert Smith, Min. Mag. 13 (1902) 125; Z. Kristallogr. u. Mineral. 37 (1903) 209.

7) S.L. Penfiel and W.E. Ford, Z. Kristallogr. u. Mineral. 35 (1902) 435.

8) J.D.H. Donnay, Ann. Soc. Geol. Belg. 18 (1935) B222.

9) G. Tunell and C.J. Ksanda, J. Wash. Acad. Sci. 25 (1935) 32.

10) G. Tunell and C. J. Ksanda, J. Wash. Acad. Sci. 26 (1936) 507; 26 (1936) 509.

11) G. Tunell and L. Pauling, Acta Cryst. 5 (1952) 375.

12) F. Pertlik, Z. Kristallogr. 169 (1984) 227

13) S. Sueno, M. Kimata and M. Ohmasa in: Modulated Structures-(1979), AIP Conference Proceedings vol.53, edited by J.M. Cowley, J.B. Cohen, M.B. Salomon and B.J. Wuensch (American Institute of Physics, New York, 1979) p333.

14) J. de Boer, Private Communication (1986).

15) B. Dam and A. Janner, Acta Cryst. in press.

16) P.M. de Wolff, T. Janssen and A. Janner A37 (1981) 625.

17) M.J. Buerger, Am. Miner. 30 (1945) 469.

Curriculum Vitae Bernard Dam

Geboortedatum en -plaats: 12 november 1956, Arnhem

Middelbare school: Gymnasium β,
Thorbecke Scholengemeenschap,
Arnhem, 1969-1975

Kandidaats Scheikunde: KU Nijmegen, 1975-1978
-Scheikunde en natuurkunde hoofdvak met wiskunde bijvak, S3

Doctoraal Scheikunde: KU Nijmegen, 1978-1982 (cum laude)
-Hoofdvak Vaste Stof Chemie (Prof. P. Bennema)
Stage-onderwerp: Oppervlaktemorfologie en enige strukturele eigenschappen van KDP en ADP
scriptie: Ferroelectriciteit in KDP en andere tetragonale fosfaten
-Bijvak (met de omvang van een hoofdvak)
Molekuul Spektroskopie, ESR (prof. E. de Boer)
Stage-onderwerp: meting, simulatie en theorie van zwakke exchange interacties
-Caput college: Filosofie der Natuurwetenschappen
Scriptie: Inductie, een demarcatie-criterium?

Gedurende 1-1-82 tot 1-4-82 in tijdelijke dienst van de KU bij Prof. dr. J. Bloem op de afdeling Vaste Stof Fysica III, ten behoeve van een door de N.V. Philips gesponsord project getiteld: Gasfase groei van Silicium 1-kristallen.

Vanaf 1 april 1982 op de afdeling Vaste Stof Chemie werkzaam aan een promotie-onderzoek in dienst van ZWO/SON. Gedurende deze periode werd als onderwijstaak werkcollege thermodynamica gegeven.

STELLINGEN

1) Voor de kristalmorfologie is het bestaan van fundamentele periodiciteiten belangrijker dan een 3-dimensionale rooster symmetrie.
   - Dit proefschrift

2) Oppervlaktereconstructie kan gezien worden als een modulatie van de oppervlaktestructuur. De identificatie en notatie van deze oppervlaktestructuren zouden vereenvoudigd kunnen worden door het gebruik van (2+n)-dimensionale superruimtegroepen.
   - T. Janssen, A. Janner and P.M. de Wolff, Proceedings of the Seminar Group Theoretical Methods in Physics, Zvenigorod, USSR, 1979.

3) Het verband tussen oppervlaktereconstructie van een bepaalde kristalorientatie en de ermee corresponderende afstand tussen equivalente roostervlakken is onvoldoende onderzocht.

4) Het succes van de morfologische wetten van Bravais-Friedel-Donnay-Harker is slechts ten dele begrepen.

5) De discrepantie tussen de berekende en gemeten randenergie van de zijvlakken van paraffinekristallen zoals door Simon, Grassi and Boistelle is gevonden, kan worden toegeschreven aan een te primitief gekozen bindingsgraaf.
   - B. Simon, A. Grassi and R. Boistelle, J. Crystal Growth 26 (1974) 77.

6) Bij de experimentele bepaling van de Burgersvector van een randdislocatie met behulp van de foto-elastische methode wordt ten onrechte geen rekening gehouden met de beperkte scherptediepte van de microscoop.
   - V.I. Nitenko and L.M. Dedukh, Phys. Stat. Sol. (a) 3 (1970) 383.

7) Bij de berekening van intensiteitsprofielen van spanningsdubbelbrekingsbeelden van dislokaties die parallel aan een kristaloppervlak en loodrecht op de optische as van een polarisatiemicroscoop liggen, mogen de zogenaamde image forces niet verwaarloosd worden.
   - B.K. Tanner, Phil. Mag. A49 (1984) 435.

8) De conclusie van Woods en Collins dat in type I diamanten waterstofcomplexen gesitueerd zijn aan de oppervlakken van submicroscopische holtes of aan diamant/inclusie opppervlakken is voorbarig.
- G.S. Woods en A.T. Collins, J. Phys. Chem. Solids 44 (1983) 471.

9) De waarde van experimenteel onderzoek lijkt, bij gebrek aan beter, vaak gerelateerd te worden aan de geldswaarde van de gebruikte apparatuur.

10) Voor het boek van Paul Davies met als centrale these `the new physics offers a surer path to God than religion', zou de titel `The God of the new physics' meer voor de hand hebben gelegen.
- Paul Davies, God and the new physics (Simon and Schuster, New York, 1984).

11) Het `reductionalisme' van de natuurwetenschappelijke methode is vooral gevaarlijk als de natuurwetenschap `holistisch', d.w.z. als heersende ideologie of als religie, geïnterpreteerd wordt.

12) Bij de pogingen om natuurwetenschappelijke theorieën te gebruiken als basis voor religieuze beschouwingen wordt het principieel feilbare karakter van deze theorieën veronachtzaamd.

13) In de handeling van de Mozart/Da Ponte opera `Don Giovanni' doet de hoofdpersoon zijn naam geen eer aan.

17 april 1986, Bernard Dam.